The Study of the Corrosion Behavior of Gas Nitriding Treated L80 Steel in Simulated

Environment for the Slotted Liners of SAGD

by

Xueyuan Chen

A thesis submitted in partial fulfilment of the requirements for the degree of

Master of Science

in

Materials Engineering

Department of Chemical and Materials Engineering

University of Alberta

Abstract

The oil sand in Alberta province is mainly extracted by Steam Assisted Gravity Drainage (SAGD) technique which employs the slotted liners as the primary sand screening system. However, the slotted liners made of L80 carbon steel suffer from severe corrosion and erosion problems in the downhole environment containing aggressive species. However, conventional protection methods, such as inhibitors and cathodic protection methods are not applicable to this environment. Gas nitriding, as a well-established surface treatment method, has been widely applied in metallurgical processes to form an erosion resistance surface layer in extreme environment since this treatment grows a high hardness layer of ceramic iron nitrides (Fe-N) on the surface of carbon steel. Iron nitrides are also believed to have great potential to boost the corrosion resistance in various environment, but the corrosion behavior and the stability of GN carbon steel is seldom studied in any environment similar to the one that slotted liners have. Therefore, gas nitriding (GN) was selected as a coating candidate for liners in this thesis. The lab-scale GN treatment in tube furnace on L80 carbon steel was optimized by varying nitriding time, temperature and ammonia gas flowrate to grow a thick, compact and pure compound layer on L80. The corrosion behavior of GN treated L80 will be tested in the simulated environment by using various electrochemical tests such as Potentiodynamic Polarization (PD) curves and Electrochemical Impedance Spectroscopy (EIS). The surface characterization techniques such as digital microscope (DM), Scanning Electron Microscope (SEM), Energy-Dispersive X-ray Spectroscopy (EDX) and X-ray Diffraction (XRD) are also employed to investigate the microstructure, morphology and compositions of GN treated L80.

With a treatment at 40 mL/min of flowrate at 530 °C for 15 h, GN treated L80 achieved a significantly decreased corrosion rate of 0.023 mm/year in the simulated environment with

saturated carbon dioxide (CO_2) at 20°C. The significantly decreased corrosion rate was about one order of magnitude lower than that of L80 without treatment tested in the same environment. The longer GN duration increased the thickness of the compound layer but the temperature and flowrate were treated as a pair for the optimized dissociation rate to produce a compact compound layer. Double-layer equivalent circuit was used to fit the EIS data and the results suggested that the R_p, 3.96×10^5 $\Omega \cdot cm^2$, of GN treated L80 tested in the simulated environment was very close to that of alloy 800, which is one of the corrosion resistant materials applied in oil sand industry, and two orders of magnitude larger than that of L80. GN treated L80 was believed to be a more suitable material for the application of slotted liners due to wider and more stable passivation zone shown in PD curve. The XRD results showed that the surface composition of GN treated L80 did not have significant change before and after the immersion test, while the SEM and EDX provided the same confirmative evidence that both of the compositional and dimensional stability of GN treated L80 maintained after 24 h immersion test. From the potentiostatic polarization test at the applied potential of + 0.2 V vs. Ag/AgCl, the stable and decreased current density indicated that GN treated L80 not only had stable corrosion resistance in the simulated environment but also had lower overall corrosion rate than the value predicted by PD test. Therefore, GN treated L80 had significantly improved corrosion resistance of L80 in the simulated environment and it was a competitive candidate for the application as a corrosion resistant material for the slotted liners of SAGD system.

Preface

Chapter 1 is the introduction of my research work. It includes the background of my research, the defining of problems and my motivation and objective of the work.

Chapter 2 is the literature review relate to my research.

Chapter 3 is the brief introduction of the principles of the main techniques and methods that I used to conduct my research.

Chapter 4 is the optimization of GN process by varying the duration, temperature and flowrate.

Chapter 5 is the comparisons of L80, GN treated L80 and alloy 800 in the simulated environment by using electrochemical tests.

Chapter 6 is the investigations of the compositional, dimensional and electrochemical stabilities of the GN treated L80.

None of the experimental results used in this thesis has been published as journal article, books, conference papers etc. My supervisor, Dr. Jing-Li Luo, provided me valuable suggestions on the experimental design and results interpretation. She also helped me on revising the grammar and vocabulary of my thesis. Dr. Hong Luo, PDF fellow in our corrosion lab, helped me with designing and setting up GN system and corrosion cell. Dr. Qinying Wang, PDF in our corrosion lab taught me the EIS analysis. Hongbo Shi, a 4th year petroleum engineering student, helped me on sample pretreatment as a volunteer. Some of the surface characterization tests were done by the technicians from other departments, such as the XRD done by Nancy Zhang in NanoFAB and SEM by Gerein Nathan in Department of Erath and Atmospheric Science at University of Alberta. I performed most of the experiments, data analysis and results interpretations and the writings.

Acknowledgement

I would like to take this opportunity to express my gratitude to all the people who gave great helps for my master studies in Department of Chemical and Materials at University of Alberta.

Firstly, I would like to give my most sincere gratitude to my supervisor, Dr. Jing-Li Luo, who gave me numerous kind and patient helps not only on the academic and research areas, but also on my personal life and career development. Without her support, I could not complete my research. I will not forget the knowledge she taught me, the skills she helped me to developed, the professional ethics and the enthusiasm of scientific researches she delivered and these will give me great helps for my life and career as a material science engineer.

Then, I would like to thank to Dr. Hong Luo and Dr. Qinying Wang for giving me valuable suggestions and assistance on the experimental design and data analysis. Without your effort on my experimental design and research, my work could not be smoothly proceeded. I do appreciate every experiments you helped me with and the data analysis methods and experience you provided me.

My deep appreciation also goes to my exam chair, Dr. Leijun Li, supervisor committee members, Dr. Thomas Etsell, Dr. Qi Liu and Dr. Jing-Li Luo for their great suggestions to help the progress of my research.

Most importantly, I must express my thanks to my group members from corrosion lab, Dr. Chen Shen, Xianzong Wang, Dr. Yashar Behnamian, Zeynab Shirband, Ermia Aghaie, Zhong Li and Kaiyang Li. Thanks for the valuable suggestions you raised during the group meeting. The same thanks to the group members in fuel cell group: Dr. Bin Hua, Yaqian Zhang, Subiao Liu, Yifei Sun, Lin Cui, Wenfei Zhang, for the advice you provided to fill out some of my knowledge gaps.

Table of Contents

List of Figures

xiii

List of Tables

List of Abbreviations

SAGD	Steam-assisted Gravity Drainage
HPHT	High Pressure and High Temperature
GN	Gas Nitriding
PD	Potentiodynamic Polarization
EIS	Electrochemical Impedance Spectroscopy
SEM	Scanning Electron Microscope
XRD	X-ray Diffraction
AES	Auger Electron Spectroscopy
EDX	Energy Dispersive X-ray
API	American Petroleum Institute
CP	Cathodic Protection
FBE	Fusion Bonded Epoxy
PTFE	Polytetrafluoroethene
SS	Stainless Steel
AMS	American Society for Materials
WE	Working Electrode
RE	Reference Electrode
CE	Counter Electrode
AC	Alternative Current
EC	Equivalent Circuit
DM	Digital Microscope
CRA	Corrosion Resistance Alloy

Nomenclature

ε	$Fe_{2-3}N$ phase
γ'	Fe_4N phase
Z	Impedance, Ω
R	Resistance, Ω
Z_{re}	The real component of the impedance, Ω
Z_{im}	The imaginary component of the impedance, Ω
θ	Phase angle, °
C	Capacitance, F
E	Potential, V or mV
I	Current, A or μA
τ	Time constant, s
R_s	Resistance of solution, Ω
R_p	Resistance to solution to surface interface, Ω
C_{dl}	Capacitance of double layer, $S\text{-}s^n$
C_c	Capacitance of coating, $S\text{-}s^n$
R_{po}, R_{pf}	Resistance of the pore, Ω
R_{ct}	Resistance of the coating, Ω
E_{corr}	Free corrosion potential, V or mV
I_{corr}	Free corrosion Current, A or μA
$β_A$,	Anodic Tafel constants
$β_C$	Cathodic Tafel constants
E.W.	Equivalent weight of the working electrode, g
d	Density of the corroding species, $g/cm2$

λ   Wavelength of incident wave, nm

d   Lattice spacing, nm

θ   Incident angle in Bragg's Equation, °

Chapter 1. Introduction

1.1 The Introduction of Steam Assisted Gravity Drainage System

Alberta has the world third largest crude oil reserves (Figure 1-1), which is about 13% of the total amount reserves in the world. The daily crude oil production barrels from oil sand reservoirs in Alberta was as high as 1.9 million in 2011[1]. However, 80% of the oil sands are not suitable for surface mining since they are deposited in deep ground. Therefore, *in-situ* methods such as steam assisted gravity drainage (SAGD) must be applied to pump up the bitumen for further treatment. With this technique, steam is injected into bitumen-rich oil sand trough the upper horizontal well. Steam lowers the viscosity of bitumen, which allows it flowing into the slotted liner of the bottom producer well. The heated and diluted bitumen is pumped to the ground and stored for upgrading (Figure 1-2) [2]. However, various corrosive agents either generated during aquathermolysis process or intrinsically contained in the formation, significantly reduce the service life of slotted liners by degradation processes such as sweet corrosion (CO_2 corrosion), sour corrosion (H_2S corrosion), H_2S/CO_2 synergism corrosion, sulfide stress corrosion (SSC) and erosion [4]. The Faculty of Engineering at the University of Alberta is currently collaborating with RGL Reservoir Management Inc., a leading supplier of completions tools for enhanced oil recovery, for the designing of SAGD sand control and tooling system. One of the objectives of this collaborative project is to reduce the corrosion and erosion damage of the slotted liners by development of protective coatings with the ultimate goal of reducing the manufacturing cost and increase production efficiency.
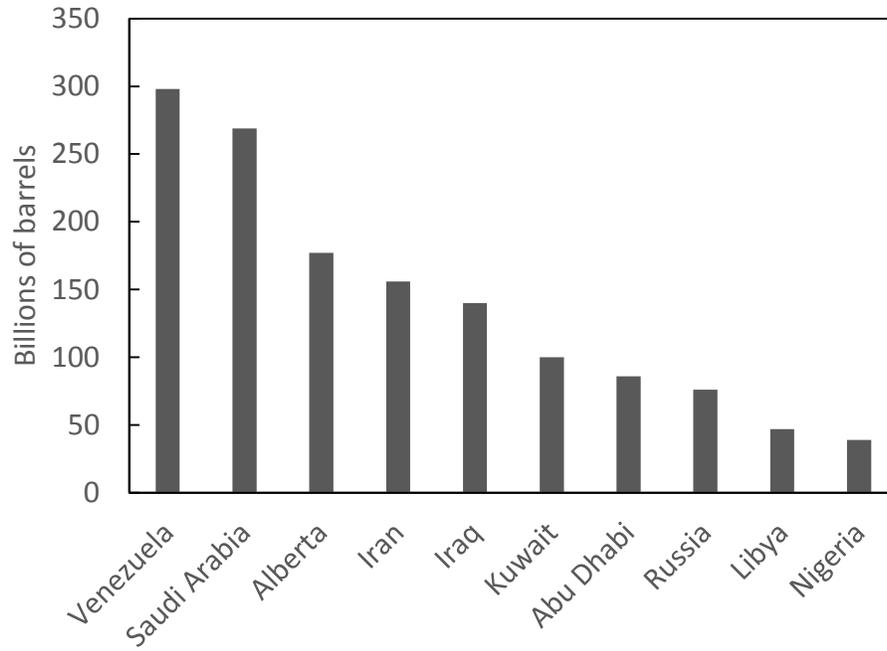
Figure 1-1. The world oil reserves ranking [1].
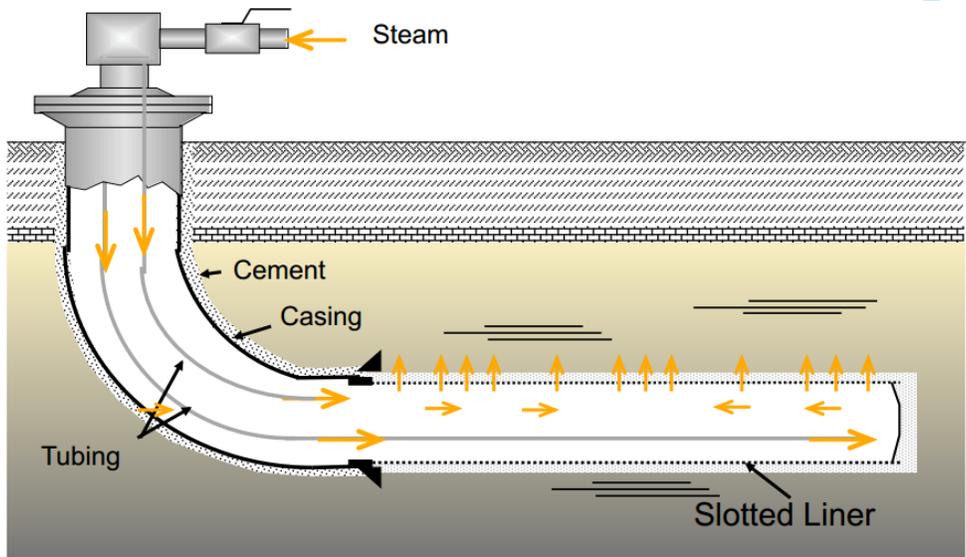
Figure 1-2. The working principle of SAGD well completion [3].

1.2 The Problems: Corrosion and Erosion

The corrosion and erosion of slotted liners could be severe after long terms of service. The corrosion rates of carbon steel in sweet and sour environments depend on various parameters such as fluid chemistry, steel surface treatment and temperatures etc. The main corrosion products formed by sweet corrosion, iron carbonate ($FeCO_3$), can either precipitate on the steel surface as a protective layer especially at elevated temperature or disperse into the fluid, which results in unacceptable corrosion rate [6]. The corrosion and erosion roughen the liners wall and result in deformation. They cause problems such as the fouling, plugging, passing of oversized particles and reduced oil quality. Many different protections have been developed to mitigate the corrosion of carbon steels as oil liners; however, commonly used corrosion control methods such as inhibitors and cathodic protection are not suitable for slotted liners due to high costs and environmental issues [5]. Therefore, surface treatment or coating is the only feasible protection method to increase both of the corrosion and erosion resistances of carbon steel in sweet and sour environment.

Figure 1-3. A failed section of slotted liner with considerable amount of corrosion stains [5].

1.3 The Objective and Scope of My Research

Therefore, to maintain the screening efficiency and increase the lifetime of slotted liners, our group had been working on the development of an economic coating that can be industrially applied on slotted liners to increase both the corrosion and erosion resistance in the sweet and sour environment. Dr. Hong Luo had been working on the development of tungsten carbide-embedded nickel coating by electro plating and Dr. Qinying Wang had been working on the investigation of chromized coating by pack cementation. The objective of my work is to explore the feasibility of the GN to improve the corrosion resistance of L80 in the simulated environment of slotted liners. In this experiment, lab-scale GN by using tube furnace was constructed to form iron nitride coating on L80 carbon steel. The optimizations of GN treatment schedule by varying nitriding time, nitriding temperature and ammonia gas flowrate were conducted in this research. The corrosion resistance of GN treated L80 was tested in the simulated environment of slotted liners. The corrosion behavior of nitriding treated specimens were compared with L80 carbon steel which is the current material used for slotted liners and alloy 800 which is commonly used in the oil well injector for H_2S-rich environment. This research examined the corrosion resistance and the stability of the GN treated L80 in the simulated environment of slotted liners.

1.4 The Significance and Innovation of My Approaches

Although GN is a widely applied industrial method, the systematical investigations of the corrosion resistance of GN treated steel in the solution with CO_2 are seldom conducted since the application of GN treated material is generally in dry environment as a material with the primary purpose for high wear resistance [7]. Lack of researches and reports of the behavioral analysis of the corrosion of GN treated carbon steel in solution drove me to research the feasibility of this well-established and economic technique for the application on the slotted liners. Most labs used

the plasma nitriding treated carbon steels as their tests subjects. Due to the different mechanisms, the plasma nitriding treated carbon steel is expected to have much better corrosion resistance than GN treated carbon steel. However, this technique could not be used for industrial-scale mass-production. There is one group, headed by Dr. Bingying Wang, in China University of Petroleum, did some preliminary researches on the investigation of the corrosion resistance of GN treated steel in CO_2 containing environment. However, they did not systematically optimize their nitriding process and they did not perform any stability test. Moreover, the composition of carbon steel is also a crucial factor which significantly alters the composition and formation of the nitriding layers. Therefore, their data could not be directly referred to predict the corrosion resistance of GN treated L80 in the simulated environment. Furthermore, the conventional nitriding treatment aims for the primary purpose of case hardening but not the high corrosion resistance. Consequently, the GN treatment schedule must be modified to maximize the density and purity of compound layer, which results in significantly increased corrosion resistance. However, it is usually not the conventional industrial practice. Therefore, self-developed GN treatments must be done to predict the corrosion behavior of GN treated L80 in simulated environment of slotted liners.

1.5 Techniques Used to Conducted My Research

The GN treatment of L80 carbon steel was mainly achieved by using a tube furnace with a quartz tube. For the corrosion behavior analysis, electrochemical measurements and tests such as potentiodynamic polarization curves and electrochemical impedance spectroscopy (EIS) were used to test electrochemical behavior of specimen in simulated environment. Tafel fitting and equivalent circuit modeling were the main analysis methods applied to interpret the data from electrochemical tests. Surface analysis methods such as digital microscopy (DM) and scanning electron microscopy (SEM) were used to characterize the surface morphology and microstructure

of specimen. The surface compositional analysis before and after the immersion tests were achieved by using X-ray diffraction (XRD) and energy dispersive x-ray (EDX). Last but not least, the tests of stability and degradation resistance were accomplished by immersion test and potentiostatic polarization test. With both the assistance of electrochemical tests and surface characterization analysis techniques, the corrosion behavior of the coatings can be systematically and comprehensively evaluated.

Chapter 2. Literature Review

2.1 The Corrosion Environment of Slotted Liners
2.1.1 Acid Gases
The generation of acid gases such as CO_2, H_2S and sulphur dioxide (SO_2) along with small amount

of hydrogen (H_2) and methane (CH_4) are usually from the aquathermolysis process, which is the

in-situ technology used to reduce the viscosity of bitumen by injecting HPHT water steam into the

oil sand well [8]. This gaseous phase separated from this process usually contains as high as 35 -

40 mol% of CO_2 and 2 - 3 mol% of H_2S [9]. Some researchers argued that the sweet corrosion

itself does not significant increase the corrosion rate since the operation temperature (higher than

200°C) significantly decreases the solubility of CO_2 in the water phase. Therefore, the pH of

produced water is usually not acidic, which passive corrosion behavior is generally expected [9].

Therefore, the water chemistries were predicted with only mild corrosion effects with uniform

corrosion rate of 0.06 mm/y on carbon steel in this operation environment. However, according to

the field data gathered by Whittaker et al. [10] from the corrosion products of liners after only five-

year of service, the actual uniform corrosion rate of failed segment from McMurray reserves was

measured as high as 8 mm/year. In their study, the XRD results showed that 80 % of corrosion

products resulted from the corrosion involves CO_2 and only 15 % iron sulfide were from H_2S

corrosion. They also concluded that the acidic environment usually resulted in much porous

corrosion products deposition than neutral or alkaline environment. Therefore, my research started

with the most common and dominated sweet corrosion as the main corrosion mechanism of the

simulated environment.

2.1.2 The Chemical Compositions of Bitumen and Formation Water

The tar sand usually consists of 86 % of silica sand and clay, which are designed to be partially

removed by the slotted liners. The crude bitumen is only about 10 % from the tar sand, and the rest

is 4 % saline water [11]. The injected steam increases the moisture level of the tar sand and three phases form. The erosion of the liners is mainly caused by the solid particles; but the water phase accounts for the corrosion. The produced water usually contains ion or anions groups such as chloride (Cl^-), carbonate (CO_3^{2-}), bicarbonate (HCO_3^-) and sulfate (SO_4^{2-}), and cations such as Na^+, Ca^{2+}, Mg^{2+} and K^+ [9]. The concentration of different species varies significantly in different oil reserves. These species may have either inhibiting or detrimental effect on the corrosion behavior of steel in this environment. For example, Cl^-, as a common species in oil sand, has a well-known detrimental effect on accelerating the localized corrosion by the breakdown of passive films formed on stainless steel (SS) [12]. By contrast, the formation water from McMurray and Grand Rapids formations contains 750 ppm HCO_3^-, which inhibits the corrosion by increasing the pH of water [10]. This research selected the "sodium-chloride-bicarbonate" basal water type, which is a common type from McMurray formation [13], as the reference solution for the simulated solution for the tests.

2.1.3 Casing Grade of Slotted Liners

In this study, L80 was selected as the core material since L80 is the existing material in application for slotted liners. L80 is manufactured under American Petroleum Institute (API) specification 5CT, which has a minimum yield strength of 565 MPa [14]. L80 is available in type 1, 9Cr and 13Cr. 9Cr was popular in the past for CO_2 and H_2S contaminated wells, but it has been replaced by the most costly 13Cr, which has better CO_2 induced weight-loss corrosion resistance; however, the high susceptibility of corrosion induced by sour environment limits 13Cr to the application in reservoirs where the partial pressure of H_2S is lower than 1.5 psi. Type 1 L80, which is usually abbreviated as L80, is the least expensive L80 steel, but it is more susceptible to weight-loss

corrosion. It is one of the most commonly applied pipeline materials for oil and gas field nowadays [15].

2.2 The Corrosion Mechanism in this Simulated Environment

2.2.1 The Effect of Carbon Dioxide (CO_2)

The corrosion of carbon steel in water with dissolved CO_2 has been studied for several decades to investigate and predict the corrosion behavior of carbon steel in oil and gas field. The solubility of CO_2 mainly depends on the partial pressure of CO_2, temperature and also the species present in bitumen. The corrosion processes involve CO_2, H_2O and Fe generally go through the reactions list below[16] [17],

Absorption of gaseous CO_2,

$$CO_2(g) + H_2O(l) \leftrightarrow H_2CO_3(aq) \text{ (eq. 2-1)}$$

The acidification,

$$H_2CO_3 \leftrightarrow H^+ + HCO_3^- \text{ (eq. 2-2)}$$

$$HCO_3^- \leftrightarrow H^+ + CO_3^{2-} \text{ (eq. 2-3)}$$
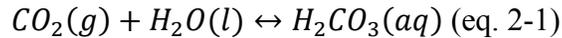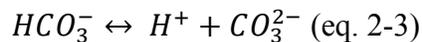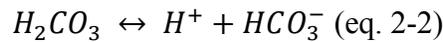
The anodic reaction is simply the oxidation of iron,

$$Fe \rightarrow Fe^{2+} + 2e^- \text{ (eq. 2-4)}$$
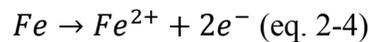
The cathodic reactions occur either by the direct reduction of hydrogen,

$$2H^+ + 2e^- \rightarrow H_2 \text{(eq. 2-5)}$$
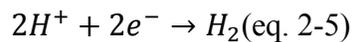
Or by the reduction of carbonate,

$$H_2CO_3 + e^- \rightarrow \frac{1}{2}H_2 + HCO_3^- \text{ (eq. 2-6)}$$

9

$$HCO_3^- \rightarrow \frac{1}{2}H_2 + CO_3^{2-} \text{ (eq. 2-7)}$$
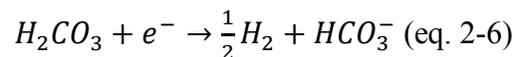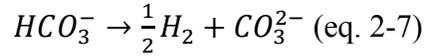
Oxides may form either with carbonates,

$$CO_3^{2-} + Fe^{2+} \rightarrow FeCO_3 \text{ (eq. 2-8)}$$
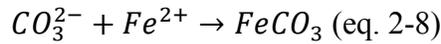
Or react with bicarbonates,

$$Fe^{2+} + 2HCO_3^- \rightarrow Fe(HCO_3)_2 \text{ (eq. 2-9)}$$

$$Fe(HCO_3)_2 \rightarrow FeCO_3 + CO_2 + H_2O \text{ (eq. 2-10)}$$
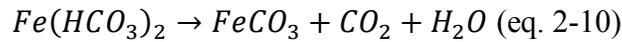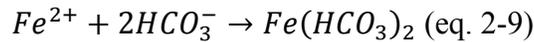
A protective film with brittle and loosely adhered iron carbonate ($FeCO_3$) is the main corrosion product. Finely dispersed Fe_3C formed during heat treatment provide better adhesion for protective layer since $FeCO_3$ tends to segregate in the voids where Fe selectively dissolved [18]. The solubility of $FeCO_3$ is faster in more acidic solution due to the accelerated Fe^{2+} products formation [16]. When the amount of Fe^{2+} and CO_3^{2-} exceed their solubilities in the aqueous phase, they precipitate onto the steel surface with different morphologies [18]. From Palacious and Shadley' study [19], they suggested that the $FeCO_3$ is usually porous, which allows Cl^-, CO_3^{2-}, and HCO_3^- transfer from the solution into the corrosion production to reach the alloy interface. The thin protective film become more compact with time as the deposition of newly formed corrosion product filling in the voids of previous formed corrosion products. The porosity of film decreases with the increase of Cl^- due to the segregation of Cl^- [20]. The corrosion products can be easily removed by the flow due to the Cl^--induced coating spallation [10] and solid impurities in the real operation environment. Therefore, the corrosion products generally did not provide sufficient protections based on the data obtained in their immersion tests [20].

2.2.2 The Effect of Bicarbonate (HCO_3^-)

Various bicarbonates may act as inhibitors or accelerators to the corrosion of carbon steel. Videm and Koren [15] investigated the effect of the level of sodium bicarbonate ($NaHCO_3$) on the corrosion behavior of carbon steel in CO_2 saturated aqueous solution with different concentrations of sodium chloride (NaCl), surface roughness and pH. The presence of $NaHCO_3$ increased the pH of the CO_2 saturated solution, which resulted in the inhibition effects of the corrosion by lowering the solubility of corrosion films. Even very low level of the HCO_3^- concentration changed the dissolution mechanisms of carbon steel in CO_2 containing aqueous solutions. For example, the "prepassive" dissolution mechanisms was observed in solutions contains low level of HCO_3^- (i.e. 0.01 M and less) compared with the passive dissolution mechanism at higher level of HCO_3^- (i.e. 0.1 M and up). No passivity occurred in 0.01 M $NaHCO_3$ solution with saturated CO_2 and 1 M NaCl which has a pH of 5.63. The corrosion mechanisms involving HCO_3^- had been proposed by Davis and Burstein [21].

$$Fe + 2H_2O \rightarrow Fe(OH)_2 + 2H^+ + 2e^- \text{ (eq. 2-11)}$$

$$Fe + HCO_3^- \rightarrow FeCO_3 + H^+ + 2e^- \text{ (eq. 2-12)}$$

$$Fe(OH)_2 + HCO_3^- \rightarrow FeCO_3 + H_2O + OH^- \text{(eq. 2-13)}$$

$$FeCO_3 + HCO_3^- \rightarrow Fe(CO_3)_2^{2-} + H^+ \text{ (eq. 2-14)}$$
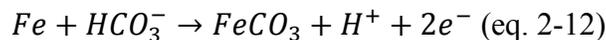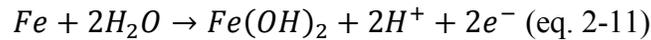
They also proposed that the complex anion $Fe(CO_3)_2^{2-}$ governed the anodic reactions and this complex formed deposited into the pits, which inhibited the corrosion rate of the steel [21].

2.2.3 The Effect of Chloride

Chloride salts are common species in oil sand well but their concentration level and types may vary significantly with different well locations. The effect of chloride groups on pipelines is often

complex as reported. The content of Cl⁻ cannot change the composition of corrosion product films but it assists the breakdown of film since the size of Cl⁻ is small enough to penetrate through the protective film to segregate as clusters between the film and metal interface, which decreases the adhesiveness of the film [20]. The proposed anodic reactions are:

$$Fe + Cl^- + H_2O \rightarrow [FeCl(OH)]_{ad}^- + H^+ + e^- \text{ (eq. 2-15)}$$

$$[FeCl(OH)]_{ad}^- \rightarrow FeClOH + e^- \text{ (eq. 2-16)}$$

$$FeClOH + H^+ \rightarrow Fe^{2+} + Cl^- + H_2O \text{ (eq. 2-17)}$$
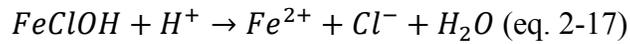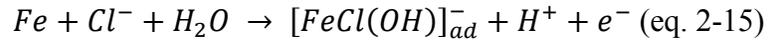
The concentration of NaCl may be up to 3M in some oil reserves [16]. The presence of Cl⁻ always relates to the initiation of pitting corrosion. Liu et al. studied the effects of chloride content on CO_2 corrosion of N80 carbon steel in simulated oil and gas well environments. They concluded that the corrosion rate of N80 in solution with 25 g/mol of Cl⁻ and anions such as Ca^{2+} and Mg^{2+} resulted in a peaked corrosion rate of about 4.0 mm/yr in an environment with 20 bar partial pressure of CO_2. This corrosion rate was about twice of the corrosion rate in the brine without Cl⁻. High level of Cl⁻ , which was larger than 80 g/L, might inhibit the corrosion process since it decreased the solubility of CO_2 in aqueous phase [20].

2.3 Corrosion Protection Methods

2.3.1 Inhibitors

Inhibitors are commonly added into the injected steam to modify the environment in deep well. For example, in the wells in McMurray reserves, oxygen scavenger ammonium bisulfite ($(NH_4)HSO_4$) is added to reduce the corrosion induced by dissolved oxygen. Caustic injection of sodium hydroxide (NaOH) is adapted to increase the pH of environment by reducing the solubility of carbon dioxide in water phase [10]. However, due to the special structure of slotted liners, both

the efficiency and the recovery of the inhibitors are extremely low in this case [22]. Moreover, the inhibitors built up through the operation not only contaminate the basal water, but also significantly lower the quality of oil production. Therefore, inhibitors could not be used as a major corrosion protection method for slotted liners.

2.3.2 Cathodic Protection

Although cathodic protection (CP) for oil well is expensive and difficult to perform in most cases, it is still another avenue to protect the liners by either sacrificing a more active piece of metal to draw corrosion away from the pipe itself (galvanic action) or impress a certain protective current [23]. The CP system for well casing (Figure 2-1) is an impressed current CP system which requires a large active anode bed to protect the well casing [24]. Although CP is a powerful tool to protect the well casing, its efficiency is limited especially at the deep end of the well [25]. Oliphant from Devon Canada tried in determining the current requirement for oil well by using average current density, the E-log test, casing potential profiles and mathematical modeling. He concluded that coated well casings were observed with lower current requirements and better current distribution, which increased the protection efficiency and lowered the operation costs [26]. Therefore, to have a coating as the primary corrosion protection method is necessary for the corrosion protection of slotted liners.
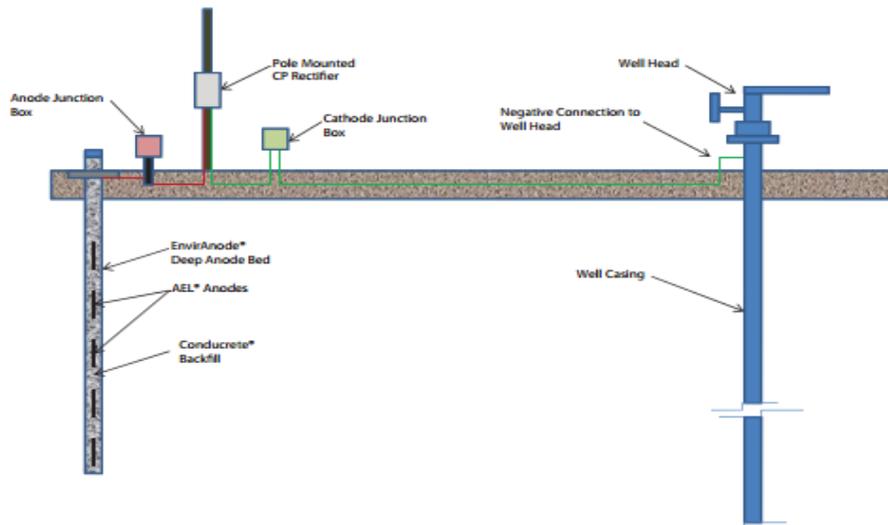
Figure 2-1. The typical cathodic protection system for well casing [24].

2.3.3 Coatings

Coating is the most common method to prevent the external corrosion of oil pipelines by sealing fusion bonded epoxy (FBE) and polyethylene on the outer surface of the pipelines [27]. However, the conventional methods could not be applied on slotted liners because the operation temperature of slotted liners is typical around 250°C, which is higher than the maximum service temperature of FBE. Moreover, the slotted liners require both internal and external coating, but the FBE cannot be evenly applied on the slotted liners with such a complex geometry [27]. Therefore, new methods or improvements must be developed to effectively protect the liners from corrosion. Ceramic coating was our primary candidate since ceramic coating is believed to have both outstanding corrosion and erosion resistance at high temperature. Several researches on various nitriding coating showed promising results in the application in oil industry.

2.3.3.1 Diffusion Coating

Diffusion coating is a heat treatment method to form a corrosion, wear and fatigue resistant coating at the surface of metal or alloy at high temperature. Diffusion coating produces a diffusion zone

with compositional gradient which formed by the chemical reactions between substrate and treatment media. The treatment media could be solid, liquid or gas [28]. Generally, diffusion coating will have better coating adhesion due to the presence of diffusion layer. Therefore, it has higher resistance to the thermal shock induced coating spallation [29]. Moreover, diffusion coating is a well-established and cost-efficient industrial treatment. Therefore, I selected GN as the primary coating candidate for the corrosion protection coating on slotted liners. The researches on the corrosion resistance of nitriding treated alloy will be discussed in sections 2.5 and 2.6.

2.3.4. Other Approaches of Coatings Candidates for Slotted Liners

Beside the GN treatment mentioned in previous sections, the researches on many other coating techniques for the slotted liners are also in progress. For example, EnCana Corporation conducted several tests on the polytetrafluoroethene (PTFE), or so called Teflon^{TM} coating (Figure 2-2) [30], which has a maximum operation temperature above 260℃. Another feature of this material is the "non-sticky" property to oil which results in the mitigation of plugging of solid particles [31, 32]. On the other hand, ceramic coatings are also being investigated due to their inert chemical properties and high strength at high temperatures. Silonite^{TM} coating (Figure 2-3), mainly consists of SiO_2, was also developed by EnTech® especially due to its extremely high resistance in sour corrosion environment [30]. This dense and smooth ultra-thin coating was tested to have outstanding corrosion and wear resistance in many aggressive environment. However, the thermal expansion coefficient of PTFE is more than ten times of the thermal expansion of steel. The disbondment at high temperature due to expansion induced cracks may be a concern for the application of this material [34]. Moreover, silica deposited by hot fusion technique has an intrinsically weak bonding with ferrous material, which may indicate that this coating is more susceptible to coating spallation induced by mechanical forces [35].

Figure 2-2. Teflon^{TM} coated pipes [30].

Figure 2-3. Silonite^{TM} coated parts [33].

2.4 Nitriding Treatment

2.4.1 Gas Nitriding

Gas nitriding (GN), which had been developed since early 1900s, is the most widely applied industrial-scale nitriding method [36]. GN process involves the diffusion of nitrogen into the surface of steels by dissociation of ammonia (NH_3) at 500°C to 580°C. The composition and microstructure of iron nitrides formed on the steel surface in this process are effected by the

controls of nitriding parameters such as the nitriding duration and temperature. "Single-stage" GN, which is the schedule applied in this research, is the simplest GN schedule. It requires lower operation temperatures and forms a shallower nitride-rich layer but with higher hardness and less dimensional distortion. Moreover, GN is the most economic nitriding treatment. Although the drawback of this method is the long treatment duration and low efficiency, it is so far the most industrially favorable nitriding method [36]. GN treated steel with improved chemical and mechanical properties is considered as a promising candidate for the slotted liner of SAGD system; therefore, lab-scale gas nitriding was developed and optimized for the surface treatment of L80 steel in this research.

2.4.2 Salt-bath nitriding

Salt bath nitriding is another industrial-scale nitriding treatment, which was firstly developed as an alternative of gas nitriding. It involves the dissociation of cyanide to cyanate at the same temperature with GN treatment and leads to the liberated nitrogen to be readily diffused into the iron matrix. Compared with GN, salt bath nitriding shortens the process time to less than 10 h but the toxicity of the cyanide salts and its hazardous impact on environment let it fall out of favor for the industrial application in recent decades [36]. Although some of the companies still adopt this method as their primary nitriding method, our lab did not attempt this method for our research by considering the accessibility and toxicity of the raw materials.

2.4.3 Plasma nitriding

Plasma nitriding is the latest nitriding technique, which achieves the nitriding effect by the ionization of nitrogen gas at lower temperature (Figure 2-4). Therefore, this method is also called "glow discharge" nitriding. Plasma nitriding is the most efficient nitriding method; it not only further shortens the process time, but also has the highest precision of properties control. However,

both the capital and operation costs of this technique are much higher than the GN and salt-bath nitriding [36]. This technique cannot be applied to process large pieces. However, most experiments conducted in the lab refer to this technique as their fabrication method. Therefore, their interpretations are only partially adopted as the reference to my research in section 2.6.
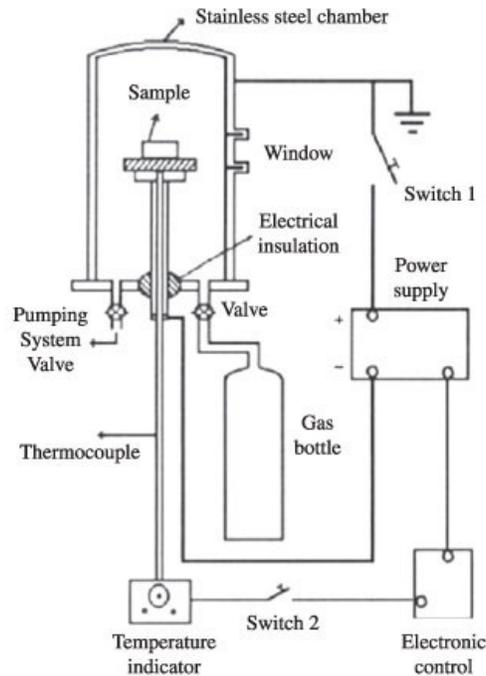
Figure 2-4. The schematic of plasma nitriding [39].

2.5 Gas Nitriding

2.5.1 Mechanism

The GN process usually involves the partially dissociation of ammonia gas at 500°C to 580°C by the following simple reaction:

$$2NH_3 \leftrightarrow 2N + 3H_2 \text{ (eq. 2-18)}$$
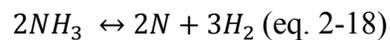
Some of liberated nitrogen atoms recombine into nitrogen gas and flow out with undissociated ammonia and produced hydrogen. The remaining of liberated nitrogen atoms slowly diffuse into the steel at these temperatures (Figure 2-5) to form either face-centered cubic γ' phase, Fe$_4$N,

which dissolves 5.7 to 6.1 wt% N and hexagonal ε phase, Fe$_{2-3}$N, which contains 8 to 11 wt% of

N (Figure 2-6) [36].
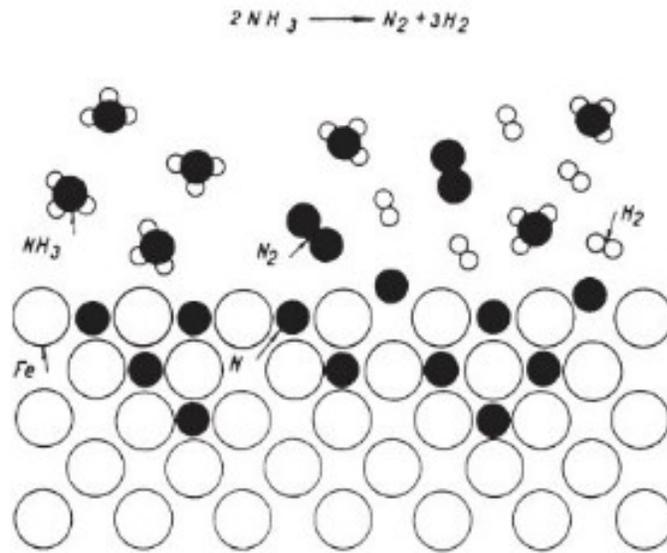
Figure 2-5. The Schematic of ammonia decomposition and nitrogen interstitial diffusion [38]
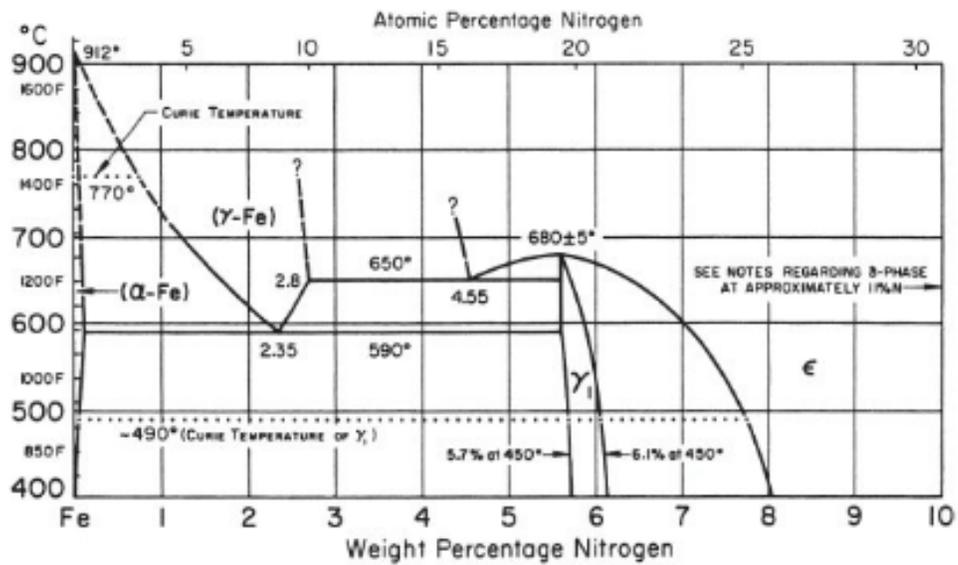
Figure 2-6. Iron-Nitrogen equilibrium diagram [36].

2.5.2 Procedure

Since the industrial-scale GN furnace was not available in this research, I constructed the lab-scale gas nitriding set-up according to the industrial-scale gas nitriding furnace by using a tube furnace as the heating equipment and quartz tube as the gas chamber and sample holder (Figure 2-7). The working gas was the high purity anhydrous ammonia gas. Nitrogen gas was used as the purge gas before the gas nitriding process in order to prevent explosion caused by the mixing of ammonia gas and air, and flushing gas after the gas nitriding in order to remove the ammonia gas from the tube for its irritant smell. The tube furnace was programed based on the "one-stage" gas nitriding schedule (Figure 2-8) since this treatment only have one diffusion stage (Table 2-1). The reason to use this nitriding schedule was because this schedule results in the least specimen deformation [36] which is important to the dimensional uniformity of slotted liners. The gas washing bottle was applied to minimize the discharge of ammonia directly into the atmosphere since the solubility of ammonia is very high (maximum solubility: 700 mL ammonia gas in 1 mL of water at standard atmosphere pressure at 25°C [36]) in water. The GN set-up was placed in the fumehood to prevent gas leaks during the treatment. The industrial-scale (Figure 2-9) GN furnace nowadays has been developed with computer controlled system, which is capable of extremely precise temperature and flowrate control. The industrial GN furnace follows the same principle of the lab set-up but with a stirring fan on the top to ensure the temperature and the uniformity of gases phase (Figure 2-10).
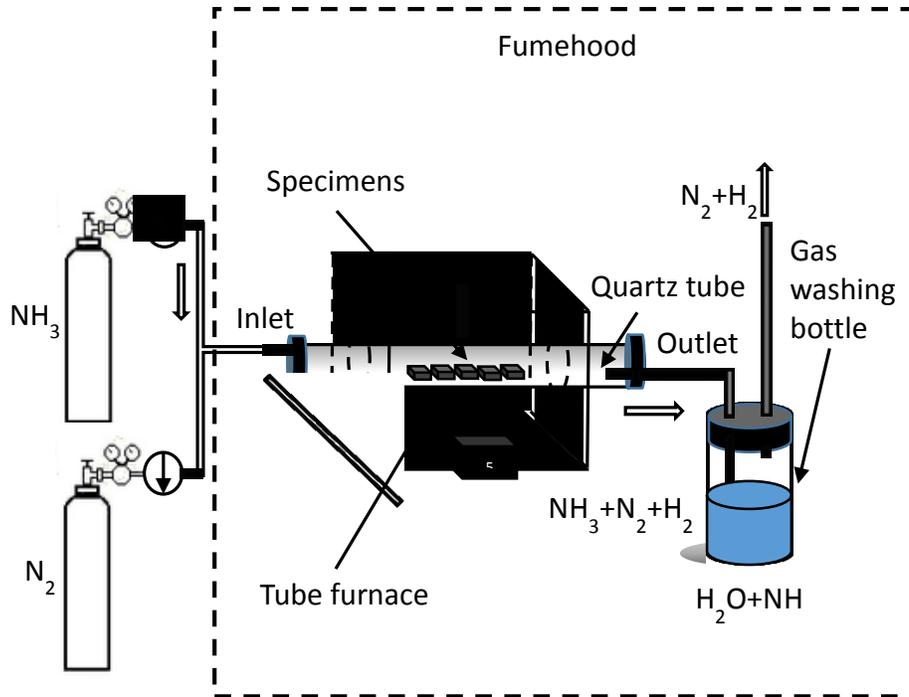
Figure 2-7. The Schematic of lab-scale gas nitriding set up.
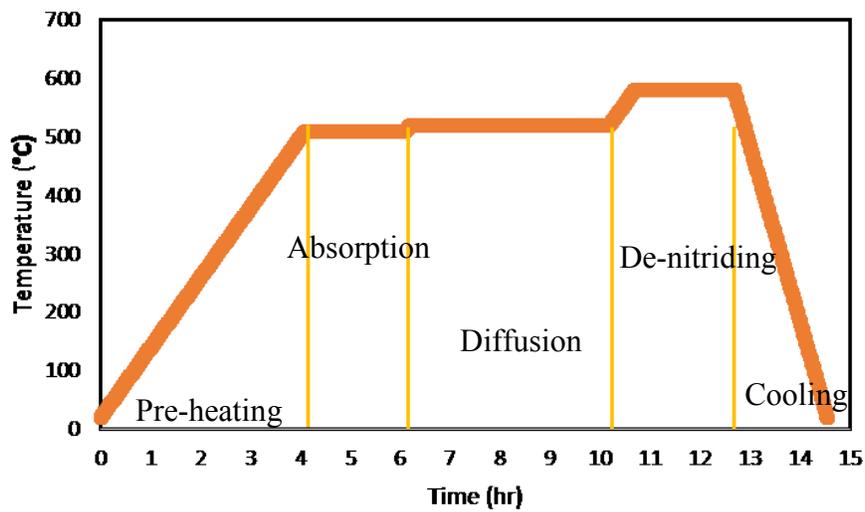
Figure 2-8. The sample time and temperature schedule of a "one-stage" gas nitriding process.

Table 2-1. The purpose of each stages of a "one-stage" gas nitriding process [36].

Stage	Purpose
Pre-heating	To preheat the specimens to nitriding temperature; to allow ammonia expel the nitrogen injected to prevent the mixing of air and ammonia.
Absorption	To allow the dissociated nitrogen steadily and slowly absorbing onto the surface of specimens.
Diffusion	To create a large diffusional layer by increasing the dissociation rate of ammonia and diffusion rate of nitrogen into the core material.
De-nitriding	To decrease the brittleness of surface compound layer by removing the surplus nitrogen from this layer.
Cooling	To cool the temperature of nitrided specimens to room temperature for specimens collection.

Figure 2-9. The industrial-scale "pot-type" gas nitriding furnace [38].
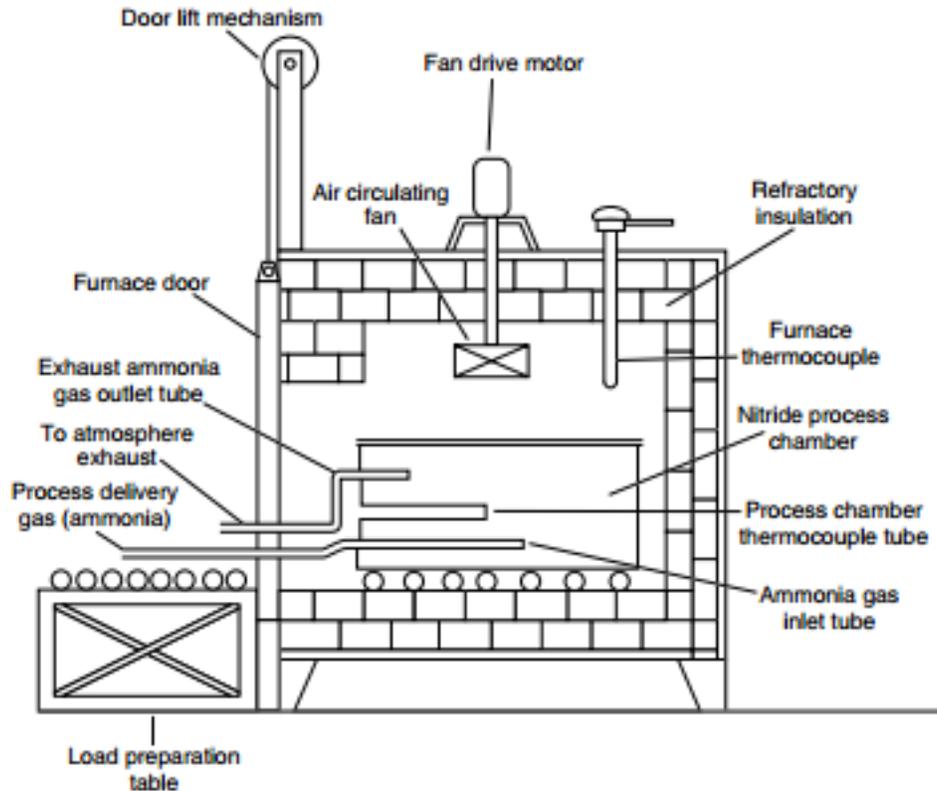
Figure 2-10. The schematic of industrial-scale gas nitriding furnace [36].

2.5.3 Microstructure and Composition

The surface structure of nitriding steel highly depends on the chemical compositions and the nitriding conditions. However, it generally consists of a compound layer with mixture of γ' (Fe_4N) and ε ($Fe_{2-3}N$) and a diffusion zone (Figure 2-11,12), which is the substrate with diffused nitrides [39]. The compound layer with higher hardness and inert chemical properties is the effective layer to resist the corrosion and erosion. The thickness of compound layer is usually around 10 μm but the diffusion zone can extend to 200 μm from the interface of compound layer toward the core of substrate [39]. ε phase is reported with higher corrosion resistance and less brittleness [36]. Therefore, treatment schedule needs to be varied to obtain the ε phase as much as possible. Alloying elements, such as chromium (Cr) and vanadium (V), are beneficial for the nitriding

process since the formation of nitrides zone increases the microhardness of the diffusion layer. Therefore, SS usually forms more complex diffusion layer due to higher amount of alloying elements [36]. Since L80 is a plain carbon steel with very limited amount of alloying elements, the GN process of L80 and expected properties should be similar to those of normal carbon steel.
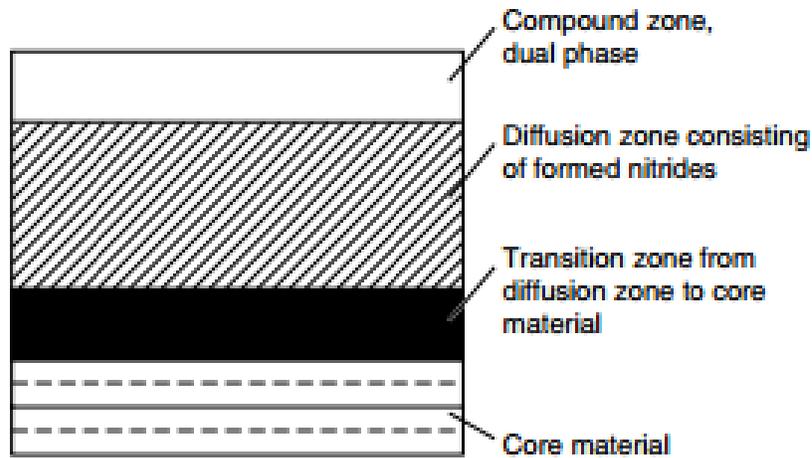
Figure 2-11. Schematic of a typical nitriding treated structure [36].
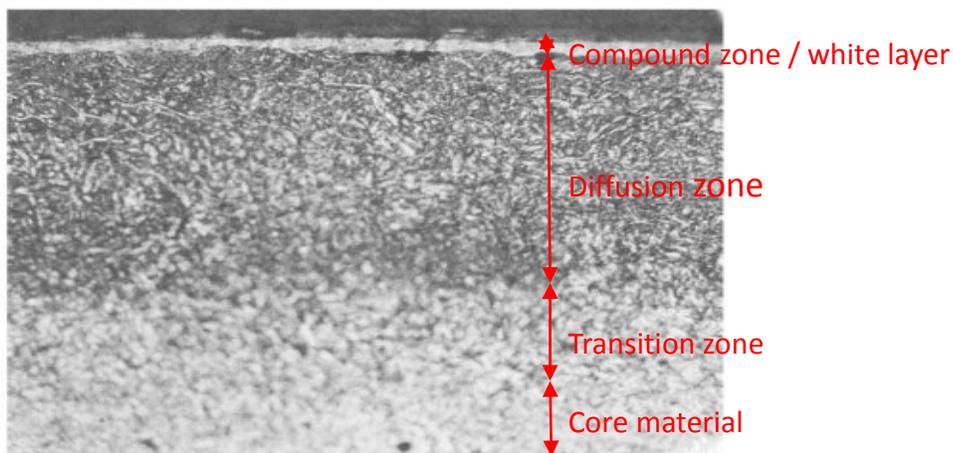
Figure 2-12. The typical microstructure of GN treated specimen [36].

2.5.5 Applications and Advantages

The most commonly known application of GN treated steel is for the hot-work forming tools such as forging dies since this technique significantly increases both the hardness of surface and

diffusion zone (Figure 2-13). The operation environment of GN treated steels are typically as high as 500°C; therefore, nitriding treated steel is thermally stable at high temperature [40]. GN treated steels are also widely used as heavy duty machine components in automotive and aerospace industries due to its high wear resistance. The compound layer is ductile enough to maintain the dimensional stability after long term of service [40]. The corrosion resistance of compound layer also has great potential to be used as anticorrosion nitriding material. One of the examples is the rams for hydraulic systems of excavators working in salt and copper mines [40]. The ram made of 40HM or 18G2A steel as heavy as 320 kg was GN treated in a pit furnace at 570°C for 4 hr. The nitriding ram had successfully withstood the exposure to salt spray exceeding 264 h without signs of corrosion. The corrosion resistance retained even with some point defects detected after years of operation due to the presence of nitride - rich diffusion layer [40]. This application not only indicated that GN treated steels have great resistance to penetration of the aggressive species in solution but also suggested the promising stability of GN treated steels in humid environments.
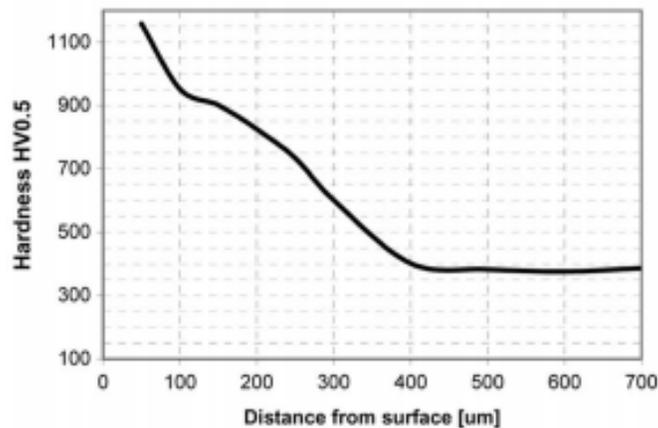
Figure 2-13. The hardness profile across of the 38HMG (Nitralloy 135) [40]

2.5.6 More Advantages

Besides the advantages mentioned in the previous subsection, some other features also allow GN to become one of the most competitive candidates for the application as slotted liners. For the industrial-scale production, the cost-effectiveness of the mass production of large pieces becomes the most crucial factor to determine the feasibility of GN technique. According to the process selection guide for surface hardening process of steels published by American Society for Materials (SM) International in 2002 [41], nitriding method was reported to have the second lowest fabrication cost among 15 most prevalent surface treatments (Figure 2-14). Moreover, unlike the conventional oil transportation pipelines, both internal and external sides of slotted liners are operated in extreme environment; therefore, the selected coating technique must fulfill the demand of applying coating on each exposed surface. GN is capable of applying coating on complex geometry, even on the tiny slots surface since the treatment requires the immersion in the gaseous phase. Lastly, the "non-sticky" property to oil and water of coating is also extremely important to the application on slotted liners. Nitriding treated steel has significantly lowered liquid wettability [42] [43], which may have the potential to minimize the fouling and plugging problems of the slotted liners.
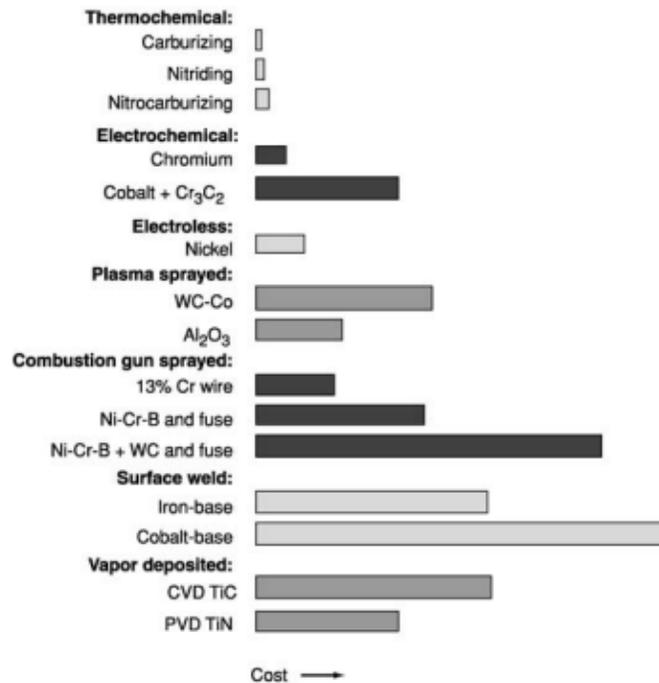
Figure 2-14. Approximate relative costs of various surface treatments [41].

2.6 The Corrosion and Wear Resistance of Nitriding Steels

The excellent wear resistance of GN treated specimens at dry HTHP environment has been proven. However, the corrosion behavior of GN treated carbon steel is not well-studied, especially in CO_2 containing solution because the existing application of gas nitriding steel in humid environment or solution is very limited. Since the water acts as the electrolyte to corrosive species, the operation environment of slotted liners is prone to cause much severer corrosion behavior on GN treated specimens and the driving corrosion mechanisms may be different from the environment without much water. Dr. Bingying Wang's group in China University of Petroleum [44, 45] was working on the effect of CO_2 containing solution on the corrosion behavior of GN treated steels. Their studies were focused on steels with typically higher amount of Cr content than L80, which has no Cr in the matrix. Since the chromium nitride has higher corrosion resistance than iron nitride, to directly use their results to predict the corrosion mechanism and behavior of L80 carbon steel in

27

the simulated environment of slotted liners is not reliable. Furthermore, they did not report any stability tests, which is essential to the characterization of coating performance in extreme environment. Therefore, the GN schedules for L80 were optimized in this research for long term uses in the simulated environment of slotted liners.

2.6.1 The Sweet Corrosion of Nitriding Steels

Wang et al. [44] carried a series of corrosion and wear resistance tests on GN treated steels. Significant increases of hardness from 275 HV (substrate) to 675 HV (compound layer) were observed for the 40Cr steel GN treated in ammonia at 550°C for 10 hrs. The gradual change of hardness resulted from the formation of diffusion layer ensures the firm bond between the nitride rich layer and substrate. The SEM results of 40Cr steel after 10 h of GN treatment showed that their treatment tended forming finer, more compact and ordered scale of corrosion product $FeCO_3$ in 3.5% NaCl solution with 80 psi CO_2 pressure at 60°C. The weight loss experiment suggested a decreased corrosion rate from 9.929 mg/m^2 ·h of untreated specimen to 7.555 mg/m^2 ·h (GN treated). However, they only compared the corrosion resistance of the effect on nitriding duration by doing electrochemical tests on GN steel treated for 2 h and 10 h. The typical industrial application of gas nitriding treatment is usually much longer than 10 h [36]. Therefore, I doubt that with such a short nitriding time, the formation of a surface nitrides layer would not be compact enough to characterize the effects of nitriding layer. Moreover, they did not investigate the relationship between nitriding duration to the corrosion resistance. Only two nitriding durations could not suggest a reliable relation between the nitriding duration to the corrosion resistance of nitriding steel.

Wang et al. [45] also observed that the corrosion potential of gas nitriding treated Cr40 steel was elevated from -599.0 mV vs. SCE (untreated) to -265.9 mV vs. SCE (GN treated for 10 h) in the

same solution with 3.5 wt% NaCl and 80 psi CO_2 at 30 °C. The corrosion current significantly decreased from 42.68 $\mu A/cm^2$ to 8.550 $\mu A/cm^2$, which indicated a great drop of corrosion rate in this environment. The passivation region of GN treated specimen showed great corrosion inhibition effect. By contrast, the Cr40 steel without GN treatment tends to active dissolution. These electrochemical results indicated GN steel was a promising corrosion resistant material in a CO_2 containing solution. However, a single value of corrosion rate and a potentiodynamic curve cannot determine the corrosion behavior of GN treated L80. Therefore, I decided to take an insight of the corrosion behavior of GN treated L80 in CO_2 containing environment by using equivalent circuit modeling for the EIS tests.

According to another research by Wang et al. on 35CrMo [46], nitriding steels were also reported with better anchoring effect on the corrosion products deposited on the surface to further inhibit the sweet corrosion. Unlike the loosely attached porous corrosion products obtained from the sweet corrosion on carbon steel in CO_2 environment, the corrosion product $FeCO_3$ deposited on nitriding steel was observed with fine and compact crystalline morphology. This greatly enhanced property suggested that the nitriding layer retained the protection effect by the deposition of compact corrosion products even with a slight degree of coating degradation. It is an important property for the long term service of GN treated steel in the real operation environment. Therefore, a series of stability tests were designed to verify these observations of corrosion product depositions in my research.

Liu [47] studied the corrosion resistance of nitriding treated 45 steel in the CO_2 containing produced water from oil well. He reported that the corrosion current increased with the decreases of pH of solution by varying the amount of CO_2 dissolved; however, the corrosion current increased with the increase of temperature even when the solubility of CO_2 in the solution dropped

significantly. These results suggested that the effect of CO_2 may not be an issue at the operation temperature of slotted liners because the corrosion mechanism at high temperature was not dominated by the sweet corrosion mechanism. However, the corrosion mechanism of nitriding steels might significantly vary in the HPHT environment since the high pressure dramatically increases the solubility of CO_2 in water. Therefore, further researches on the corrosion resistance of GN treated steel applied as slotted liners should also be conducted at HPHT environment.

2.6.2 The Effect of Alloy Elements on Nitriding in Acidic Environment

Generally, the presence of alloy elements increases the corrosion resistances of nitriding steels due to the formation of complex nitrides [36]. For example, Chen et al. [48] tested the corrosion resistance of GN treated Fe-9.0Al-30Mn-1.8C alloy at 550 °C for 4 h in 10% HCl solution. The pitting potential of this treated alloy in this environment shifts from -750 mV vs SCE to +30 mV vs. SCE. The corrosion current was approximately three orders of magnitude smaller than the untreated alloy in the same environment. Moreover, only nano-sized pits were observed after the immersion test after 24 h. This observation suggested GN treated alloy had significantly increased corrosion resistance and stability in acidic solution. However, since this alloy contained about 9 wt% of Al, this allows the co-formation of Al-N and Fe-N as the nitrides group in the compound layer. By contrast, L80 has limited types and amount of alloy elements. Therefore, this strong inhibition effect reported from Chen et al. might not be observed on GN treated L80. Most researches were conducted on alloys with various alloying elements. Therefore, the electrochemical tests should be conducted exclusively on GN treated L80 to predict the corrosion resistance of it in the simulated environment.

2.6.3 The Effect of Cl- on Nitriding Steels

Most of the corrosion tests on nitriding steels were conducted in solutions containing NaCl. Cl- has very well-known detrimental effects on the penetration and breakdown of passive layer [20]. Therefore, the penetration and segregation of Cl- in the interface between compound layer and diffusion layer may result in localized corrosion and coating spallation. Fortunately, most of the literature revealed that GN treated steels have outstanding resistance to the penetration of Cl-. Yeh et al. [49] conducted series of tests on corrosion behaviors of GN SACM 645 steel at 530°C for several different nitriding duration. They reported that the corrosion current density of GN treated SACM 645 for 12 h tested in 3.5 wt% NaCl solution decreased form 1.0×10^{-5} A/cm^2 to 3.0×10^{-7} A/cm^2. They explained that the decrease of corrosion current density was because Cl- neither reacted nor penetrated through the nitride layer to react with substrate. However, it could diffuse through the opening crack of compound layer to react with the substrate. Therefore, the corrosion resistances of nitriding steels obtained were determined by the composition and microstructure of substrates [50]. This finding addressed the importance of the compactness of compound layer since the fact that the corrosion of substrate L80 is severe in this environment. Therefore, the problem that I strived to solve was to decrease the surface defects by continuously optimizing the treatment schedules.

2.6.4 Improvement on Corrosion and Wear Resistance by Other Nitriding Methods

Since GN is difficult to be directly conducted in most institutes due to the large volume of the equipment, most researches on the corrosion behavior of nitriding material were conducted by using the most innovative plasma nitriding method. Niu et al. [51] conducted the electrochemical tests on MG400 steel nitrided by laser 450 plasma nitriding technique in the ground water simulation solution. The corrosion current density tested in this environment was as low as

8.10×10^{-6} A/cm^2 which was about five times lower than that of the MG400 steel in the same environment. MG400 steel had the similar chemical composition with L80; therefore, the same magnitude of corrosion current might be expected for GN treated L80 in similar environment. However, since plasma nitriding generally produces more compact compound layer with less defects [36], a slightly lager current density should be expected for GN treated L80 in the similar environment.

Tang et al. [52] researched on the nitriding temperature effects on the 30CrMnSiA steel by using plasma nitriding. They discovered that nitrides formed at lower temperature (400°C - 500°C) mainly consist of ε phase (Fe$_{2-3}$N), which had higher wear and corrosion resistance in 3.5% NaCl solution than γ' phase (Fe$_4$N) formed at higher temperature (above 560°C). However, the lower nitriding temperature (400°C) resulted in much thinner compound layer (2 μm) than the compound layer (8 μm) of steel nitrided at higher temperature (500°C). The thin compound layer was highly susceptible to spallation during the operation. Moreover, their surface characterization also suggested that roughened surface finish was found on sample nitrided at higher temperature. Roughened surface was not beneficial for the inhibition of fouling and plugging of slotted liners. Therefore, this research provided me the clues on deciding the optimal nitriding temperatures range for my nitriding treatment.

Salt bath nitriding as another common nitriding technique is also used in the investigation of the corrosion resistance of nitriding steel. Almeida et al. [53] compared the corrosion resistance of AISI H13, AISI P20 and N-8550 treated by using salt bath nitriding, GN and plasma nitriding at 560°C. They report that salt bath nitriding by using Fe$_4$KCN as working media showed the best wear resistance since the nitrocaburization process promoted the formation of a compound layer with carbonitrides and carbides. The complex growth structure of various nitrides boosted the

microhardness of the surface. However, they did not carry out the corrosion tests on the treated specimens. According to the researches on the corrosion resistance of iron nitride and iron carbide from Weber et al. [54], they reported that the corrosion resistance of γ' phase iron nitride was two times better than the corrosion resistance of iron carbide tested in the same environment since iron nitrides generally formed a more dense and closed layer. Therefore, the corrosion resistance of salt bath nitriding steel might be lower than the corrosion resistance of the nitriding steels treated by other methods.

2.6.5 Wear Resistance of Nitriding Steel

The wear resistance of nitriding steel is a well-studied property since GN treated steels have been widely applied as heavy duty tooling parts [40]. Wang et al. [44] performed mill tests by using a MG-200 high speed friction and wear testing machine. They observed that the Cr40 steel after 10 h of GN treatment had higher micro-hardness of the diffusion layers since the nitrides that precipitated between the grain boundaries distort the lattice to increase the resistance to deformation. The presence of diffusion layer was important to the slotted liners since the diffusion layer had much higher hardness compared with the substrate (Figure 2-15). This layer with about 200 μm of thickness retained a high hardness even after the top compound layer was worn off or chipped off during long time of service. The wear resistance of GN treated steels is not emphasized in this research, but it is planned in the future work to complete the study of the erosion resistance of GN treated steel in the simulated environment.
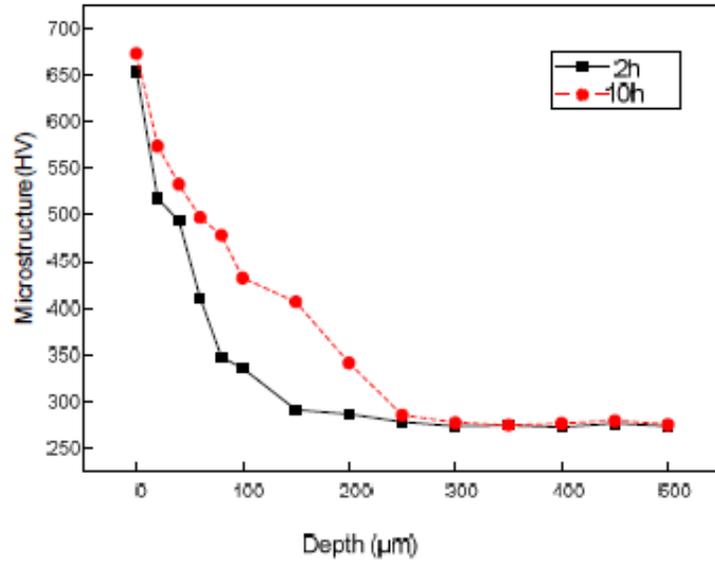
Figure 2-15. The hardness depth profile of the GN steel for 2 h and 10 h [44].

Chapter 3. Techniques

3.1 Electrochemical Tests

3.1.1 Three-Electrode Cell

Three-electrode cell is one of the most commonly used electrochemical setup for corrosion tests.

The electrode of interest, which is named working electrode (WE), acts as the anode of the reaction.

The potential of WE is measured with respect to the reference electrode (RE), which provides a

constant potential E_{ref} to be compared with the measured potential of WE in different tests. The

RE used in my research is Ag/AgCl in saturated KCl electrode, which has a constant potential of

0.199 V at 298.15 K, because it is thermally stable even when used at a temperature as high as

80°C. A platinum (Pt) plate is used as the counter electrode (CE) which allows the transfer of

current. It functions as a cathode to WE to provide a circuit for current to be measured [55, 56].
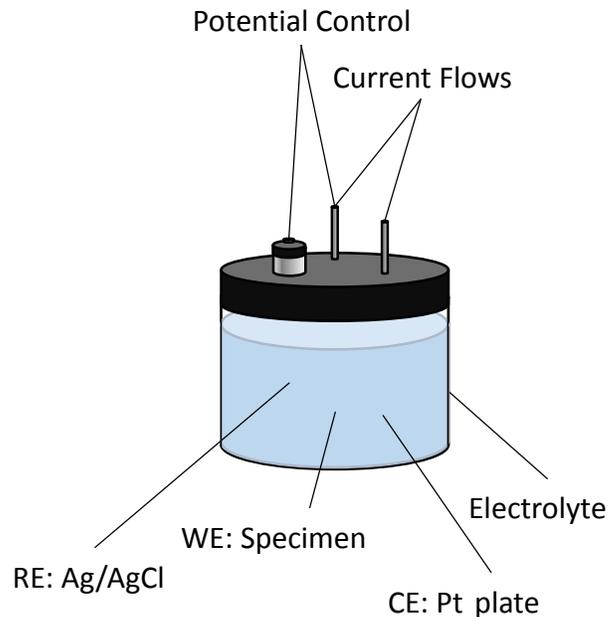
Figure 3-1. The Schematic of a three-electrode cell setup.

3.1.2 Electrochemical Impedance Spectroscopy

3.1.2.1 Bode and Nyquist Plots

Electrochemical impedance spectroscopy (EIS) is a non-destructive test which is used to measure the resistivity and capacity of specimen by collecting the current response to the alternative current (AC) potential signal at different applied frequencies. It is a widely used standardized characterization technique for electrochemical tests. The fluctuations reveal the chemical reactions undergoing [57]. Impedance (Z) or resistance (R) is the ability of a circuit to resist the flow of current in response to an AC. The total impedance of the system can be expressed as equation 3-1, where Z_{re} denotes the real component of the impedance and Z_{im} represents the imaginary part of the impendence. With the Z_{re} on x-axis and Z_{im} on y-axis, the vector $|Z|$ can be calculated [58]. EIS data may be presented as a Bode plot (Figure 3-2) or a Nyquist plot (Figure 3-3). The Bode plots examine the dependence of the impedance or phase angle (θ) on the frequency. On the other hand, the Nyquist plot is a more popular representation of the EIS data. These plots directly compare the impedance of different tests conducted separately. Both of the plots are used to interpret the corrosion behavior of the specimens tested in the simulated environment in this research [58].

$$|Z| = Z_{re} + Z_{im} \quad \text{(eq. 3-1)}$$
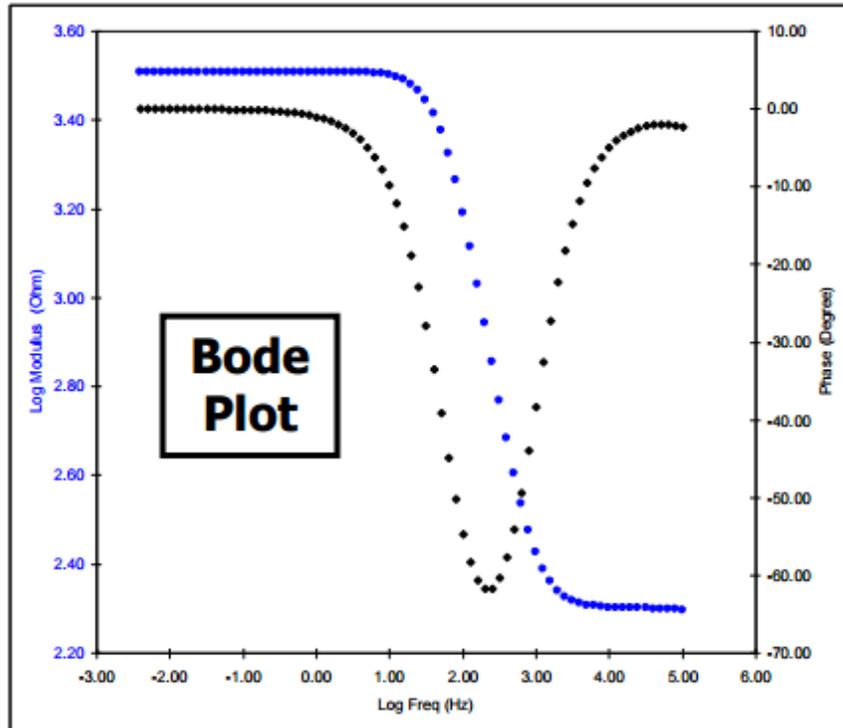
Figure 3-2. A typical Impedance Bode plot [58]
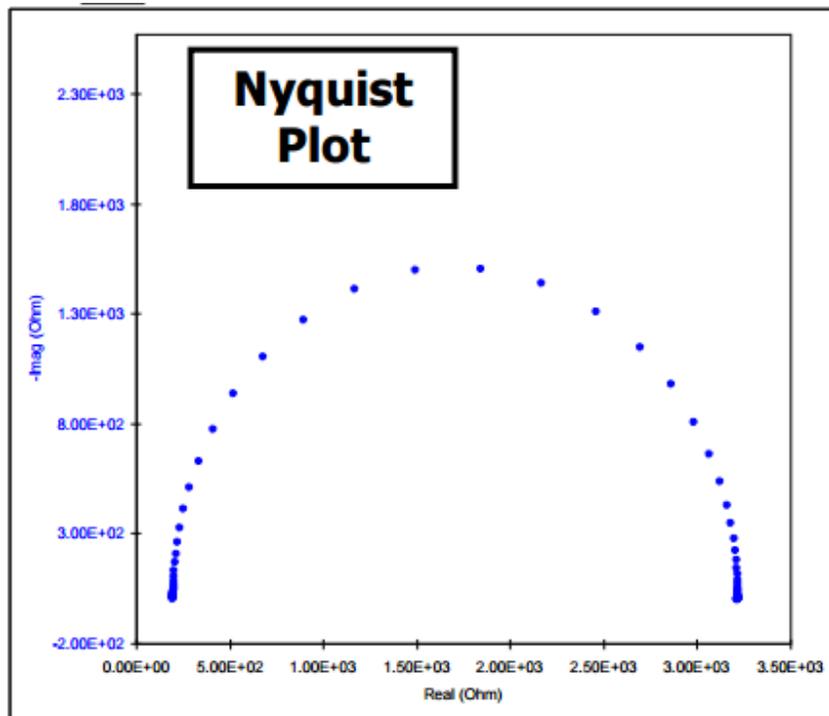
Figure 3-3. A typical Nyquist plot [58]

3.1.2.2 Equivalent Circuit

Besides the Bode and Nyquist plots, the data of EIS measurement can be interpreted by using electrical circuit elements called equivalent circuit (EC) modeling [59]. Most of the circuit elements in the model are common electrical elements such as resistors, capacitors, and inductors (Table 3-1).

Table 3-1. The common electrical elements for EC model [59].

Component	Current vs. Potential	Impedance
Resistor	E= IR	$Z = R$
Inductor	E = L di/dt	$Z = j\omega L$
Capacitor	I = C dE/dt	$Z = 1/j\omega C$

Z, impedance (R), is the resistance of current. The total impedance of the system is the sum of R and capacitance (C, farads), shown by eq. 3-2.

$$Z(\omega) = R + \frac{1}{j\omega C} \text{ (eq. 3-2)}$$

The time constant τ, in s, calculated by multiplying the impedance of resistor and capacitor (eq. 3-3), measures the accumulation of charge at the interface,

$$\tau = RC \text{ (eq. 3-3)}$$

Two EC models were applied in this research. Randles cell is for the EIS data of L80 tested in the simulated environment. The schematic of equivalent circuit (Figure 3-4) consists of three parts: a

resistor R_s, which stands for the resistance to current flow in solution, and a resistor R_p, which stands for the resistance of the surface to solution interface; and the capacitance C_{dl}, or the charge storage capacity, of the surface.
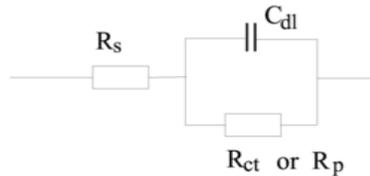
Figure 3-4. The schematic diagram of a simplified Randles cell [59].

The other model used is a commonly accepted model for a porous coating on an active metal (Figure 3-5). The capacitance of the coating, repressed by C_c, is usually smaller than the double layer capacitance (C_{dl}). The pore resistance (R_{po}) is the resistance of ionic conduction passing the pores of the coating, and the R_{ct} represents the resistance of the coating [59-61].
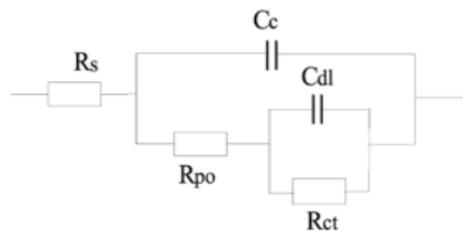
Figure 3-5. The schematic diagram of a coating system [59].

3.1.3 Polarization Curves

3.1.3.1 Potentiodynamic Polarization

The potentiodynamic polarization curve is one of the most commonly used methods to examine the corrosion behavior of a system by plotting potential (E) versus log current (I). This technique records the change of current with respect to the potential versus the reference electrode applied.

Free corrosion potential (E_{corr}) and free corrosion current (I_{corr}) are obtained by the Tafel extrapolation within ± 25 mV versus reference electrode of anodic polarization curve and cathodic polarization curve (Figure 3-6) [62]. Most active alloys, like the carbon steel, exhibit dynamic dissolution in some environments by showing a continuous increase of current with respect to the increase of potential, but some materials may have a passive region, shown in Figure 3-7, the inhibition effect within a range of potential applied is shown by a small and stable current generation [62]. A good coating should have a small I_{corr} and more positive E_{corr} in a test environment. The presence or formation of passive zone is also essential for a coating system.
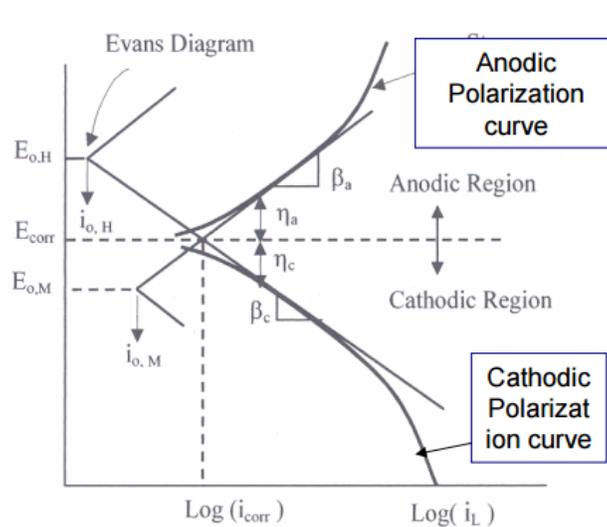
Figure 3-6. The Tafel extrapolation to estimate the I_{corr} and E_{corr} of the potentiodynamic polarization curves [62].
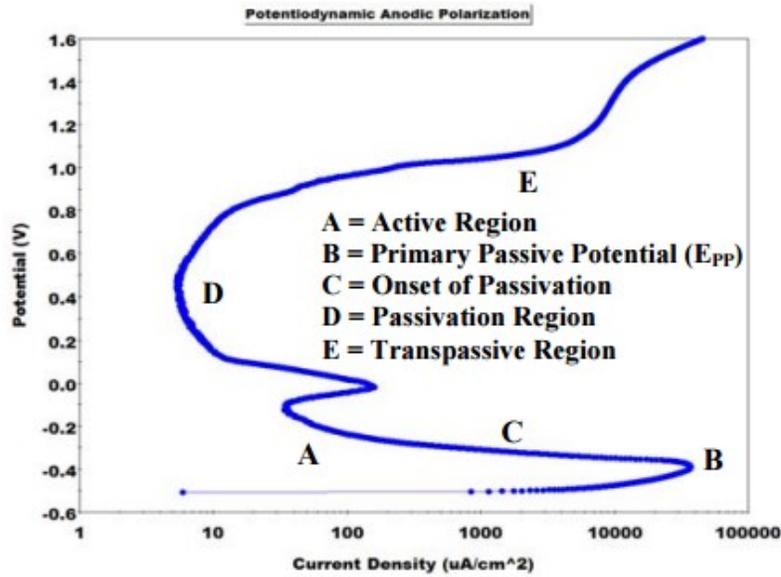
Figure 3-7. A standard potentiodynamic anodic polarization plot of 430 SS [63].

3.1.3.2 Corrosion Rate

The potentiodynamic polarization test measures the corrosion rate, usually expressed in mm/year. The I_{corr} can be calculated by equation 3-4 [63],

$$I_{corr} = \frac{\beta_A \beta_C}{2.3(\beta_A + \beta_C)} \frac{\Delta i}{\Delta E} \text{ (eq. 3-4)}$$

$\frac{\Delta i}{\Delta E}$ = reciprocal of the slope of the linear polarization,

β_A, β_C = anodic and cathodic Tafel constants,

I_{corr} = corrosion current density in $\mu A/cm^2$.

Then, the corrosion rate can be calculated by using equation 3-15 [63],

$$Corrosion\ Rate\ (mm/year) = \frac{3.27 \times 10^{-3} I_{corr}(E.W.)}{d} \text{ (eq. 3-5)}$$

E.W. = equivalent weight of the working electrode (g),

d = density of the corroding species (g/cm2),

I_{corr}= corrosion current density ($\mu A/cm2$).

This calculated corrosion rate can predict the real corrosion rate of the material in its operating environment.

3.1.4 Potentiostatic Polarization

The potentiostatic polarization test collects the current generated with respect to the time at a constantly applied potential to observe the electrochemical performance of a system [63]. The fluctuation and tendency of current density indicate the stability of the tested specimen within a period of time. A good coating should maintain a small current generation with small fluctuation within a long time period. This technique was used to determine the electrochemical behavior of the specimen in simulated environment in this research.

3.2 Surface Characterization

3.2.1 Microscopy

Digital microscopes (DM) and scanning electron microscope (SEM) were two microscopies employed to provide highly magnified images of the specimen for the surface microstructure and morphology analysis in this research. Optical microscope magnifies the image of small sample by using visible light and a series of lenses (Figure 3-8). Digital microscope, which is the combination of an optical microscope and a camera, allows the capture and measurement of images with magnifications up to 1000X [64]. This technique is perfect to measure the thickness of the compound layer but the surface morphology is analyzed by using SEM. SEM uses an electron beam to excite the surface of sample to emit electrons and photons, which are collected by the secondary electron or backscatter detectors (Figure 3-9). Secondary electron detector was used in this research since this detector provides nm-scale resolution images, which facilitated the morphology analysis of my specimens [65].
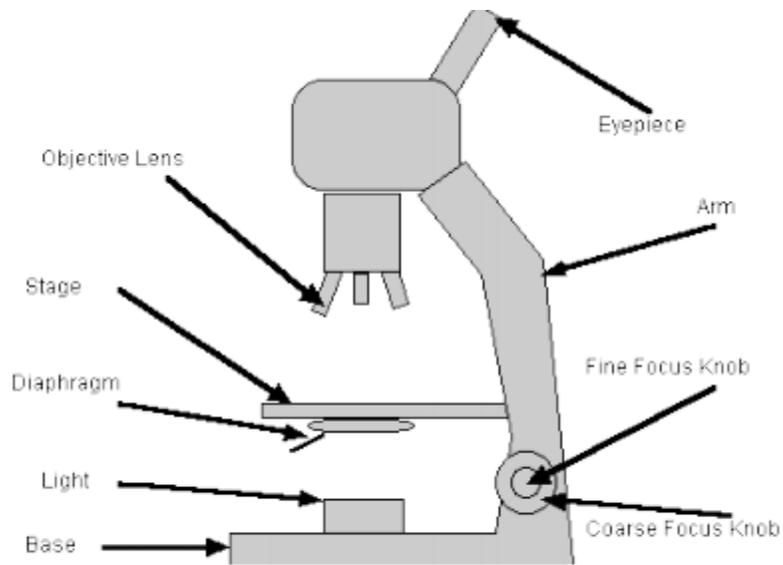
Figure 3-8. The schematic setup of an optical microscope [64].
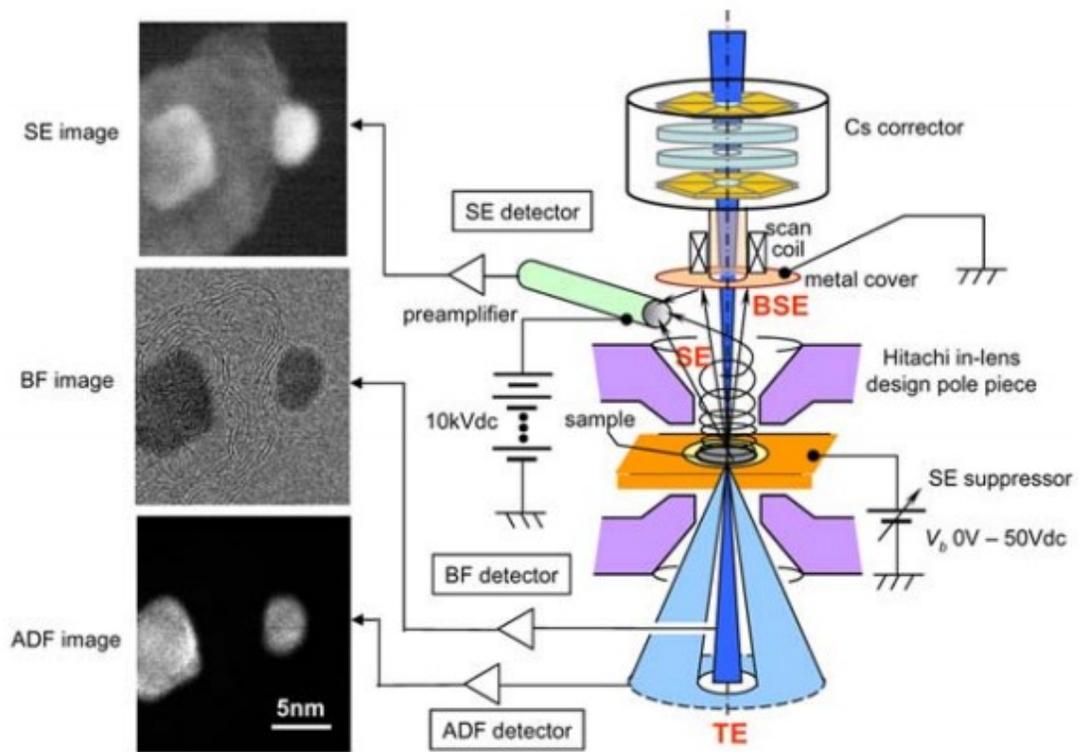
Figure 3-9. The schematic setup of SEM [65].

3.2.2 Energy-Dispersive X-ray Spectroscopy

Energy-Dispersive x-ray spectroscopy is a detector that can be coupled with SEM to identify the compositional distribution and elementary abundance of the sample. This detector captures the energy released by filling the inner shell electrons to the vacancies left by the excitement of outer shell electrons. This technique produces EDX spectrum with intensity peaks of different elements [66]. The EDX spectrum and composition calculation were used to determine the compositions of the nitriding specimens before and after the immersion tests in this research.

3.2.3 X-ray Diffraction

Compared with EDX, X-ray diffraction (XRD) provides a more precise compositional analysis of the compound. X-rays are emitted by the bombardment of metal target on the sample. The incident beam ionizes the electrons from the outer most shell and the detector captures signal to identify the "foot print", lattice spacing d, of each material by using Bragg Equation (eq. 3-4) [67].

$$n\lambda = 2d\sin\theta \text{ (eq. 3-4)}$$

n = positive order integer,

λ = wavelength of incident wave, nm,

d = lattice spacing, nm,

θ = incident angle, °,

Each compound has it unique and identical diffraction pattern, which can be used to determine the composition of a complex material. Both bulk and thin-film XRD modes were used to reveal the compositions of substrate and coating layer in this research.

Chapter 4.The Optimization of Gas Nitriding Schedule

The nitriding schedules for L80 carbon steel were optimized in this chapter in order to obtain a GN treated L80 specimen with the best corrosion resistance in the simulated environment. The optimization of nitriding process is a tedious process since the formation of nitrides layer depends on various factors, such as the sample pretreatment, the composition of substrate, nitriding duration, nitriding temperature, ammonia flowrate, gas pressure etc. The nitriding schedule should always be modified based on the properties of the material treated to fulfill different application purposes. In this research, three factors, nitriding duration, temperature and ammonia flowrate were selected to optimize the nitriding schedule to produce a highly corrosion resistant nitrides layer on L80 substrate. The morphologies of nitrides layers and the corrosion resistances of specimens treated with different schedules will be compared and studied in this chapter.

4.1 Experimental Procedure

4.1.1 Gas Nitriding of L80

4.1.1.1 Sample Preparation

L80 (Table 4-1) specimens were cut from as-received plate with 1.00 cm × 1.00 cm × 0.15 cm dimensions. A square surface was polished with 240, 400, 600, 800 and 1200 grid LECO silicon carbide sand papers, respectively. Then, the samples were further polished by using LECO polish cloth with 1.0 μm Buehler alumina micropolish powder (standard polishing procedure). The polished L80 specimens were preserved in acetone to prevent corrosion and the formation of an oxides layer. The polished samples were rinsed with acetone, ethanol and deionized water for 5 min in ultrasound water bath respectively (standard rinsing procedure). The rinsed samples were dried by pressurized air flow at room temperature and kept dry in sample bag before the gas nitriding process. All the chemicals used in this process were analytical grade reagents.

Table 4-1. The chemical compositions of L80 [68].

	C	Mn	Cr	Ni	Cu	S	Si	Fe
Max	0.430	1.900	-	0.250	0.030	0.030	0.450	Balanced

4.1.1.2 Gas Nitriding

Firstly, water was used to clean and dry both inside and outside of the quartz tube and its cap especially the parts around the opening. The specimens were placed inside an alumina tray inside the quartz tube as near as possible to the center. No more than eight specimens were placed in the tube each time since overlay of samples was not allowed. The polished surfaces of specimens were placed upward to ensure the largest contact volume with gaseous phase. After the specimens had been properly placed in the tube, the quartz cap was sealed tightly. The tube was placed in the Thermolyne 79300 tube furnace (Figure 4-1) by lifting its front latch. The center of the tube was placed right below the temperature sensor for temperature accuracy. The sealing of cap and connections must be double checked since the cap and connections might loosen during the movement of tube. The furnace latch was closed. The furnace and gas washing bottle were placed inside the fumehood. All the pipes were connected as shown in Figure 2-7.
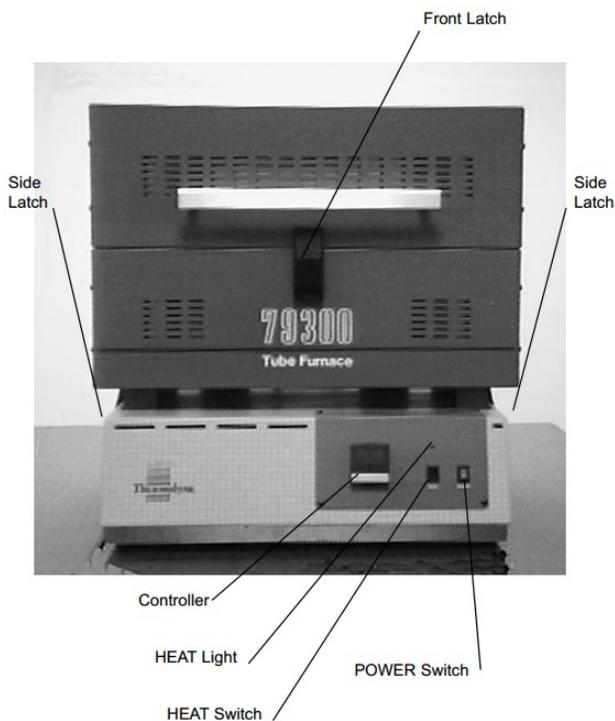
Figure 4-1. Thermolyne 79300 tube furnace [69].

When the tube was sealed and the furnace was closed, set the flowrate of nitrogen gas (99.9999% purity, Praxair) to 1000 mL/min at a pressure of 20 psi. A small amount of soapy water was sprayed onto all the connection parts. If bubbles were observed, the leak source were tighten or sealed and the leak test was carried again until no leak source was detected. The nitrogen gas flow was set for more than 10 minutes before introducing the ammonia gas. The controller of the furnace was programed for the heating process. Before shutting down the nitrogen gas flow, the anhydrous ammonia (99.995% purity, Praxair) was introduced to the quartz tube at the designed flowrate with a pressure of 20 psi.

When the furnace cooled below 120°C, nitrogen gas (99.9999% purity, Praxair) was introduced at a flowrate of 1000 mL/min and 20 psi pressure into the quartz tube for 10 min. The ammonia gas supply was shut down after introducing nitrogen gas. When the furnace cooled to room

temperature, the latch of the furnace could be opened and the quartz tube was taken out. Nitrided samples were removed carefully form the tube.

4.1.1.3 Sample Post-Treatment

A group of nitrided specimens was used for the electrochemical tests. The back side of the nitriding surface was welded with 1/24' 062-60/40 Canada Metal soldering wire by using Weller WLC 100™ soldering station. The sealing agent used was the West System epoxy resin 205™. All the sides were sealed with epoxy resin except a nitriding surface with an average exposure area of 0.85 cm^2. Before each electrochemical experiment, sealed specimens were rinsed following the standard rinsing procedure. The other group of nitrided specimens were directly sealed inside the epoxy resin without the welding procedure. A 1.00 cm × 0.15 cm surface (cross-section) area was polished by the standard polishing procedure. The polished cross-section after the standard rinsing procedure was etched with Nital solution (5 wt% nitric acid in ethanol) for 15 s. After the etching, the etched cross-section was rinsed by deionized water and air dried for observation by using DM. The L80 without nitriding treatments was directly welded with wire, polished with standard polishing procedure, sealed with epoxy, rinsed by standard procedure and dried for the electrochemical tests.

4.1.2 Solution Preparation

The composition of standard simulated solution used in this research was listed in Table 4-2. All the chemicals used were reagent grade. If not specially stated, all the tests used this standard solution for the simulated solution.

Table 4-2. The composition of standard simulated solution.

NaCl (g)	$NaHCO_3$ (g)	Deionized water (L)
58.44	0.84	1.00

4.1.3 Electrochemical Tests

The electrochemical tests used the three-electrode cell shown in figure 4-2. The WE was the GN treated L80, the RE was the Accun.et® Cat.313-6 Ag/AgCl in saturated KCl solution, and the CE was a Pt plate. N_2 was pumped into the container with 200 mL simulated solution with a flow rate of 500 mL/min at an inlet pressure of 20 psi for the deaeration of the solution for 15 min. After the deaeration, CO_2 was pumped into the simulated solution at 20 mL/min and 20 psi before the test for at least 30 min to ensure the saturation of CO_2. All three electrodes connected to the electrochemical workstation Gamry reference 3000^{TM} potentiostat well. The specimen, rinsed by standard rinsing procedure and air dried right before each test, was immersed into the solution 30 min before the EIS for stabilization. EIS measurements were performed at the free corrosion potential with a 10 mV amplitude signal and a range of applied frequencies from 100 kHz to 0.01 Hz. The initial delay for the open circuit potential measurement was set to be 30 min. Potentiodynamic polarization is a surface destructive measurement; therefore, it was applied after EIS measurement by sweeping the potential with a constant rate of 1 mV/s from -800 mV vs. Ag/AgCl to 1500 mV/s vs. Ag/AgCl or ceased when the current generated was larger than 30mA. The test data were collected by using Gamry Instruments Framework 5.58a and analyzed by using Gamry Echem Analyst 5.58. At least five times of electrochemical tests were carried out for each nitriding schedule to ensure the reliability of the data.
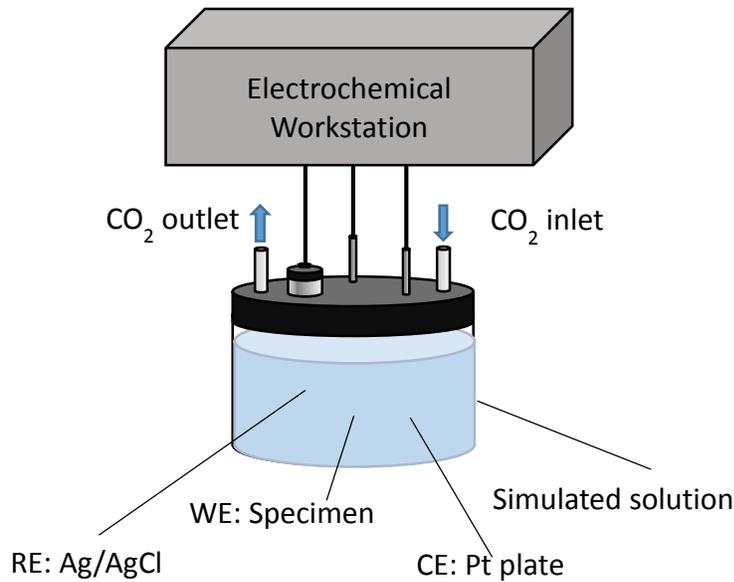
Figure 4-2. The schematic of three-electrode cell for specimens immersed in standard simulated solution with saturated CO_2 at 20°C, 1 atm.

4.1.4 Surface Characterization

The sealed and etched cross-section of GN treated L80 was observed by using Keyence VH-Z100R DM. The images of cross-section at magnifications of 400X and 1000X were taken for the comparison of the thickness of compound and diffusional layers. The tested specimens were rinsed by the standard rinsing process before and after the electrochemical tests.

4.2 Optimization of Nitriding Duration

Nitriding duration can influence the formation of nitrides layer and the electrochemical properties of the nitriding specimen. The optimization of nitriding duration selected three time durations, 8 h, 12 h, and 16 h, based on the literature and my preliminary optimization process (Table 4-3) [36, 44, 45]. A group of eight samples were GN treated with either schedule. Each schedule was performed at least three times. A schedule with optimized nitriding duration which produces the most corrosion resistant nitrides layer were selected and studied in this section.

Table 4-3. The matrix of optimization of nitriding duration.

	Schedule (#)	Duration (h)	Temperature (°C)	Flowrate (mL/min)
The Effect of **Nitriding Duration**	D1	**8**	530	40
	D2	**12**	530	40
	D3	**16**	530	40

4.2.1 Surface Characterization

To seal the nitriding specimen in epoxy was to prevent the error of compound layer thickness produced by non-uniform polishing. The cross-section images of GN treated L80 treated with different nitriding duration are shown in Figure 4-3. The images taken at 400X show the length and microstructure of the diffusion layer. Diffusion layer was not very observable in these images since L80 is a plain carbon steel with a very limit amount of alloying elements (Table 4-1). Therefore, it did not show a clear microstructure gradient from the compound layer to the core material. The images taken at 1000X showed the length and microstructure of the compound layer, which was the white layer on top of the diffusion layer in Figure 4-3. b. It showed that after 8 h of nitriding treatment, a compound layer cannot be observed even at 1000X. However, after 12 h of treatment, a thin compound layer started to deposit on the diffusion layer (Figure 4-3. d), but this layer was not uniform and thick enough to protect the surface from corrosion because the partially exposed diffusion layer might result in localized corrosion in the test environment. Figure 4-3. f showed the GN treated L80 after 16 h of treatment, a thick ($\approx$ 10 µm) and uniform compound layer could be observed on top of the diffusion layer. The boundary between the compound layer

and diffusion layer was very distinct. It indicated the purity of the compound layer should be higher than that of the specimens treated by the previous two schedules. These results suggested that with the increase of GN duration, the thickness of compound layer increased. Generally, the higher the thickness of the coating, the better the corrosion resistance of it since the coating created a thick boundary, which made it difficult or took longer time to be penetrated by the aggressive species. However, the corrosion resistance of a coating is not solely based on the thickness. The compactness is also a vital factor, which was tested by the electrochemical tests in the next section.
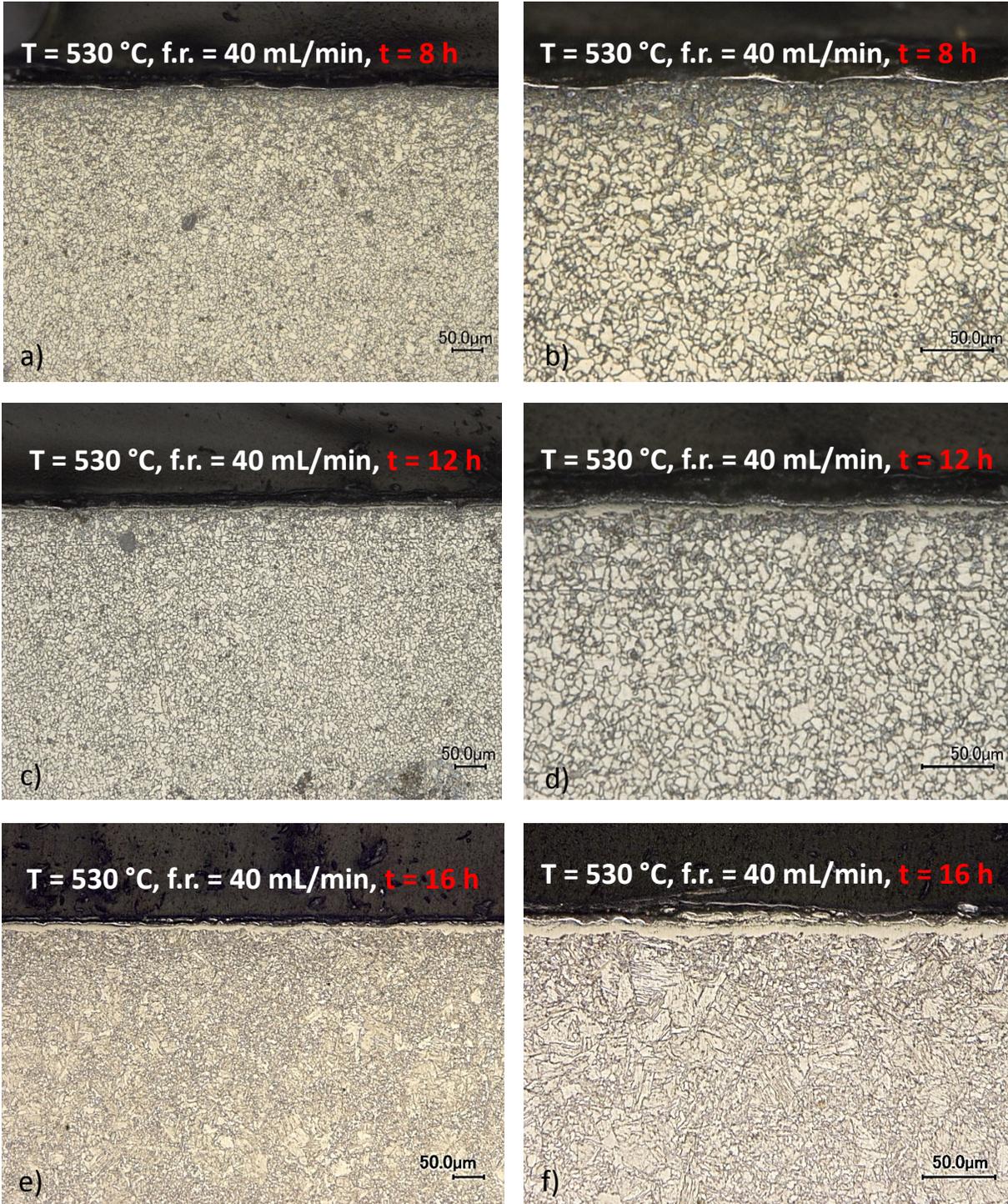
Figure 4-3. The DM images of cross-section of GN treated L80 treated with different nitriding duration taken at 400X and 1000X. a) T = 530°C, f.r. = 40 mL/min, t = 8 h, 400X; a) T = 530°C, f.r. = 40 mL/min, t = 8 h, 1000X; a) T = 530°C, f.r. = 40 mL/min, t = 12 h, 400X; a) T = 530°C,

f.r. = 40 mL/min, t = 12 h, 1000X; a) T = 530°C, f.r. = 40 mL/min, t = 16 h, 400X; a) T = 530°C, f.r. = 40 mL/min, t = 16 h, 1000X.

4.2.2 Electrochemical Tests

The potentiodynamic polarization curves of specimens treated with different nitriding schedule and L80 without GN treatment tested in the simulation environment are shown in Figure 4-4. The most representative curves of each schedule were selected to be shown in this figure. L80 in this environment showed an active dissolution behavior in which the increase of current density with the increase of potential applied was large, and 30 mA/cm^2 of current density was achieved before the penitential reached 0 V vs. Ag/AgCl. It indicated that L80 had very poor corrosion resistance in this environment since the corrosion products formed in this near neutral but slightly acidic (pH = 5.78) environment was non-protective [70]. Therefore, the corrosion rate of L80, calculated by using eq. 3-5, was as large as 0.222 mm/year. By contrast, the GN treated L80 specimens with either schedule had passivation zones, where the increase of current densities with an increase of potential within a range was not apparent. Although the corrosion current of L80 after 8 h of treatment was similar to that of L80 without nitriding treatment, the formation of nitrides on the surface enhanced the corrosion resistance of L80 due to the presence of a passivation zone since the iron nitrides had a much higher corrosion potential [45]. Therefore, the corrosion occurred preferentially at the boundary of the surface inclusions or partially exposed core material [50]. The surface pits formed during nitriding had a better anchoring effect for the deposition of corrosion products than a uniformly corroded surface [46]. Therefore, passivation effects could be observed for GN treated specimens with thin and non-uniform compound layers. After 12 h of treatment, with the increase of compactness and amounts of surface nitrides, the corrosion potential of specimens treated after longer duration increased from -0.68 V vs. Ag/AgCl to -0.58 V vs.

54

Ag/AgCl. The increase of E_{corr} was more evident after 16 h of treatment due to the formation of a more compact and thick compound layer. The E_{corr} shifted to -0.36 V vs Ag/AgCl and the I_{corr} dramatically decreased to 1.96 $\mu A/cm^2$. The corrosion rate was lowered to 0.023 mm/year which was about an order of magnitude smaller than that of L80 without GN treatment. This effect indicated that the formation of a thick, pure and compact compound layer effectively inhibited the corrosion reaction occurring on the surface of the nitriding treated specimens. The surface imperfections in the compound layer were very limited; therefore, the sweet corrosion could only be generated in limited locations. Therefore, an overall decreased corrosion current density and a more positive corrosion potential could be observed on the samples treated with longer duration in the test environment.
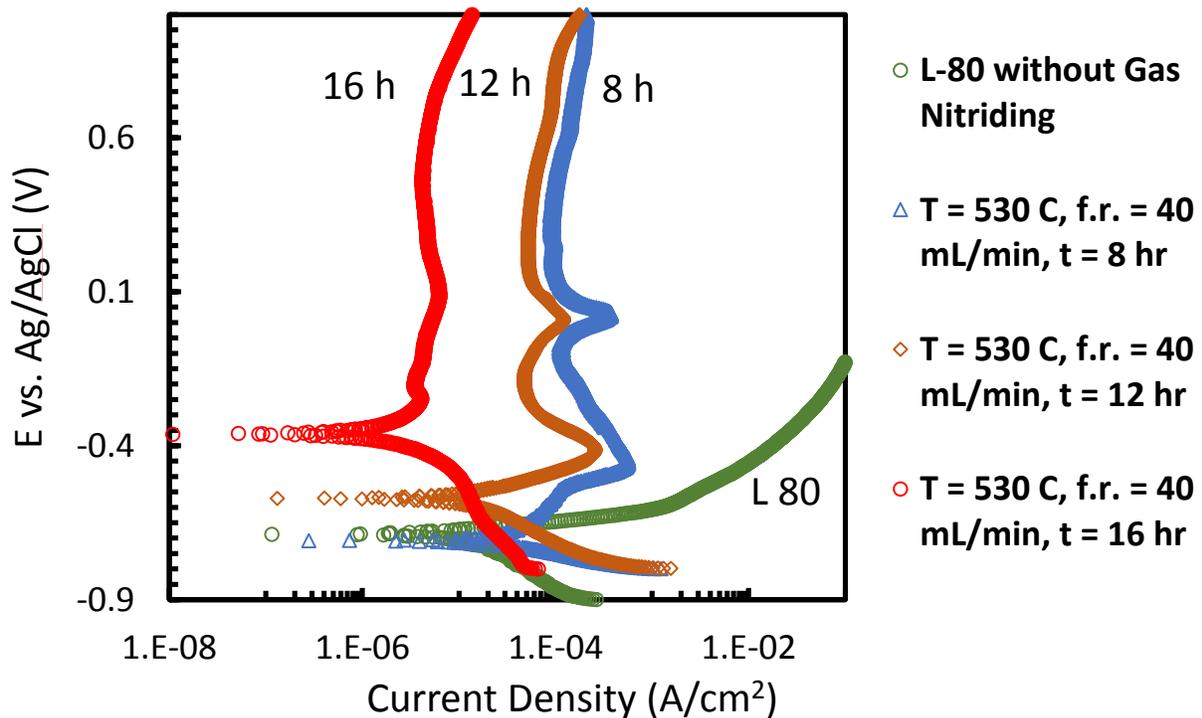
Figure 4–4. The effect of nitriding duration on the potentiodynamic polarization curves of nitriding treated specimens in CO_2 saturated simulation environment at 20°C.

Table 4–4. The effect of nitriding duration on the corrosion current and corrosion rate of GN L80.

Schedule	I_{corr} ($\mu A/cm^2$)	Corrosion rate (mm/year)
L-80	19.2	0.222
T = 530 °C, f.r. = 40 mL/min, t = 8 h	18.2	0.211
T = 530 °C, f.r. = 40 mL/min, t = 12 h	16.3	0.189
T = 530 °C, f.r. = 40 mL/min, t = 16 h	1.96	0.023

The EIS data of GN treated specimens and L80 without GN represented in the Nyquist plot (Figure 4-5) showed the same trend with the potentiodynamic polarization curves, where the specimens with the longest nitriding treatment had the largest radius of capacitance curve. Generally, the larger the radius capacitance curve, the better the corrosion resistance of the test specimens [9]. Therefore, GN L80 after 16 h of treatment had the highest corrosion resistance in the simulated environment. The detailed analysis of EIS tests will be discussed in Chapter 5.
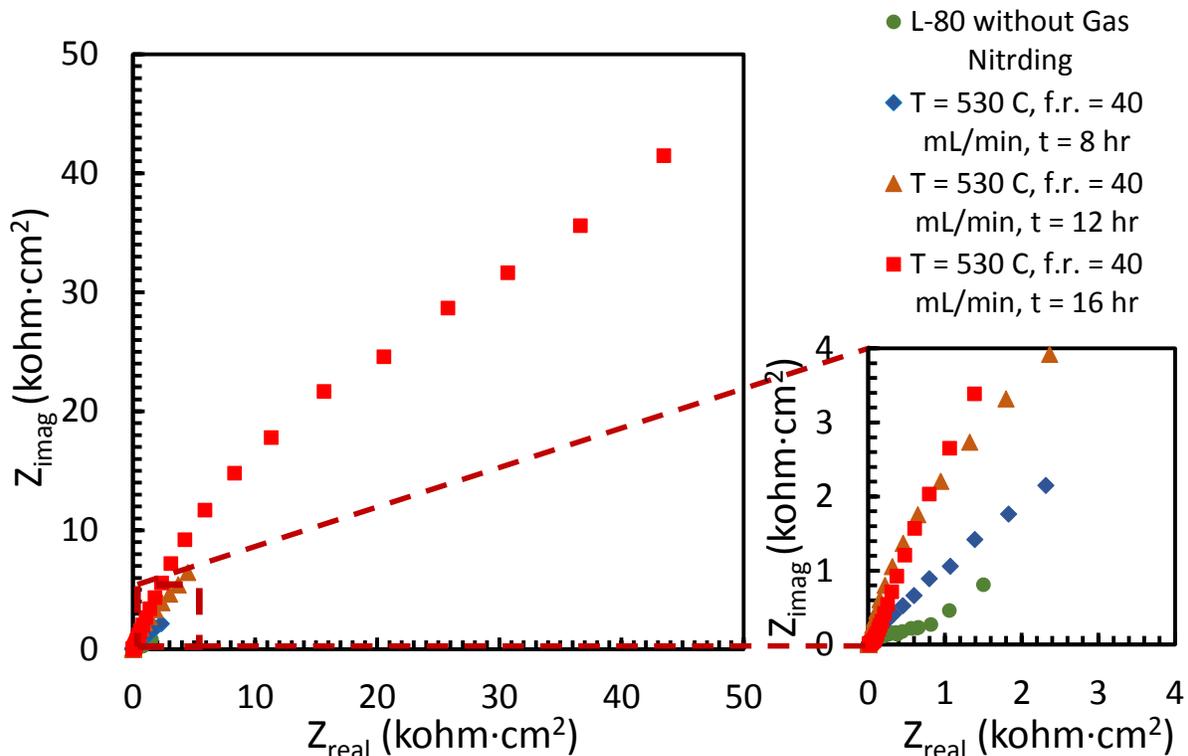
Figure 4-5. The effect of nitriding duration on the EIS (Nyquist plot) of nitriding treated specimens in the CO_2 saturated simulated environment at 20°C

4.2.3 The Effect of Nitriding Duration on the Industrial Application for Slotted Liners

The results of the optimization of nitriding duration revealed a simple relationship that the longer the nitriding time, the better the corrosion resistance. However, it did not indicate that a "perfect" corrosion free coating for the steel would be produced after an infinite long time of treatment. The deposition rate of compound layer slows down after a long term treatment since the diffusion of liberated nitrogen into the compound layer becomes more difficult when the compactness of the compound layer was higher [36]. Moreover, the inclusions such as Fe_3C, intrinsically present at the surface, always interrupted the formation of nitrides and the compactness. The purity of the iron nitrides will not achieve the perfect state. Therefore, after long term of treatment, usually

longer than 96 h [36], the specimen may reach a "saturation state", which the growth of compound layer is too slow for industrial-scale production. However, the corrosion resistance of the saturated nitriding steel is not necessarily larger than the corrosion resistance of "non-saturated" nitriding steel. Furthermore, due to the special geometry requirements of slotted liners, the thickness of the coating should be thin as the purpose of corrosion protection is fulfilled. A thicker coating decreases the screening efficiency of the slotted liners, and most importantly, it requires extra revision of the existing design and production, which may not be acceptable for the sponsors of the project.

4.2.4 Conclusions

The effect of nitriding duration on the corrosion resistance of GN treated L80 in the simulated environment was examined in section 4.2. Based on the etched cross-sectional images taken by using DM, longer nitriding duration could produce a thicker and more uniform compound layer on the L80 specimen. The potentiodynamic polarization curves suggested that the corrosion potential of GN treated L80 with optimized duration shifted to the most positive region and the corrosion current density of GN treated L80 with optimized duration dramatically decreased compared to those of L80 without nitriding treatment. The corrosion rate of specimen with the optimized nitriding duration lowered the corrosion rate in the simulated environment about one order of magnitude because the compound layer was sufficiently pure and compact to prevent the corrosion occurring in the weak spots such as inclusions and cracks. GN treatment with either duration produced passivation zones that showed in the potentiodynamic polarization curves, which indicated that GN produces surface nitrides with better anchoring effect of the corrosion products. The corrosion products deposited in a protective manner significantly inhibited the corrosion reactions. The EIS data also suggested that the specimen with the longest treatment

showed the best corrosion resistance because of the largest radius of capacitance curve obtained in this measurement. The results of optimization of GN duration suggested that specimen with 16 h of treatment had much higher corrosion resistance than the specimens treated with 12 h or 8 h. However, a "saturated" nitriding steel is not cost-effective because it takes longer time to produce and the corrosion resistance is not necessarily higher than "non-saturated" nitriding steel. An extremely thick coating is also not acceptable for slotted liners.

4.3 The Optimization of Nitriding Temperature

Nitriding temperature is the main factor to influence the composition of compound layer and the growth rate of compound layer [36]. The optimization of nitriding temperature selected three temperature, 520°C, 530°C and 540°C based on the literature and my preliminary optimization process (Table 4-5) [36, 44]. A group of eight samples were GN treated with either schedule. Each schedule was performed at least three times. In this optimization process, a schedule with optimized nitriding temperature at specified flowrate, which produced the most corrosion resistant nitrides layer, was selected and studied.

Table 4-5. The matrix of optimization of nitriding temperature.

	Schedule (#)	Duration (h)	Temperature (°C)	Flowrate (mL/min)
The Effect of **Nitriding Temperature**	T1	16	**520**	40
	T2	16	**530**	40
	T3	16	**540**	40

4.3.1 Surface Characterization

The cross-section images of GN treated L80 with different nitriding temperatures are shown in Figure 4-6. The images taken at 400X show the length and microstructure of the diffusion layer and the images taken at 1000X show the length and microstructure of compound layer. Figure 4-6. b shows that at a treatment of 520°C, a uniform but thin compound layer could be observed on top of the diffusion layer. The compound layer tended to become thicker and more uniform by treatment at 530°C (Figure 4-6. d). However, the increase of temperature did not guarantee the increase of compound layer. The compound layer formed at 540°C was not uniform and the thickness could not be measured. These results indicated there was an optimal nitriding temperature at a certain flow rate which resulted in the optimal dissociation rate of the ammonia gas. The optimal dissociation rate enabled the uniform and effective deposition of the compound layer. Lower temperature resulted in low deposition rate; thus, a thin compound layer was produced with limited resistance to the penetration of aggressive species. By contrast, high temperature enabled the rapid dissociation of ammonia gas, which resulted in the non-uniform and cluster growth mechanisms [36]. The discontinuous and porous formation of the compound layer was not expected to have improved resistance in the simulated environment.
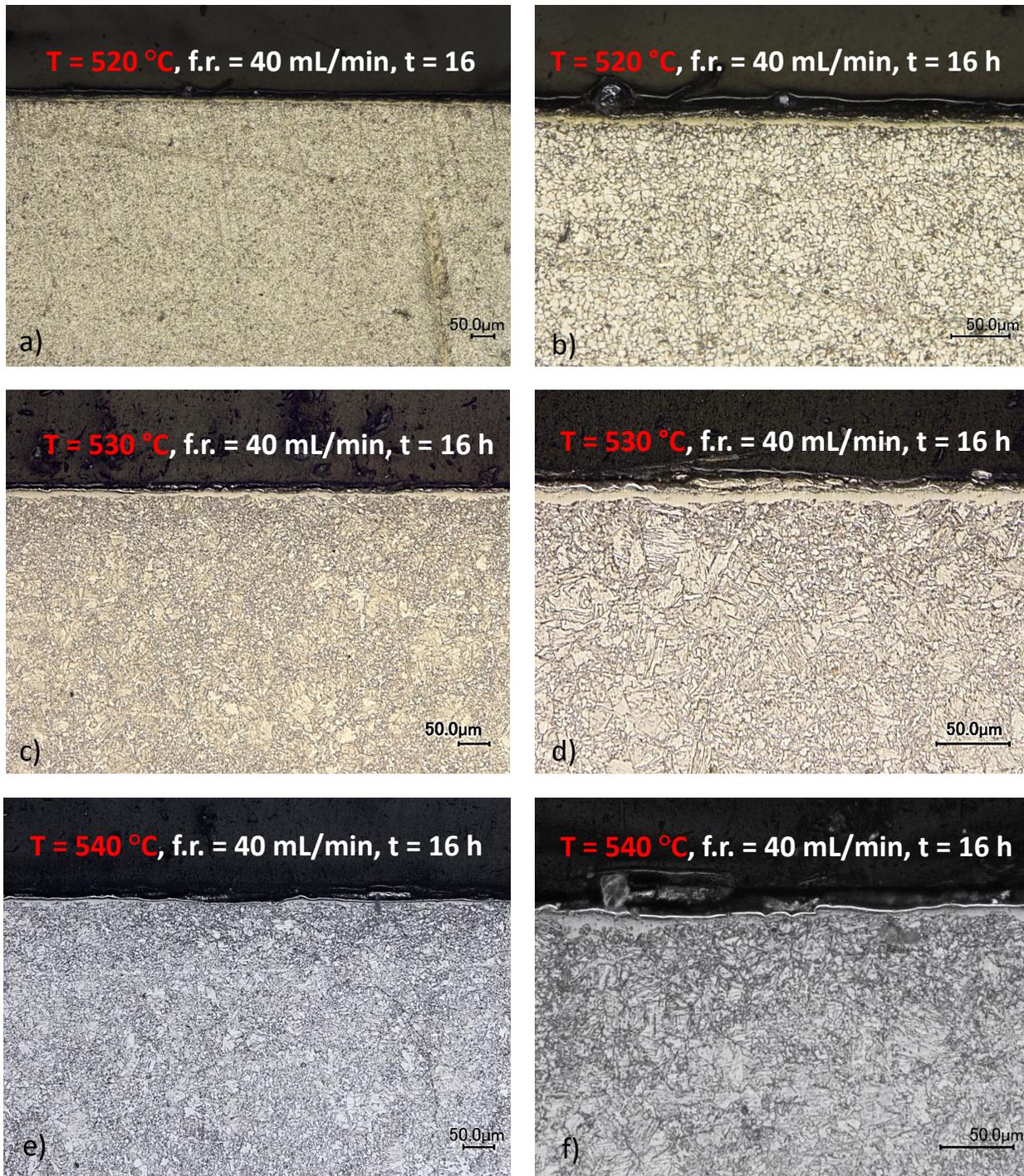
Figure 4-6. The DM images of cross-section of GN treated L80 treated with different nitriding temperature taken at 400X and 1000X. a) T = 520°C, f.r. = 40 mL/min, t = 16 h, 400X; a) T = 520°C, f.r. = 40 mL/min, t = 16 h, 1000X; a) T = 530°C, f.r. = 40 mL/min, t = 16 h, 400X; a) T =

530°C, f.r. = 40 mL/min, t = 16 h, 1000X; a) T = 540°C, f.r. = 40 mL/min, t = 16 h, 400X; a) T = 540°C, f.r. = 40 mL/min, t = 16 h, 1000X.

4.3.2 Electrochemical Tests

The effect of nitriding temperature on the potentiodynamic polarization curves of nitriding treated L80 specimens in the simulated environment is shown in Figure 4-7. The curves of specimens treated at 520°C and 540°C showed very similar patterns because the nitrides layers formed at both treatment were either too thin or too porous to prevent the penetration of corrosive species in the simulated solution. Although the deposition of corrosion products enhanced the corrosion resistance of the treated specimens, indicated by the presence of passivation zones, the corrosion rates and corrosion potentials measured from the specimens treated with non-optimal temperatures were of the same order of magnitude, which was around 0.200 mm/year (Table 4-6) and -0.68 V vs. Ag/AgCl, of L80 without treatment. By contrast, the specimen treated at 530°C showed superior corrosion resistance due to the formation of a thick, uniform, compact and pure compound layer. These results indicated that at a specified flow rate, there was an optimal temperature to allow the effective formation of corrosion resistant compound layer.
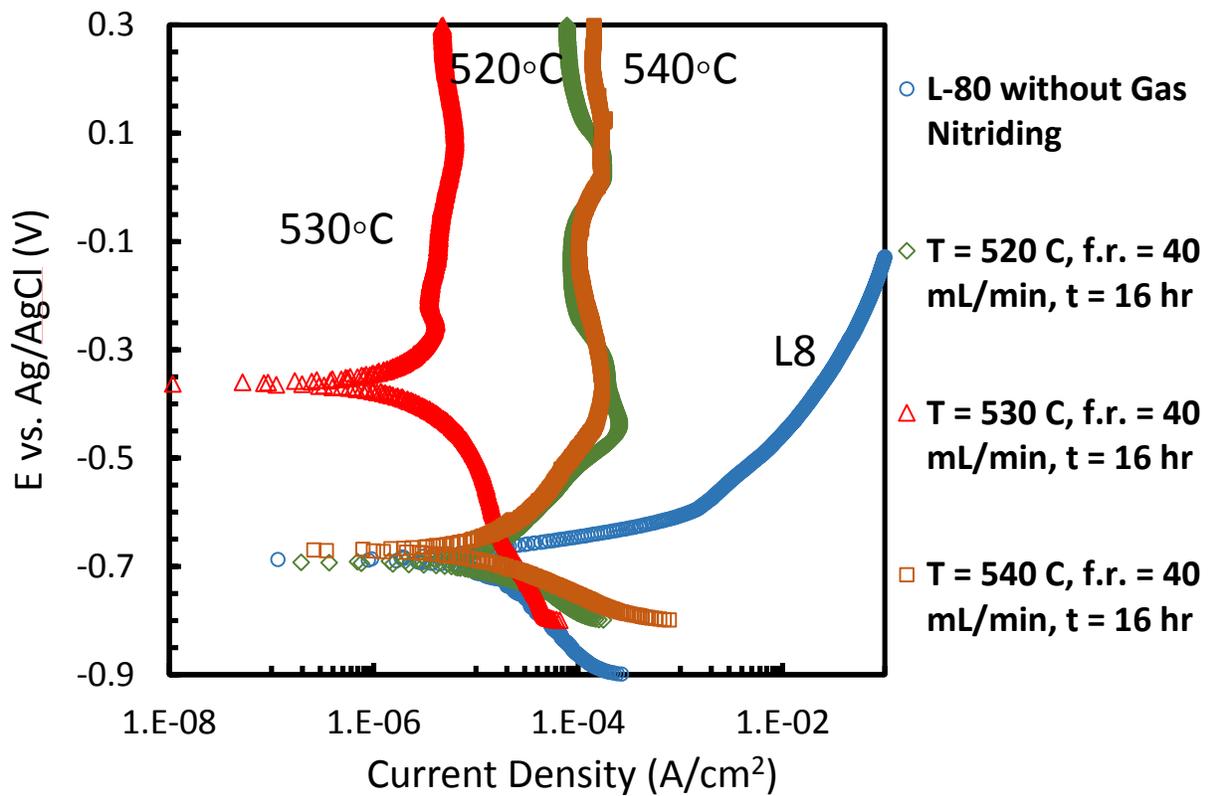
Figure 4-7. The effect of nitriding temperature on the potentiodynamic polarization curves of nitriding treated L80 specimens in CO_2 saturated simulated environment at 20°C.

Table 4-6. The effect of nitriding temperature on the corrosion current and corrosion rate of GN L80.

Schedule	I_{corr} ($\mu A/cm^2$)	Corrosion rate (mm/year)
L-80	19.2	0.222
T = 520 °C, f.r. = 40 mL/min, t =16 h	16.8	0.194
T = 530 °C, f.r. = 40 mL/min, t = 16 h	1.96	0.023
T = 540 °C, f.r. = 40 mL/min, t = 16 h	17.8	0.206

The EIS data of GN treated specimens and L80 without GN represented in Nyquist plot (Figure 4-8) showed the same trend with the potentiodynamic polarization curves, where the specimens treated at the optimal temperature at this flow rate had the largest radius of capacitance curve. Therefore, GN treated L80 at 530°C at a flow rate of 40 mL/min had the highest corrosion resistance in the simulated environment.
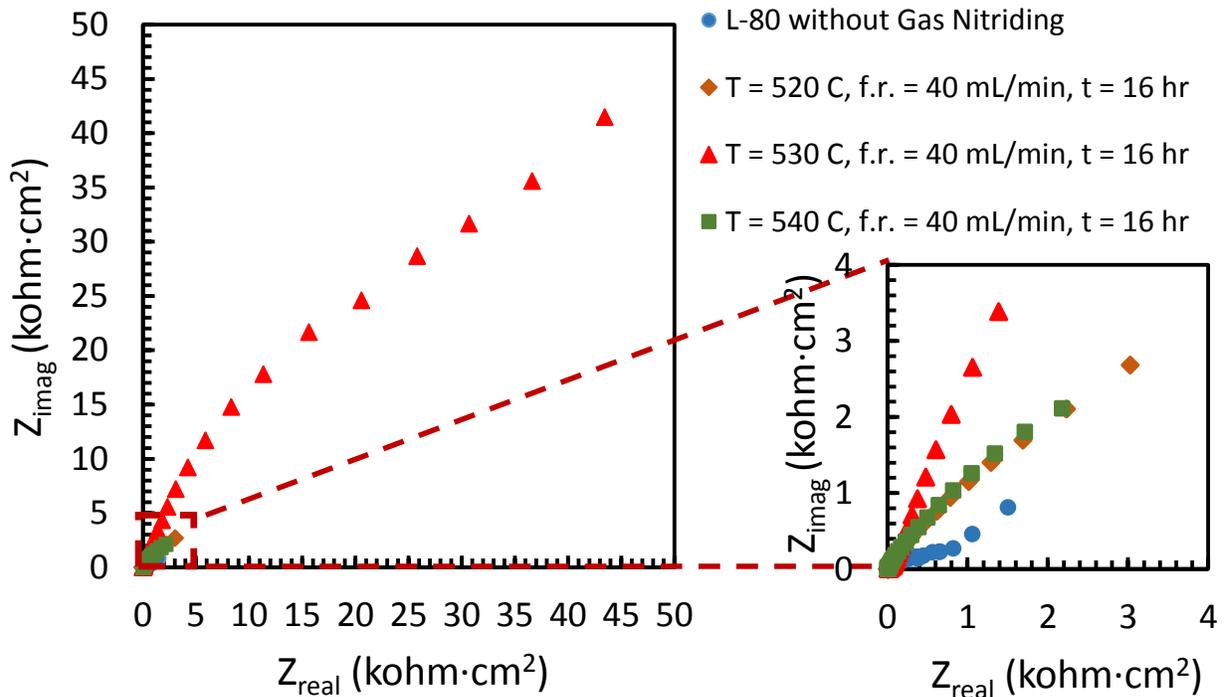
Figure 4-8. The effect of nitriding temperature on the EIS (Nyquist plot) test of nitriding treated specimens in CO_2 saturated simulated solution at 20°C.

4.3.3 The Sensitivity of Nitriding Temperature

The sensitivity of the treatment temperature range seems to be an issue for industrial application since the lab data showed such short temperature range which resulted in significantly different corrosion resistances. Some people may question that the high sensitivity of the narrow temperature range may not be applicable to the industrial-scale production. However, the

sensitivity of the temperature range is actually not an issue because the geometry of the lab apparatus exaggerated the effect of temperature changes on the overall dissociation rate of ammonia gas. The heating zone of gas chamber of this nitriding treatment was less than 300 mL with a point thermal detector. Unlike the industrial-scale pot furnace (Figure 2-9), the lab-scale furnace did not have an air circulating system which facilitates the uniform distribution of temperature and gaseous phase. Therefore, in such a confined and static space with a slow flow rate, the subtle change of temperature had considerable effects on the dissociation rate of the system. The industrial-scale production may yield a result that specimens treated at both 520°C and 540°C are measured with higher corrosion resistances than the lab data, but the discussion of optimal nitriding temperature is still valid but with a wider temperature range. The industrial-scale nitriding temperature is around 500°C - 580°C [36]. However, based on the composition and different application purposes of nitriding steels, the industrial applied nitriding temperature range is usually narrowed down to less than 30°C at a reasonable gas flow rate [36].

4.3.4 Conclusions

The effect of GN temperature on the corrosion resistance of GN treated L80 in the simulated environment was examined in section 4.3. Based on the etched cross-section images taken by using DM, only the treatment at the optimal nitriding temperature produced a thick and uniform compound layer. The potentiodynamic polarization curves suggested that the corrosion potential of the specimen treated at the optimal temperature shifted to the more positive region and the corrosion current density was about one order of magnitude smaller than the corrosion current density of L80 without treatment. The treatments done at non-optimal temperatures showed similar corrosion current densities with L80 without treatment because the thin and porous compound layers were not protective in the simulated environment. The EIS data also suggested that the

specimen treated at the optimal temperature showed the best corrosion resistance because of the largest radius of capacitance curve obtained in this measurement. The results of optimization of GN temperature suggested that specimen treated at 530°C at 40 mL/min had the best corrosion resistance in the simulated environment than the specimens treated at 520°C and 540°C. The high sensitivity of temperature range is not an issue in the industrial-scale application because the geometry and setup of lab-scale nitriding apparatus exaggerated the effect of temperature changes on the properties of nitriding steels. The optimization of nitriding temperature was still valid but with a wider temperature range for the industrial application.

4.4 The Optimization of Ammonia Flow rate

Ammonia gas flow rate is the trickiest parameter among all the three parameters. Nitriding duration and temperature are intrinsic properties, which are not varied with the size of apparatus. However, the ammonia gas flow rate is an extrinsic parameter, which must be altered based on the geometry and volume of the heating chamber. Generally, researchers do not mention the flow rate of their experiments since the flow rate they used only worked for their specific setup, which cannot be directly referenced in my research. Therefore, the selection of flow rate for optimization of schedules was based on my own preliminary optimization processes. The optimization of ammonia flow rate selected three flow rate, 35 mL/min, 40 mL/min and 45 mL/min (Table 4-7). A group of eight samples were GN treated with either schedule. Each schedule was performed at least three times. A schedule with specific ammonia flow rate at the optimized temperature, which produces the most corrosion resistant nitrides layer, was selected and studied in this section.

Table 4-7. The matrix of optimization of ammonia flowrate.

	Schedule (#)	Duration (h)	Temperature (°C)	Flowrate (mL/min)
The Effect of **Ammonia Flowrate**	F1	16	530	**35**
	F2	16	530	**40**
	F3	16	530	**45**

4.4.1 Surface Characterization

The cross-section images of GN treated L80 with different ammonia flow rates are shown in Figure 4-9. The images taken at 400X show the length and microstructure of diffusion layer and the images taken at 1000X show the length and microstructure of compound layer. Figure 4-9. a and b show the cross-section images of specimen treated at 35 mL/min of ammonia flowrate. A thick but non-uniform compound layer could be observed on the top of the diffusion layer. The boundary between the compound layer and diffusion layer was vague, which indicated that the large dissociate rate produced higher amount of liberated nitrogen atoms, which were forced to be rapidly diffused into the matrix at higher partial pressure [36]. However, this rapid diffusion was not favorable for the formation of compact compound layer but a layer with a considerable amount of un-reacted iron. The specimen treated at 45 mL/min of flow rate .Figure 4-9. e and f showed a compound layer with similar thickness compared with other specimens treated at different flow rates. However, due to the low dissociation rate, the density of compound layer was lower since the amount of liberated nitrogen that entered the compound layer was limited [36]. Therefore, the diffusion was not effective and a porous structure with micro-cracks was produced. These results suggested that at a certain nitriding temperature, there was an optimal ammonia flow rate to allow

the effective growth of a compact compound layer. The thickness of the compound layer was not determined by the flow rate of ammonia gas since the diffusion of nitrogen was a temperature and time determined variable. However, the flow rate had strong effects on the compactness of the compound layer, which was examined by electrochemical tests.
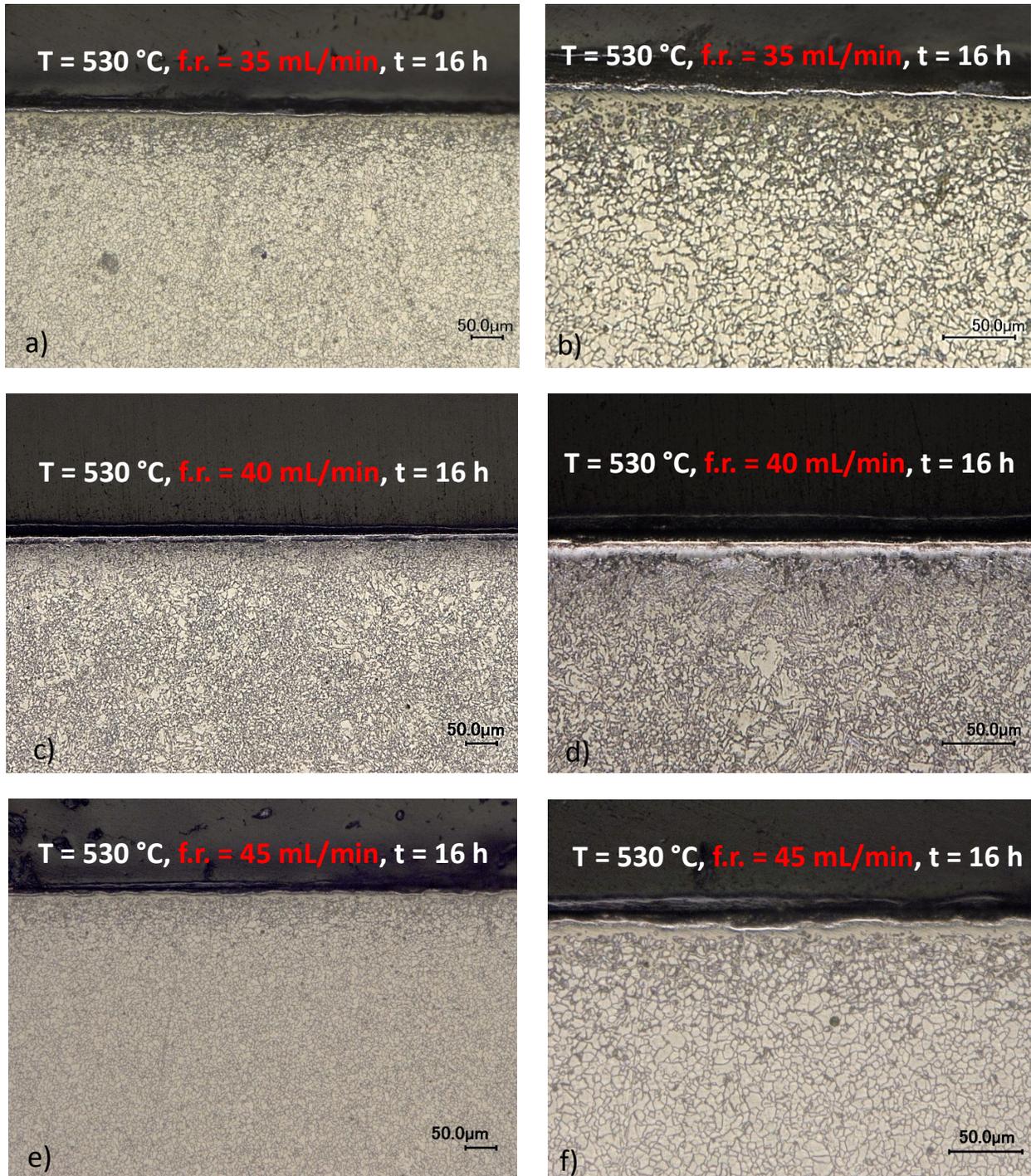
Figure 4-9. The DM images of cross-section of GN treated L80 treated with different nitriding temperature taken at 400X and 1000X. a) T = 530°C, f.r. = 35 mL/min, t = 16 h, 400X; b) T = 530°C, f.r. = 35 mL/min, t = 16 h, 1000X; c) T = 530°C, f.r. = 40 mL/min, t = 16 h, 400X; d) T =

530°C, f.r. = 40 mL/min, t = 16 h, 1000X; e) T = 530°C, f.r. = 45 mL/min, t = 16 h, 400X; f) T = 530°C, f.r. = 45 mL/min, t = 16 h, 1000X

4.4.2 Electrochemical Tests

The effect of ammonia flow rate on the potentiodynamic polarization curves of GN treated L80 specimens in the simulated environment is shown in Figure 4-10. The curve of specimens treated with 35mL/min of flow rate did not show decreases of the current generated or the shift of corrosion potential. The passivation zone of specimen treated with this schedule was not stable as those treated with other flow rates since the large amount of non-reacted iron remaining in the compound layer still participated in the corrosion reaction. Therefore, a large free corrosion current was detected. This morphology also enhanced the occurrence of localized corrosion and a high corrosion rate would be expected. By contrast, even though the compound layer formed at 45 mL/min of flow rate was not compact, most micro-cracks might not penetrate the layer and the sufficiently small crack size prevented the occurrence of localized corrosion. Therefore, the overall corrosion resistance of this specimen increased and the corrosion rate decreased to 0.165 mm/year (Table 4-8). The specimen treated with 40 mL/min of ammonia flowrate showed the best corrosion resistance due to the formation of a thick, uniform and compact compound layer. These results indicated that at a specific temperature, there was an optimal ammonia flowrate to allow the effective formation of a corrosion resistant compound layer.
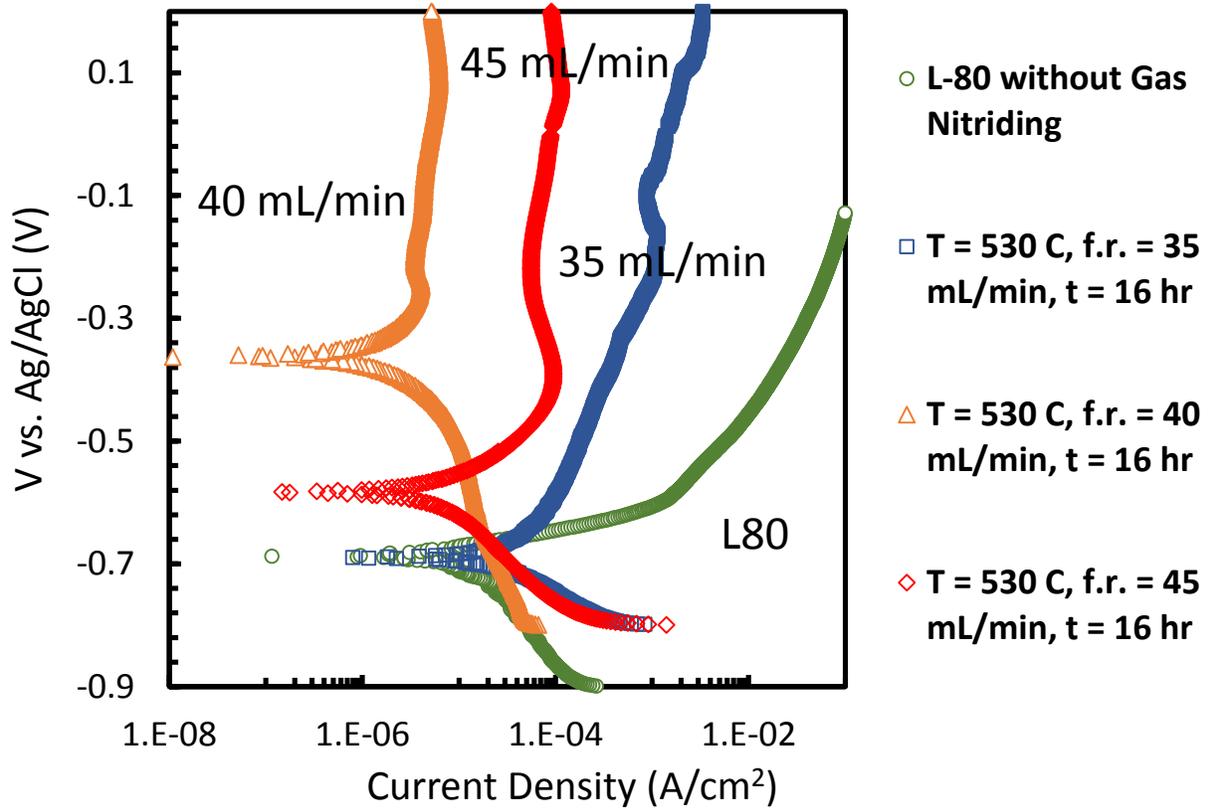
Figure 4-10. The effect of ammonia flowrate on the potentiodynamic polarization curves of nitriding treated L80 specimens in CO_2 saturated simulated environment at 20°C.

Table 4-8.The effect of ammonia flowrate on the corrosion current and corrosion rate of GN L80.

Schedule	I_{corr} ($\mu A/cm^2$)	Corrosion rate (mm/year)
L-80	19.2	0.222
T = 530 °C, f.r. = 35 mL/min, t = 16 hr	14.3	0.235
T = 530 °C, f.r. = 40 mL/min, t = 16 hr	1.96	0.023
T = 530 °C, f.r. = 45 mL/min, t = 16 hr	20.3	0.165

The EIS data of GN treated specimens and L80 without GN represented in the Nyquist plot (Figure 4-11) showed the same trend with the potentiodynamic polarization curves, where the specimens treated at the optimal flowrate at a specified temperature had the largest radius of capacitance curve. Therefore, GN treated L80 at 40 mL/min had the highest corrosion resistance in the simulated environment.
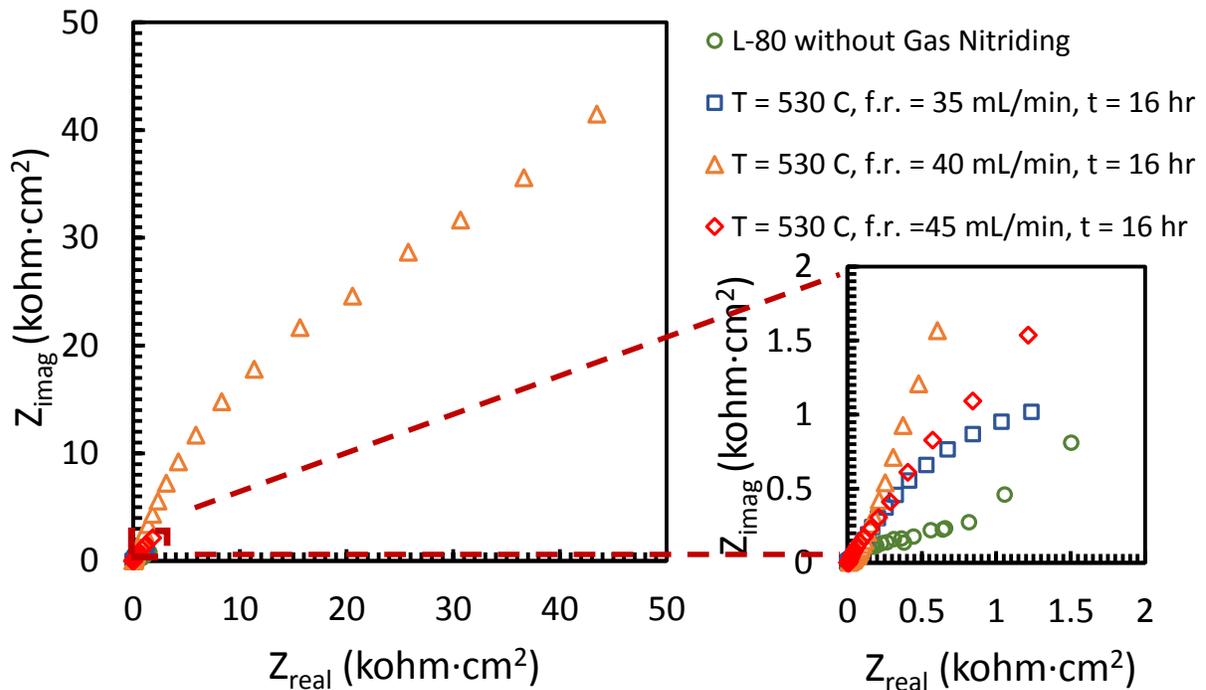
Figure 4-11. The effect of ammonia flowrate on the EIS (Nyquist plot) test of nitriding treated specimens in CO_2 saturated simulated solution at 20°C.

4.4.3 The Effect of Nitriding Temperature and Flow Rate on the Dissociation Rate

As I mentioned in the previous section, the optimized ammonia flow rate should be treated as a pair with the optimized nitriding temperature since the dissociation rate of ammonia gas is the key factor which determines the formation of the compound layer. However, the value of the dissociation rate cannot be directly referred to as a guide to design the nitriding schedule. For

example, to decrease both the nitriding temperature and flow rate of the schedule can maintain the same dissociation rate of the ammonia gas. However, the lowered temperature decreases the diffusion rate of liberated nitrogen atoms into the matrix, which results in an overall decreased efficiency of the formation of the compound layer. By contrast, to maintain a higher nitriding temperature and higher ammonia flowrate can maintain the same dissociation rate, but the treatment consumes more energy and materials, which is not cost-effective for industrial production. This research suggested an optimized pair of nitriding temperature and ammonia flow rate for this treatment set-up, but it did not indicate that other flow rates tested, such as 45 mL/min, could not be used as the optimal flowrate for this system. It was because the corresponding optimal nitriding temperature was not tested as a planned schedule. If other paired temperature and flow rates are tested and optimized, the specimen treated with the other optimized schedule may yield a similar corrosion resistance as the one optimized in my research.

4.4.4 Conclusions

The effect of ammonia flow rate on the corrosion resistance of treated L80 in the simulated environment was examined in section 4.4. Based on the etched cross-section images taken by using DM, only the treatment at the optimal nitriding flow rate at the specified nitriding temperature produced a uniform compound layer. The variation on the flow rate did not change the thickness of the compound layer but the compactness and uniformity of the compound layer. The potentiodynamic polarization curves suggested that the corrosion potential of the specimen treated at the optimal flow rate shifted to the most positive region and the corrosion current density dramatically decreased. The corrosion behavior of treatments done at non-optimal flow rates did not have significant improvements on the corrosion resistances compared with L80 without treatment because the thin and porous compound layers were not protective in the simulated

environment. The EIS data also suggested that the specimen treated at the optimal flow rate showed the best corrosion resistance because of the largest radius of capacitance curve obtained in this measurement. The results of optimization of GN flow rate suggested that specimen treated with 40 mL/min of flowrate at 530°C had the best corrosion resistance in the simulated environment than the specimens treated at 35 mL/min and 45 mL/min. The optimized flow rate should be paired with the corresponding temperature. Specimens treated with other optimized flow rate and temperature combinations might also yield similar corrosion resistances in the simulated environment once the dissociation rate is maintained. However, the dissociation rate cannot be directly referred to as a design parameter because of the non-optimal diffusion efficiency or cost-effectiveness.

4.5 Conclusions of Chapter 4

The nitriding schedules for L80 carbon steel were optimized in this chapter in order to obtain a GN treated L80 with the best corrosion resistance. Three parameters, nitriding duration, temperature and ammonia flow rate were optimized to produce a highly corrosion resistant nitrides layer on an L80 substrate. The optimization of nitriding duration suggested that a longer treatment produced a compound layer with thicker and more compact structure, which generally had better corrosion resistance. The nitriding temperature influenced the effectiveness of the growth of the compound layer. The optimized temperature showed a narrow range for the lab-scale treatment, but the optimization was valid with a wider range for industrial-scale production. The nitriding flow rate did not affect the thickness but the compactness of the compound layer. The optimized temperature and flow rate were treated as a pair for an optimized dissociation rate. However, the dissociation rate cannot be directly referred to as a design parameter due to the effectiveness and for economic reasons. GN treated L80 with either schedule showed improved corrosion resistance

by the presence of passivation zones in potentiodynamic polarization tests. The optimized schedule was a treatment at 40 mL/min at 530°C for 16 h. The corrosion current density decreased to 1.96 $\mu A/cm^2$ and the corrosion potential shifted to -0.38 mV v. Ag/AgCl. The corrosion rate of a specimen treated with the optimized schedule decreased to 0.023 mm/year, which was about one order of magnitude smaller than the corrosion rate of L80 in the same environment. Therefore, the optimized nitriding schedule significantly increased the corrosion resistance of L80 in the simulated environment.

Chapter 5. The Corrosion Behavior of Gas Nitriding Steel

In this chapter, the corrosion behavior of GN treated L80 is investigated by comparing with the corrosion behavior of L80 without treatment and alloy 800, which is a nickel-based alloy used in oil industrial for various purposes, such as the material for steam exchanger and casting liners and tubing for HPHT well [71, 72]. Alloy 800 has outstanding corrosion resistance in various aqueous media at high temperature due to the presence of chromium (19 - 23 wt%). The iron (39.5 min wt%) provides high corrosion resistance to the internal oxidation and the nickel (30 - 35 wt%) maintains the ductility and machinability of the structure [73]. Alloy 800, as a corrosion resistant alloy (CRA), might be one of the most suitable candidates for the manufactures of slotted liners. However, the high fabrication cost of this alloy limits its prevalence for large-scale application [72]. Therefore, this chapter will compare the corrosion resistances and behaviors of L80, GN treated L80 and Alloy 800 to discuss whether GN treated L80 is suitable as a corrosion resistant material for the slotted liners in the simulated environment.

5.1 Experimental Procedure

The experiments conducted in these chapter followed the same experimental procedures mentioned in Chapter 4. The sample treatment on alloy 800 was the same with that of L80 without nitriding treatment. For the electrochemical tests, Alloy 800 and L80 were treated with an additional process: after the specimen was placed in the deaerated simulated solution, a constant cathodic potential, −1V vs. Ag/AgCl, was applied for 15 min to reduce the oxide film formed on the specimen surface due to contact with humid air.

5.2 Electrochemical Tests

5.2.1 Potentiodynamic Polarization Curves

Figure 5-1 shows the potentiodynamic polarization curves tested for L80, GN treated L80 and alloy 800. L80 tested in this simulated environment showed an active dissolution corrosion behavior where the current density generated increased significantly with an increase of potential. By contrast, both GN treated L80 and alloy 800 showed passivation effects in the same test environment and the corrosion current densities generated by both materials were about one magnitude smaller than that of L80 without treatment (Figure 5-1, Table 5-1). However, the corrosion potential of alloy 800 was -0.60 V vs. Ag/AgCl, which was more negative than the corrosion potential of GN treated L80, which was -0.38 V vs. Ag/AgCl. Moreover, the passivation zone of alloy 800, from -0.45 V vs. Ag/AgCl to 0.74 V vs. Ag/AgCl was smaller and more negative than the passivation zone of GN treated L80, which was from -0.28 V vs. Ag/AgCl to 1.22 V vs. Ag/AgCl. Most importantly, alloy 800 showed a metastable pitting zone by fluctuating current densities from 0.2 V vs. Ag/AgCl to 0.6 vs. Ag/AgCl. This zone suggested that alloy 800 was more susceptible to attack by the aggressive species such as Cl⁻ in the solution [74]. When the applied potential was higher than 0.6 V vs. Ag/AgCl, the specimen subjected to rapid breakdown of passive films and large current generation. By contrast, GN treated L80 had a stable passivation zone without any sign of attack from corrosive species. Most importantly, the current density generated at high potential of 1.22 V vs. Ag/AgCl was even smaller than the free corrosion current density generated on L80 in the same environment. These tests suggested that GN treated L80 was more suitable as the material than alloy 800 for slotted liners in the simulated environment due to the more positive corrosion potential and the presence of a wider and more stable passivation zone.

77
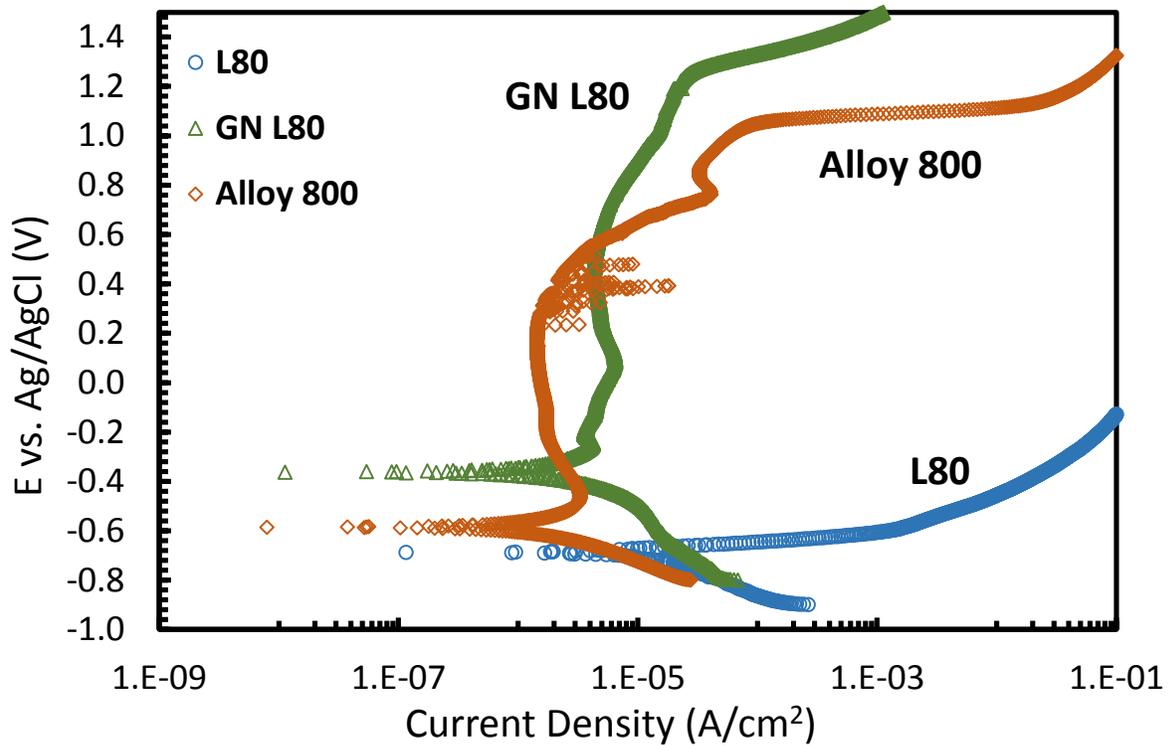
Figure 5-1. The potentiodynamic polarization curves of GN treated L80, alloy 800 and L80 in the same simulated solution with saturated CO_2 at 20°C.

Table 5-1. The comparison of corrosion current density and corrosion rate of L80, GN treated L80 and alloy 800 in the same simulated environment.

	I_{corr} ($\mu A/cm^2$)	Corrosion rate (mm/year)
L80	19.2	0.222
GN treated L80	1.96	0.023
Alloy 800	1.68	0.019

5.2.2 EIS Tests

The Nyquist plot in Figure 5-2 showed that both GN treated L80 and alloy 800 had much larger radiuses of capacitance curves than that of L80. The similar radiuses suggested that these two materials had similar corrosion resistances in the same simulated environment, but the shapes provided the clues for the equivalent circuit modeling. The shapes suggested double-layer prototype for these two materials. The detailed analysis of corrosion behavior of these three materials will be discussed in section 5.2.3. The other presentation of EIS data in a phase Bode plot are shown in Figure 5-3. Both of the GN treated L80 and alloy 800 had larger phase angles, which were closed to -75°, in the low frequency zone. Both of them were much larger than the phase angle of L80, which was - 48°. The larger phase angles of GN treated L80 and alloy 800 indicated that both materials were good capacitors with high corrosion resistance.
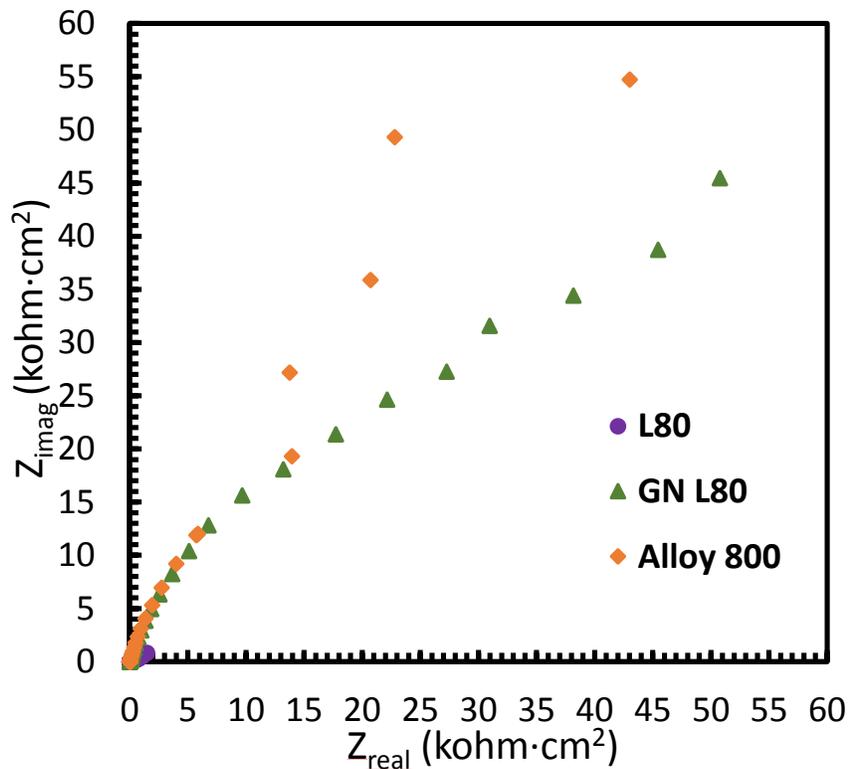
Figure 5-2. The Nyquist plot of different materials tested in the same environment.
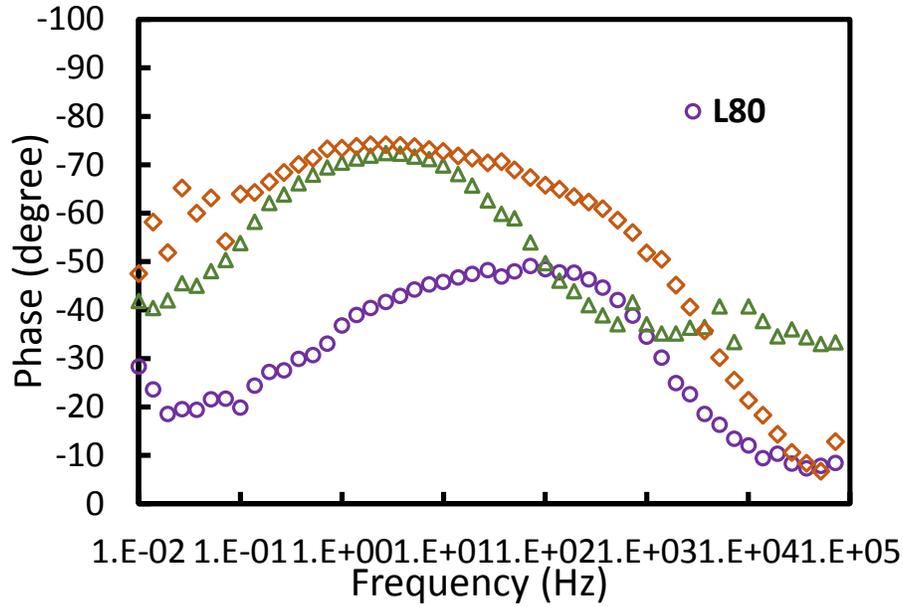
Figure 5-3. The Phase Bode plot of different materials tested in the same environment.

5.2.3 EC Modeling

According to figure 5-2, the last several measurements of the impedance curve of alloy 800 showed

large fluctuations and discontinuities, which were strong indications of the presence of a second

time constant. It suggested that the double-layer model should be applied to this material. Since

the double-layer structure of nitriding steel was known, it was also applied to GN treated L80. This

EC model (Figure 5-4) is a generally accepted model for imperfect inert coating on an active metal.

The EC model applied for L80 (Figure 5-5) was a simple Randles cell model with one time

constant. It is a generally accepted model for an active metal in a corrosive environment
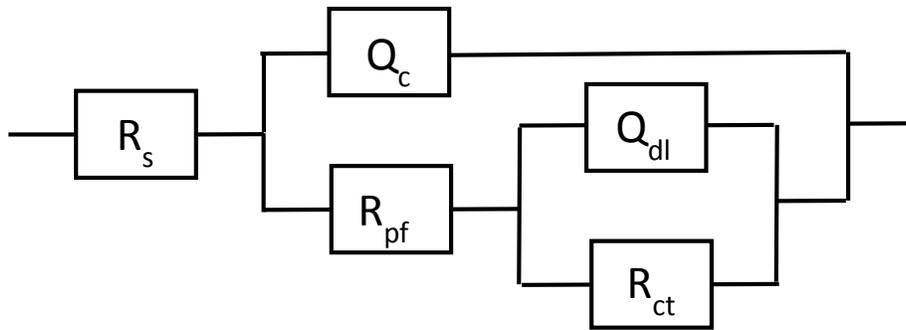
Figure 5-4. The EC fitting for the EIS data of GN treated L80 and alloy 800 tested in the simulated environment.
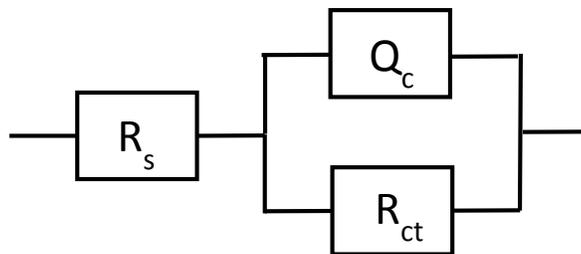
Figure 5-5. The EC fitting for the EIS data of L80 tested in the simulated environment.

Table 5-2 and 5-3 list the EC fitting results of GN treated L80, alloy 800 and L80 tested in the same simulated environment with different models applied. Q_c measures the degree of coating degradation [75], where the larger the number, the more severe the coating degradation. The Q_c of the gas nitriding treated L80, 2.06×10^{-5} S-s^n was slightly smaller but within the same magnitude of the Q_c of the alloy 800, 4.8×10^{-5} S-s^n. Both Q_c of these two materials were significantly smaller than that of L80. These results suggested both materials had excellent resistance to the degradation of surface structure.

R_{pf} is a corresponding resistance with increasing water absorption or permeability. The larger this value, the higher the resistance of the coating to the ionic species [76]. Alloy 800 had much larger R_{pf}, 5.02×10^5 $\Omega \cdot cm^2$, than that of GN treated L80, 2.12×10^2 $\Omega \cdot cm^2$. These results suggested that the coating to substrate interface of GN treated L80 was the weak part. If the aggressive species in the solution broke through the coating via the cracks and voids, the corrosion was likely to occur

in the interface and directly attack the iron in diffusion layer [76]. Therefore, a highly compact passivation layer was essential for the maintenance of corrosion resistance. However, the corrosion occurring in the interface might not always be detrimental based on the different deposition manner of corrosion products. If the deposition of corrosion products was compact, the corrosion reaction might be inhibited instead.

Q_{dl} is a strong indicator of the coating adhesion loss [75, 76]. The smaller this number, the better the coating adhesion. GN treated L80 had much smaller Q_{dl}, 9.93×10^{-6} S-s^n, than that of alloy 800, 4.35×10^{-3} S-s^n. These data were valid since the "coating" on alloy 800 was actually a passive film formed in this solution. This film was always subjected to dynamic formation and breakdown due to the preferential depletion of nickel and dehydration of the outer passive film by CO_3^{2-} [77]. This material is very sensitive to the disturbance due to turbulence in the real operation environment since once the repassivation of the passive film is interrupted, the breakdown of the passive film is rapid and irreversible.

R_{ct} represents the resistance to the charge transfer between the coating and solution interface [75]. This parameter is inversely proportional to the corrosion rate. The R_{ct} of alloy 800, 5.474 $\Omega \cdot cm^2$ was much smaller than the R_{ct} of GN treated L80, 3.96×10^5 $\Omega \cdot cm^2$. These results indicated that the coating material itself had extremely high corrosion resistance because iron nitride was chemically stable in this environment. Therefore, very limited corrosion occurred at this interface. By contrast, alloy 800 did not have a stable passivation layer in this environment. The most dynamic reactions occurred on the outer shell of the passive film [77]. Therefore, for GN treated L80, the corrosion occurred between this interface dominated the corrosion rate calculated for the whole specimen in the test environment.

R_p, which is the sum of all the R modules in the EC models, is the total polarization resistance of the specimen measured. Both of the R_p of GN treated L80, 3.96×10^5 $\Omega \cdot cm^2$ and alloy 800, 5.02×10^5 $\Omega \cdot cm^2$ were significantly larger than the R_p of L80, 2.32×10^3 $\Omega \cdot cm^2$. These results indicated both GN treated L80 and alloy 800 had excellent corrosion resistance in the test environment. Although R_p of these two materials were within the same magnitude, their corrosion behaviors were totally different. R_{pf} was the most dominant factor of the R_p of alloy 800 in this system, but R_{ct} accounted for most of the R_p of GN treated L80. Therefore, the corrosion resistance of GN treated L80 was more sensitive to the size and amount of opening cracks in the coating, but alloy 800 was more sensitive to the stability of the outer shell of the passive film. Fortunately, the coating adhesion of GN treated L80 was very strong. This high adhesion was because the coating was not applied on the surface with mechanical force but by the growth mechanism at high temperature. Therefore, the natural spallation of the coating should not be a common issue to GN treated L80. A coating with good adhesion is extremely important for its long term service in an environment.

Table 5-2. The EC fitting of GN treated L80 and alloy 800 tested in the simulated environment.

	GN treated L80	Alloy 800
Model	R(Q(R(QR)))	R(Q(R(QR)))
R_s	19.56	5.98
Q_c	2.06E-05	4.80E-05
n	0.8	0.8262

R_{pf}	2.12E+02	5.02E+05
Q_{dl}	9.93E-06	4.35E-03
n	0.8878	0.8504
R_{ct}	3.96E+05	5.474
R_p	3.96E+05	5.02E+05

Table 5-3. The EC fitting of L80 tested in the simulated environment.

	L80
Model	R(QR)
R_s	3.334
Q_c	0.1201
n	0.8
R_{ct}	2315
R_p	2318.334

5.3 Surface Characterization

Figure 5-6 shows the images taken by DM before and after the potentiodynamic polarization tests for each material. L80 in the simulated environment suffered from severe uniform corrosion with a significantly deformed surface. The surface was roughened by the corrosion reactions and the

flake-like corrosion products loosely deposited were removed easily from the substrate by rinsing with deionized water. The roughened surface is favorable for the fouling deposition, which induces the plugging problem of the slotted liners. By contrast, GN treated L80 did not show any sign of corrosion reactions or changes of surface morphologies. It suggested that GN treated L80 was dimensionally and chemically stable in the test environment. Alloy 800 after the test showed a large amount of pits which were a sign that pitting corrosion had occurred around the inclusions and grain boundaries [77]. Therefore, the corrosion rate of alloy 800 might greatly increase with service time.
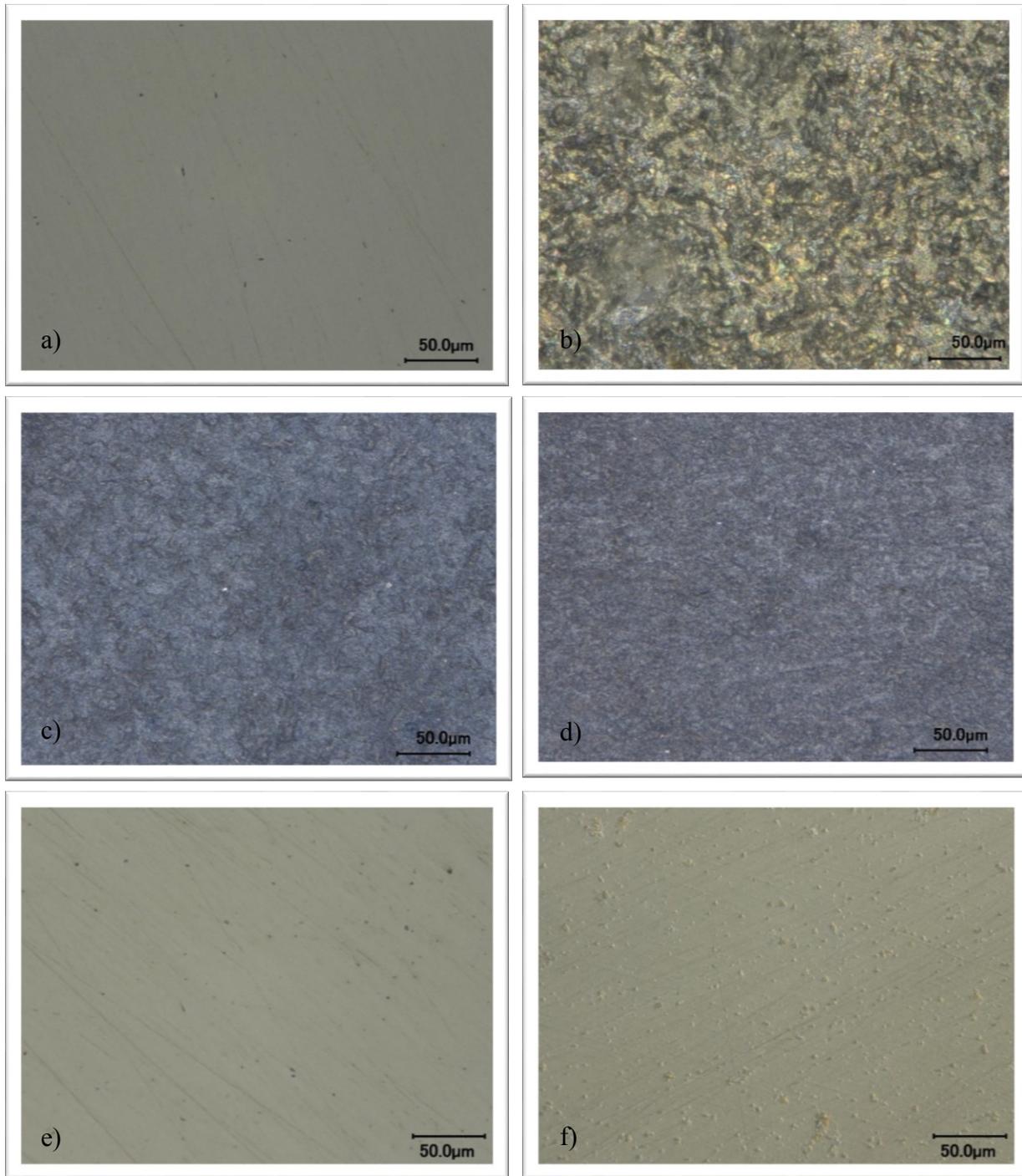
Figure 5-6. The DM images of suface morphologies of different materials before and after the potentiodynamic polarization tests in the same simulated environment, images were all taken at 1000X. a) L 80 before test; b) L80 after test; c) GN treated L80 before test; d) GN treated L80 after test; e) alloy 800 before test; f) alloy 800 after test.

5.4 Conclusions for Chapter 5

In this chapter, the corrosion behavior of L80, GN treated L80 and alloy 800 were compared by using potentiodynamic polarization tests, EIS tests and DM. GN treated L80 tested showed a more positive corrosion potential, -0.38 V vs. Ag/AgCl, and wider and more stable passivation zone, which indicated that GN treated L80 was more suitable as a corrosion resistant material in the test environment. Both GN treated L80 and alloy 800 showed large radiuses of capacitance curves and high phase angles around -75 °, which indicated that these two materials had excellent corrosion resistance in the test environment. The double-layer model was used for the EC fitting of EIS data of GN treated L80 and alloy 800. Randles cell model was used for L80. The R_p value of GN treated L80, 3.96×10^5 $\Omega \cdot cm^2$, was very close to the R_p value of alloy 800, 5.02×10^5 $\Omega \cdot cm^2$, and both values were significantly larger than the R_p of L80, 2.32×10^3 $\Omega \cdot cm^2$. However, R_{pf} was the most dominant factor of the R_p of alloy 800 in the test environment, but R_{ct} accounted for the R_p of GN treated L80. Therefore, GN treated L80 was more sensitive to cracks in the coating because corrosion was more likely to occur between the interface of the coating and diffusion layer. Fortunately, the coating adhesion of GN treated L80 was very strong indicated by an extremely small Q_{dl}, 9.93×10^{-6} $S\text{-}s^n$, since the coating grew directly on the diffusion layer. Therefore, both alloy 800 and GN treated L80 had great corrosion resistance in the test environment, but GN treated L80 was more suitable for the application as slotted liners in the simulated environment.

Chapter 6. The Stability Tests

The corrosion rate measured and corrosion behavior examined for GN treated L80 in Chapter 5 cannot give us a full picture of the corrosion resistance of this material in the simulated environment. The stability is another important property to predict the overall corrosion resistance of a coating in an environment for a long term service. The stability tests involved the immersion test with various compositional and dimensional characterizations, and electrochemical tests. Only the coating satisfying all of these criteria could be considered for the long term service as corrosion resistant materials.

6.1 Experimental Procedure

6.1.1 Immersion Tests

The immersion test was conducted in the same container as the electrochemical tests. N_2 was pumped into the container with 200 mL simulated solution at a flow rate of 500 mL/min with an inlet pressure of 20 psi for 15 min. After deaeration, CO_2 was pumped into the simulated solution at 20 mL/min and 20 psi before the test for at least 30 min to ensure the saturation of CO_2. A sealed but not welded GN treated L80 specimen was placed into the solution with the exposed surface facing up. The immersion test lasted for 24 h with a continuous injection of CO_2 to maintain saturation. The immersed specimens were cleaned with deionized water after immersion. They were air dried after rinsing and stored in a dry plastic bag for compositional and morphological tests. Immersion tests were repeated at least three times.

6.1.2 Surface Characterization

Zeiss Sigma 300 VP-FESEM located in the Department of Earth and Atmospheric Science was the SEM used for the surface morphology examination. It was equipped with a secondary electron detector and a Bruker EDX system with dual silicon drift detectors for the examination of

elemental distribution and compositional analysis. Each samples was loaded on the examination disc on a conductive adhesive tape without metal or carbon spray. The software used for the capture of SEM images was SmartSEM and the software used to process the EDX data was Esprit.

Rigaku XRD Ultimate IV located in the NanoFAB was the XRD used for the compositional analysis of this research. Both bulk diffraction and thin-film diffraction modes were used for the examinations. The 2θ was from 30° to 90° with 1° per min with copper as the target for all the samples. Jade 9.0 was the software used to process the XRD data and its build-in database was used for the compounds screening test.

6.1.3 Electrochemical Tests

Potentiostatic polarization test is used to measure the corrosion resistance of the GN treated L80. N_2 was pumped into the container with 200 mL simulated solution at a flow rate of 500 mL/min with an inlet pressure of 20 psi for 15 min. After deaeration, CO_2 was pumped into the simulated solution at 20 mL/min and 20 psi pressure before the test for at least 30 min to ensure the saturation of CO_2. All three electrodes were connected to the electrochemical workstation Gamry reference 500^{TM} potentiostat well. The sealed and welded specimen, rinsed by a standard rinsing procedure and air dried right before each test, was immersed into the solution 30 min before the potentiostat test for stabilization. A constant applied potential +0.2 V vs. Ag/AgCl which was 0.58 V larger than the corrosion potential of the system was applied on GN treated L80 with an optimized schedule. The current generated during the test was recorded per second for 72 h. The software used for this test was Gamry Instruments Framework 5.58a. Potentiostatic polarization tests were performed at least three times.

6.2 Compositional Stability

Figure 6-1 shows the XRD pattern of L80 and GN treated L80 before and after immersion. To compare the patterns of L80 and GN treated L80 before the immersion test, the pattern of GN treated L80 did not show the co-presence of iron or any impurities. These results indicated that the purity of the nitrides formed was high and pure Fe_3N (ε phase) with more than 8 wt% of N (Figure 2-6) was formed in the nitriding process. The XRD pattern of GN treated L80 after the immersion test showed that the composition of the surface compound layer did not change compared with the GN treated L80 before the immersion test. The XRD pattern of GN treated L80 after the immersion test did not show any exposure of the iron substrate. It also proved that the adhesion of compound layer to the diffusion layer was excellent. The comparison of XRD results before and after the immersion test indicated that GN treated L80 had great compositional stability in the test environment.
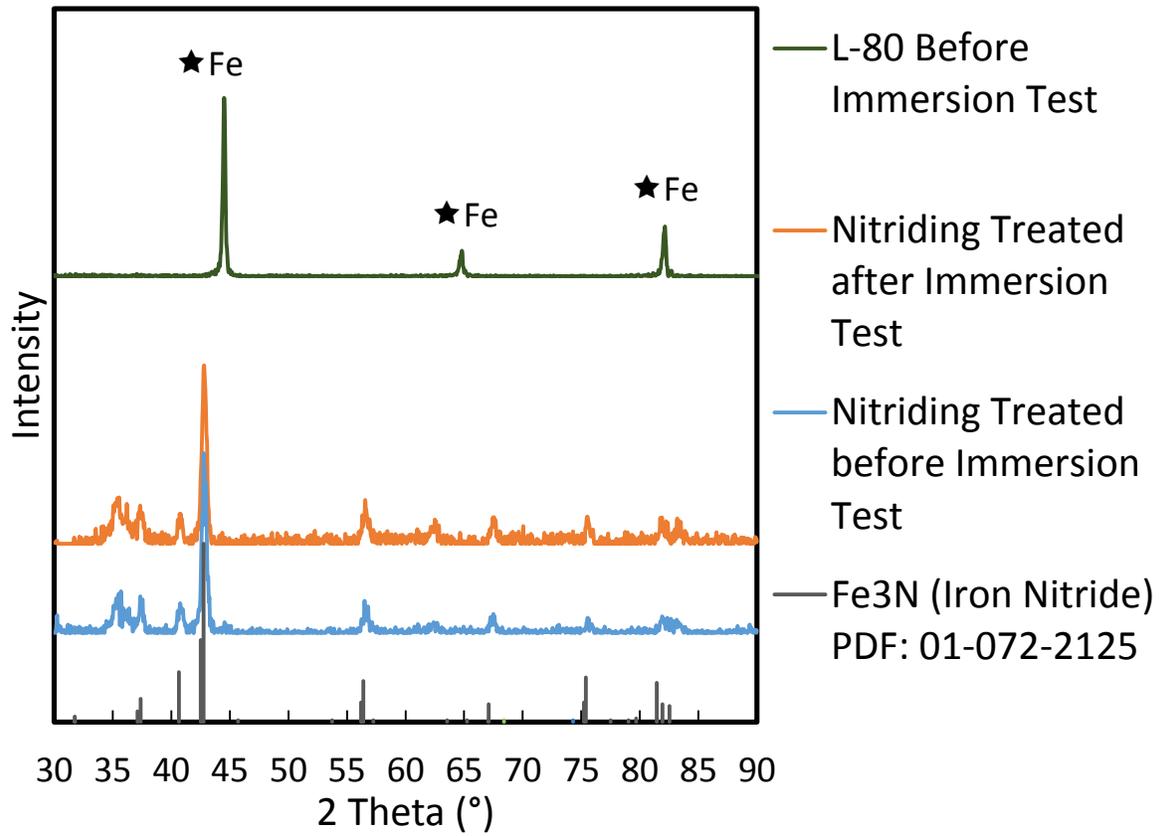
Figure 6-1. The XRD pattern of L80 and GN treated L80 specimens before and after the immersion test in CO_2 saturated simulated solution at 20 °C for 24 h.

The EDX spectrum (Figure 6-2) and EDX elemental analysis (Table 6-1) also revealed that the composition of the compound layer before and after the immersion test did not have any significant changes. The variation of compositions was sufficiently small to conclude that little reactions occurred on the GN treated L80 surface during the immersion test. Therefore, the composition stability of GN treated L80 was excellent in the test environment. The errors on the composition differences might be contributed from the organic residuals from the rinsing process and the detection limit of the equipment.
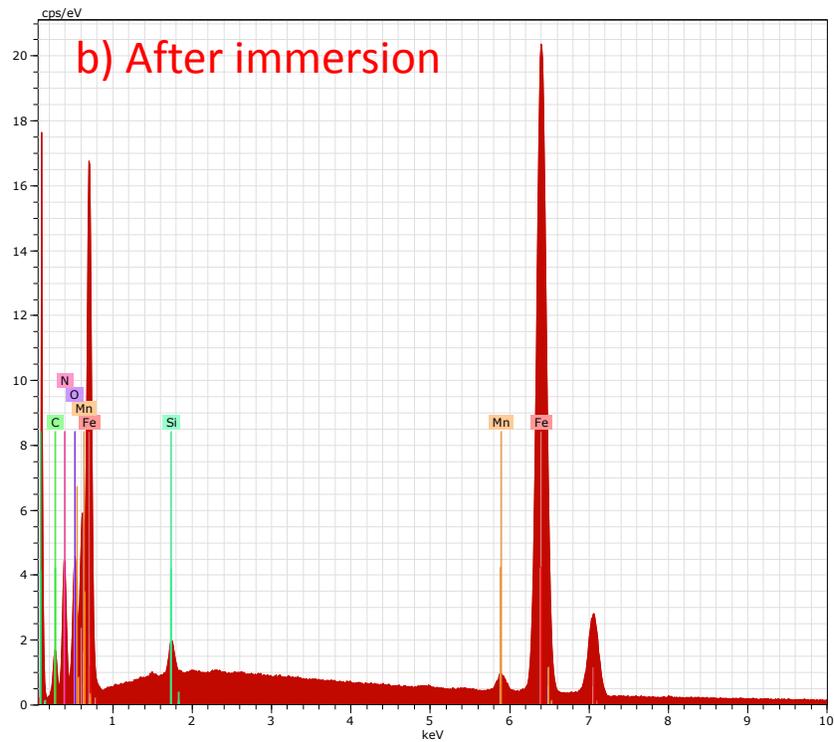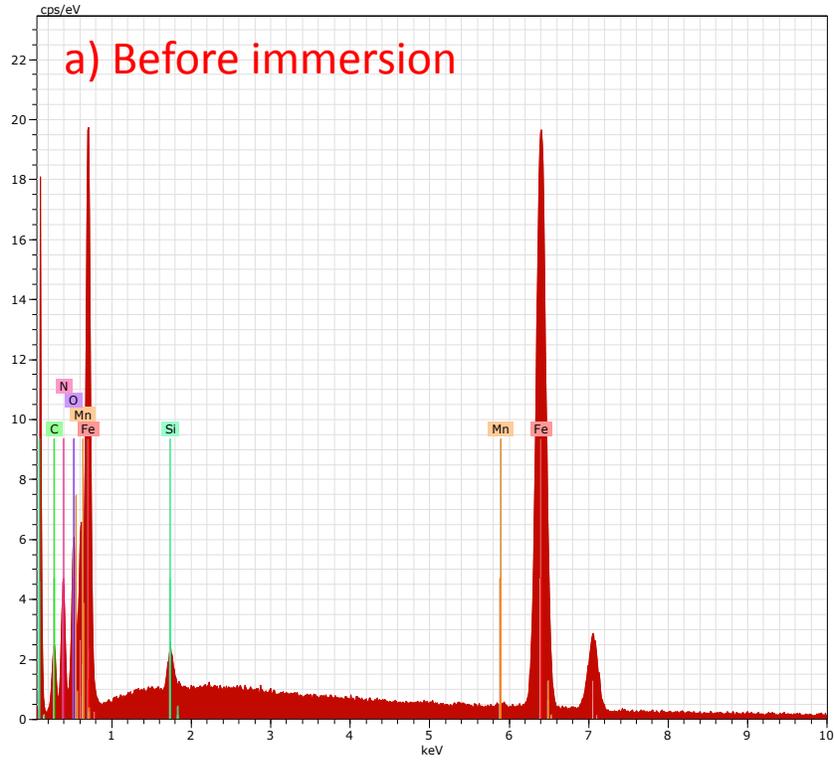
Figure 6-2. The surface EDX spectrum of GN treated L80 specimens before and after the immersion test, resolution 5 μm × 5 μm. a) before the immersion test; b) after the immersion test.

Table 6-1. The composition of compound layer before and after the immersion test.

Element	Weight percent (wt%)		Atomic percent (at%)	
	before	after	before	after
Fe	82.84	80.29	57.28	51.38
N	7.67	8.04	21.14	20.50
O	3.80	5.49	9.16	12.27
C	3.13	4.83	10.05	14.38
Mn	1.75	0.95	1.23	1.21
Si	0.82	0.40	1.13	0.26
Total	100.00	100.00	100.00	100.00

6.3 Dimensional Stability

The dimensional stability is another important factor to determine the stability of GN treated L80 in the simulated environment. It is especially important to slotted liners, which require precise dimension controls since the size of slots was careful iterated to obtain the desired screening efficiency of the bitumen. If the dimensional changes of the GN treated surface are significant either by the growth of additional layers or the removal of a coating, the screening efficiency of the slotted liners will decrease dramatically. Figure 6-3 a) shows the surface morphology of the GN treated L80 without any pretreatment. The small particles attached on the surface naturally formed on the compound layer were washed away by immersion of the specimen (Figure 6-3, b). However, the morphology of the compound layer was still dense without partially spallation or pit formation. The surface gaps were small and shallow compared with the depth of the compound layer. The gaps did not initiate and propagate into deep through the entire layer. Therefore, the compound layer had great resistance to the deformation or mass loss induced by the tests environment.
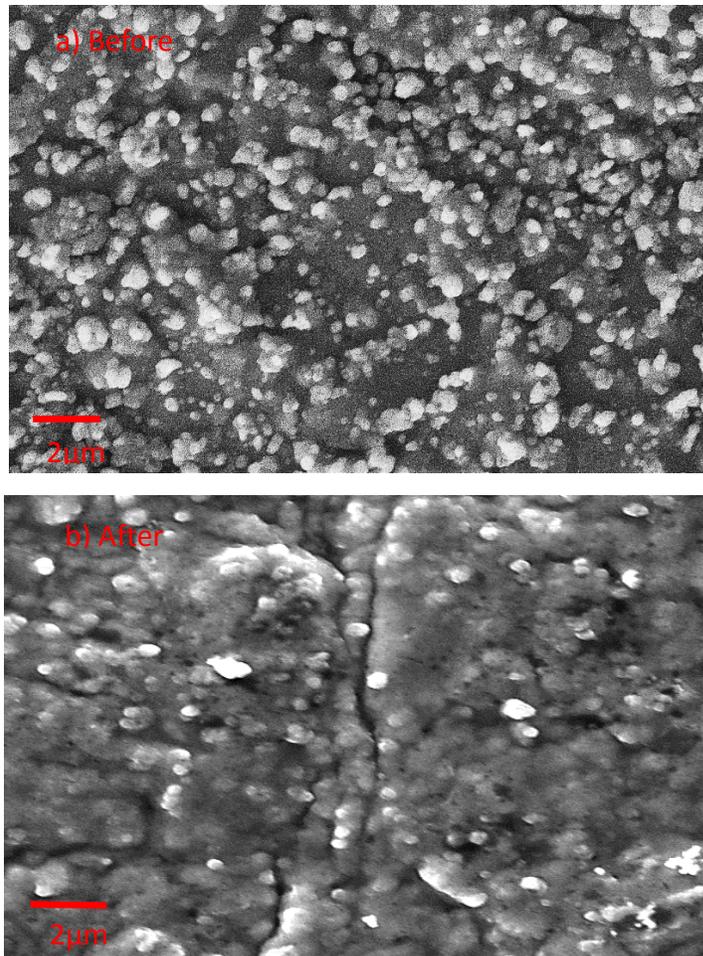
Figure 6-3. The secondary electron SEM images of surface morphologies of GN treated L80 before, a), and after, b), the immersion test, taken at 20000X.

6.4 Corrosion Resistance

The potentiostatic polarization curve of GN treated L80 tested in the simulated environment showed a small average current density, less than 10 $\mu A/cm^2$, with a constant applied potential of 0.2 V vs. Ag/AgCl for 72 h. The peak current density generated within the first hour of the test was due to the rapid formation of corrosion products in cracks and pits with fresh and active surfaces. The current density soon dropped to a stable state and gradually decreased to smaller values (log-log scale). The fluctuations of the current density were extremely small within ± 1 $\mu A/cm^2$ per hour after the first hour of the test. The current density dropped down to 1 $\mu A/cm^2$

after 10 h of test, which was even smaller than the free corrosion current density, 1.96 μA/cm^2, for GN treated L80 tested in the potentiodynamic polarization test. This fact suggested that the corrosion rate of GN treated L80 in the simulated environment would be smaller than the average value predicted by the potentiodynamic polarization test. The decrease of current density was because the corrosion products formed in the cracks and pits were deposited in a compact and protective manner, which prevented the occurrence of further corrosion [44]. Therefore, an overall decreased corrosion current density was observed.
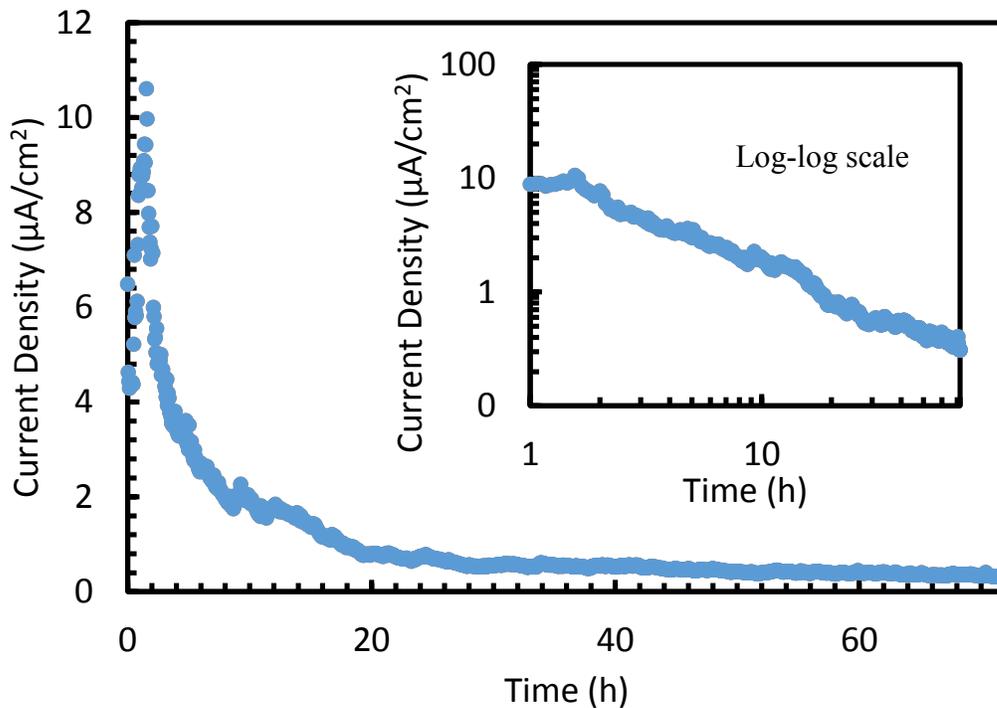
Figure 6-4. The potentiostatic polarization curve of the GN treated L80 tested in simulated environment with a constant applied potential, 0.2 V vs. Ag/AgCl, for 72 h.

6.6 Conclusions of Chapter 6

In this chapter, the stability of GN treated L80 in the simulated environment was tested and discussed. The XRD results suggested that the GN treated sample was capable of producing a compact compound layer with pure ε phase iron nitride on L80. The composition of the compound

layer after the immersion test did not show any difference. Therefore, the compositional stability of GN treated L80 was excellent in the simulated environment. The same conclusion was verified by EDX test where the elementary compositions of the compound layer before and after the test did not have significant differences. The SEM images also suggested the dimensional stability of compound layer was outstanding since the changes of the compound layer morphologies were small. The potentiostatic polarization test suggested that the GN treated L80 had excellent and stable corrosion resistance in the simulated environment. The current density generated on GN treated L80 at a constant 0.2 V Ag/AgCl potential decreased continuously with time. The corrosion current tested after 10 h of immersion was even smaller than the free corrosion density tested for GN treated L80, which indicates a smaller overall corrosion rate was expected than the one predicted by the potentiodynamic polarization test. The fluctuation of current density was sufficiently small to conclude that GN treated L80 had great electrochemical stability in the test environment.

Chapter 7. Conclusions

In chapter 4, GN treatment was optimized based on nitriding duration, temperature and ammonia flow rate to obtain the optimized corrosion resistance in the simulated environment of slotted liners. Both nitriding duration and temperature affected the thickness of compound layer, but the compactness of the compound layer was influenced by the duration and flow rate. GN treated L80 treated with either schedule showed improved corrosion resistance due to the presence of passivation zones in potentiodynamic polarization tests. The optimized schedule was a treatment at 40 mL/min of flowrate at 530°C for 16 h. The corrosion current density of optimized GN treated L80 decreased to 1.96 $\mu A/cm^2$; its corrosion potential shifted to -0.38 mV v. Ag/AgCl. Most importantly, the corrosion rate of optimized GN treated L80 decreased to 0.023 mm/year, which was about one order of magnitude smaller than the corrosion rate of L80 in the same environment. Therefore, the optimized nitriding schedule significantly increased the corrosion resistance of L80 in the simulated environment.

Chapter 5 compared the corrosion behavior of L80, GN treated L80 and alloy 800 by using potentiodynamic polarization tests, EIS tests and DM. Even though both alloy 800 and GN treated L80 had small corrosion rates, large radiuses of capacitance curves, and high phase angles in the simulated environment, GN L80 showed a more positive corrosion potential and a wider and more stable passivation zone than alloy 800. The R_p value calculated by EC fitting of GN treated L80, 3.96×10^5 $\Omega \cdot cm^2$, was very close to the R_p value of alloy 800, 5.02×10^5 $\Omega \cdot cm^2$, and both values were significantly larger than the R_p of L80, 2.32×10^3 $\Omega \cdot cm^2$. However, the corrosion behavior suggested that GN treated L80 was more sensitive to the cracks in the coating. However, the deposition of corrosion products on the surface cracks of GN treated L80 in this environment was protective and natural coating spallation was difficult due to high coating adhesion. Therefore, GN

treated L80 was the candidate with most stable and inhibited corrosion behavior for the application as slotted liners in the simulated environment.

Chapter 6 investigated the stability of GN treated L80 in the simulated environment. Both XRD and EDX results suggested that GN treatment is capable of producing a compact compound layer with pure ε phase iron nitride on L80. The small changes of composition of the compound layer before and after the immersion test proved that GN treated L80 had superior compositional stability in the simulated environment. The SEM images before and after the immersion tests suggested that the dimensional stability of the compound layer was outstanding since the changes of compound layer morphologies were limited. The potentiostatic polarization test indicated that GN treated L80 had excellent corrosion resistance and stability in the simulated environment. The current density generated on GN treated L80 at a constant 0.2 V Ag/AgCl potential decreased continuously with time. The corrosion current density tested after 10 h of immersion was even smaller than the free corrosion density tested for GN treated L80. Therefore, the overall corrosion rate of GN treated L80 in the simulated environment could be smaller than the one predicted by the potentiodynamic polarization test. The fluctuation of current density was sufficiently small to conclude that GN treated L80 had great electrochemical stability in the test environment.

In conclusion, GN treated L80 had improved corrosion resistance and inhibited corrosion behavior in the simulated environment. Most importantly, the superior stability also suggested that this material was a competitive candidate for the application as slotted liners. However, the real operation environment of slotted liners is more complex than the simulated environment. Therefore, more experiments with complex variables should be conducted to further test the applicability of GN treated L80 in the operation environment of slotted liners in future work.

Chapter 8. Future Work

8.1 Further Optimization

The optimization of GN schedule is an iteration process which should not cease even when the required performance is achieved. The optimization of treatment only emphasized on nitriding duration, temperature and ammonia flow rate in this research. However, the performance of final products is influenced by many other factors such as pre-treatment, number of stages, cooling rates, etc. For example, Chang et al. [78] investigated the effect of gas nitriding pressure on the formation of AlN in Fe-9Al-28Mn-1.8C alloy; they found that both of the thickness of the nitride layer and nitrogen concentration were increased with the increase of nitriding pressure. The corrosion resistance of a nitrided specimen in 3.5 wt% NaCl was significantly increased only after 12 h of treatment. Not only the optimization of nitriding parameters, but the schedule itself could be heavily altered to achieve better properties. The modern GN technique gradually replaced the hazardous ammonia gas by dissociating pure nitrogen gas at higher pressure (20 ksi) and higher temperature (above 1000°C) for only 3 h to achieve a nitriding layer with higher thickness and compactness [79]. Therefore, the optimization of nitriding treatment should not be limited in the adjustment of nitriding parameters. The properties of nitriding steel can also be improved by various methods.

8.2 Complex Simulated Solution

The chemistries in the simulated solution selected for this research was "sodium-chloride-bicarbonate" type, which was dominated by NaCl. The reason to select such a simplified system was to focus the research on the corrosion directly induced by dissolved CO_2. However, the real formation water is much more complex than this simulated solution. According to Abercrombie [80], the formation water of the north Athabasca oil sand region may also contain tremendous

amounts of sulphate minerals such as thenardite (Na_2SO_4) and carbonate minerals such as calcite ($CaCO_3$). Most of these chemicals were proven to have detrimental effects on the breakdown of the coating due to various mechanisms [81]. Therefore, a simulated solution with much more complex chemistries should also be tested to understand their effects on the degradation rate of GN treated L80. The real produced water separated from the bitumen from different reservoirs are the most ideal test solutions for the electrochemical tests for GN treated L80.

8.3 Effect of H_2S and Its Synergism with CO_2

Hydrogen sulfide (H_2S) is another common acidic gas released from the aquathermolysis process. According to Garverick [82], this gas is extremely harmful because it acts as a catalyst to promote the absorption of hydrogen formed by the cathodic reduction, which results in severe sulfide stress cracking of tubing. Most importantly, the corrosion product iron sulfide (FeS) deposits rapidly on the corroded surface in a porous manner, which results in severe plugging problems of the liners. The corrosion induced by H_2S (sour corrosion) may result in corrosion rates larger than hundreds of mpy. Therefore, the effect of H_2S on the GN treated L80 should also be investigated. Moreover, since the H_2S and CO_2 are generally co-present in most reserves, their synergism is the most common corrosion mechanism occurring on liners. Garverick [82] emphasizes that sour corrosion usually dominates the corrosion reactions when the mass ratio of H_2S/CO_2 exceeds to 1/500. The pitting corrosion induced by H_2S may result in more detrimental effects on GN treated L80 if the surface precipitation of FeS is not protective.

8.4 HPHT Environment with Water

Although GN treated steel has been widely applied in HPHT environment as hot forming tools and highly stressed machine components, the corrosion resistance of GN treated steel is never systematically conducted in HPHT environment in the presence of water [83]. In this research, the

temperature used for electrochemical tests was room temperature, 20°C and the pressure was about 1 atmosphere, 101.4 kPa. The temperature and pressure setting enabled the operation of *in-situ* electrochemical tests to understand the effect of CO_2 on the corrosion behavior of GN treated L80. However, both the temperature and pressure tested were far below the real operation temperature, 250°C, and pressure, 1 MPa [84]. Although conventional electrochemical tests cannot be directly conducted in this test environment, immersion tests and weight loss tests can still be carried to understand the corrosion resistance of GN treated L80 in the HPHT environment. Although high temperature decreases the solubility of CO_2 in the water, the high pressure increases the solubility of CO_2 and significantly decreases the pH of the solution, which may result in a different deposition mechanism of corrosion products [82]. Therefore, the HPHT tests on GN treated L80 in autoclave also should be done as planned for future work.

8.5 Erosion Resistance and Its Synergism with Corrosion

Numerous of tests of the wear resistance of GN treated steel have been conducted. GN treated steel is successfully applied as a heavy duty material in many industrial fields [83]. However, the erosion resistance and the synergism of corrosion and erosion on GN treated steel in humid environment are seldom studied. The erosion of slotted liners is a mechanical wear process which results in the mass loss of the material by particles such as silica (SiO_2) sand and fluid flow. Generally, the combined effects of erosion and corrosion are significantly higher than the sum of the effects of individual processes [85]. GN treated L80 may have outstanding erosion resistance; however, the segregation of corrosion products in the interface between coating and substrate may result in significant loss of coating adhesion, which can be reflected as degraded erosion resistance in the simulated environment. Therefore, the erosion and corrosion synergism of GN treated L80

in the simulated environment should be closely investigated before GN treated L80 is claimed to

be competent as the material for slotted liners.

Reference

[1] Alberta Government. "Oil Sands - The Resource (2013)". Retrieved from http://oilsands.alberta.ca/FactSheets/Resource_FSht_Sep_2013_Online.pdf

[2] Alberta Government, "Talk about SAGD (2013)", retrieved from http://www.energy.alberta.ca/OilSands/pdfs/FS_SAGD.pdf

[3] J. Been and B. Crozier. "Thermal Well Casing Corrosion Evaluation Using Hydrogen Permeation in Mini-Pipe Specimen", Alberta Innovates Technology Features (2007).

[4] J. L. Luo, Y. S. Ma and H. Zeng, "RGL-UA CRD Application Proposal - Comprehensive Design and Manufacturing Solutions for Sand Control and Tolling towards Enhanced Oil Recovery", No. 327807 (2014): pp. 1–40.

[5] J. L. Luo, H. Zeng and Y. S. Ma, "Sub-Project 5: Corrosion Mechanism Interactions with Product Design and Coating Treatment", Faculty of Engineering, University of Alberta (2014): pp.1-5.

[6] M. Koteeswaran, "CO_2 and H_2S Corrosion in Oil Pipelines", Faculty of Mathematics and Natural Science, University of Stavangers (2010).

[7] D. Pye, Chapter 1, "Practical Nitriding and Ferritic Nitrocarburizing", ASM International (2003).

[8] P. R. Kapadia, M. S. Kallos and I. D. Gates. "A New Reaction Model for Aquathermolysis of Athabasca Bitumen". The Canadian Journal of Chemical Engineering, 91, 3 (2012): pp. 475–482.

[9] R. Case, S. Mahajanam, J. Dunn, M. Joosten, M. Achour, H. Marchebois, S. Mahajanama, J. Dunn, and M. Bonis. "Evaluation of Corrosivity of Produced Fluids during SAGD Operations". Corrosion (2014), Paper no. 4273; pp 1-7.

[10] J. Whittaker and Q. Liu, "Corrosion Management and Mechanism Study on SAGD Brackish Water System". Corrosion (2014): Paper No. 3809; pp. 1-6.

[11] D. A. Katz, "The Athabasca Tar Sands Fort McMurray, Alberta, Canada". Department of Chemistry, Pima Community College – West Campus (2007): pp. 1-22.

[12] F. Y. Ma. "Corrosive Effects of Chlorides on Metals", Pitting Corrosion (2012), ISBN: 978-953-51-0275-5: pp.139-178.

[13] H. J. Abercrombie, "Evolution of Groundwater Hydrochemistry, North Athabasca Oil Sand Region", GeoConvention 2015: Geoscience New Horizons (2015): pp. 1-2.

[14] JEF Steel, "Corrosion Resistant High Cr Steel for Oil and Gas Wells", New Products & Technologies, 18 (2013): pp. 61-63.

[15] V. Palanisamy, J. K. Solberg, B. Salberg, and P. T. "Microstructure and Mechanical Propertied of API 5CT L80 Casing Grade Steel Quenched from Different Temperatures. ASME 2012 31st International Conference on Ocean, Offshore and Arctic Engineering, 6 (2012): pp. 253–259.

[16] K. Videm and A.M. Koren, "Corrosion, Passivity, and Pitting of Carbon Steel in Aqueous Solutions of HCO^{3-}, CO2, and Cl^-", Corrosion, 49, 9 (1993): pp. 746–754.

[17] I. S. Cole, P. Corrigan, S. Sim, and N. Birbillis, "Corrosion of Pipelines Used for CO2 Transport in CCS: Is it a Real Problem?", International Journal of Greenhouse Gas Control, 5, 4 (2011): pp. 749–756.

[18] Q. Wu, Z. Zhang, X. Dong, and J. Yang, "Corrosion Behavior of Low-Alloy Steel Containing 1% Chromium in CO_2 Environments", Corrosion Science, 75 (2013): pp. 400–408.

[19] C. A. Palacious and J. R. Shaldey, "Characteristics of Corrosion Scales on Steel in a CO_2-Saturated NaCl Brine", Corrosion, 47, 2 (1991): pp. 122–127.

[20] Q.Y. Liu, L. J. Mao, S. W. Zhou, "Effects of Chloride Content of CO2 Corrosion of Carbon Steel in Simulated Oil and Gas Well Environments", Corrosion Science, 84 (2014): pp. 165–171.

[21] D. H. Davies and G. T. Burstein. "The Effects of Bicarbonate on the Corrosion and Passivation of Iron". Corrosion, 36, 8 (1980): pp. 416-422.

[22] L. T. Popoola, A. S. Grema, G. K. Latiwo, B. Gutti, and A. S. Balogun. "Corrosion Problems during Oil and Gas Production and Its Mitigation", International Journal of Industrial Chemistry, 4, 35 (2013).

[23] W. T. Scannell and A. Sohanghpurwala, "Cathodic Protection as a Corrosion Control Alternative", Concorr, Inc. (1993): pp. 1-5.

[24] SAE, Enviranode, "Well Casing Cathodic Protection System" (2010).

[25] P. Malekinejad and M. S. Alavi, "Cathodic Protection of Oil and Gas Well Casing", 1st National Iranian Drilling Industry Congress, 1 (2008): pp. 1-11.

[26] S. Oliphant, "Well Casing Corrosion and Cathodic Protection", NACE Northern Area Western Conference (2010): pp. 1-32.

[27] R. Norsworthy, "Fusion Bonded Epoxy – A Field Proven Fail Safe Coating System", Corrosion - NACE International Conference (2006), no. 06044: pp. 1-9.

[28] J. S. Park, J. M. Kim, H. Y. Kim, J. S. Lee, I. H. Oh, and C. S. Kang. "Surface Protection Effect of Diffusion Pack Cementation Process by Al-Si Powders with Chloride Activator on Magnesium and Its Alloys. Materials Transactions, 49, 5 (2008): pp. 1048-1051.

[29] T. Nagashima, E. Sakuma and K.Takano, "Member for Immersion in Hot Dip Galvanizing Bath and Method for Producing the Same (2001)". US6284062 B1.

[30] Jiangnan Fluoroplastic Co., Ltd., PTFE Line Pipes.

[31] E. D. Hollies, "Use of Coated Slots for Control of Sand or Other Solids in Wells Completed for Production of Fluids (2009)". US 20090014174 A1.

[32] M. Shi, F. Miyazawa, S. Tobe and T. A. Stolarski, "The Friction and Wear Properties of PTFE Composite-Thermal Spray Metallic Binary Coatings", Materials Transactions, 46, 1 (2005): pp. 84-87.

[33] EnTech Instruments Inc., "Ultra Inert Silonite Surface Coatings", retrieved from http://www.entechinst.com/about/entech-technology.

[34] J.N. Dobbes, A.C. Anderson, "The Thermal Expansion of Teflon at Temperature below 3K", Journal of Non-Crystalline Solids, 69, 2-3 (1985): pp. 429-431.

[35] Q. Zhou, W. Lu, "A Method to Deposit Silica Coating by Electroplating on Steel (2015)", CN 102732936 B.

[36] D. Pye, Chapter 2, "Practical Nitriding and Ferritic Nitrocarburizing (2003)", ASM International.

[37] A. F. O. Skonieski, G. R. D. Santos, T. K. Hirsch, and A. D. S. Rocha, "Metallurgical Response of an AISI 4140 Steel to Different Plasma Nitriding Gas Mixtures", Materials Research, 16, 4 (2013): pp. 884–890.

[38] Eco-Thermal, "Pot Type Gas Nitriding Furnace (2014)", retrieved from http://www.eco-thermal.com/sh-series.html

[39] D. Krastev, "Improvement of Corrosion Resistance of Steels by Surface Modification", Corrosion Resistance (2012), ISBN 978-953-51-0467-4: pp. 295-316.

[40] J. Michalski, P. Wach, J. Tacikowski, M. Betuik, K. Burdynski, S. Kowalski, and A. Nakonieczny, "Contemporary Industrial Application of Nitriding and Its Modification", Materials and Manufacturing Processes, 24 (2009): pp.855–858.

[41] ASM International, "Chapter 1. Process Selection Guide", Surface Hardening of Steels: Understanding in Basics (2002), #06952G: pp. 1-15.

[42] A. Biswas, L. Li, U. K. Chatterjee, I. Manna, S.K. Pabi and J. D. Majumdar. "Mechanical and Electrochemical Properties of Laser Surface Nitrided Ti-6Al-4V", Scripta Materialia, 59 (2008): pp. 239–242.

[43] X. Wang, W.T. Zheng, H. W. Tian, S.S. Yu, W. Xu, S.H. Meng, X.D. He, J.C. Han, C.Q. Sun, and B.K. Tay, "Growth, Structural, and Magnetic Properties of Iron Nitrides Thin Films Deposited by DC Magnetron Sputtering", Applied Surface Science, 220 (2003): pp. 30-39.

[44] B. Wang, Z. Sun and S. Zhou, "Effect of Gas Nitriding on CO_2 Corrosion Behavior of 40Cr Steel", Applied Mechanics and Materials, 68 (2011): pp. 956–959.

[45] B. Wang, Z. Zhou, W. Wang, and B. Zhao, "Investigation of Gas Nitriding on Wear and Corrosion Behavior of 40Cr Steel". Advanced Materials Research, 313 (2013): pp. 674–678.

[46] B. Wang, Z. Sun, W. Jiang, and Z. Hou. "Corrosion Behavior of 35CrMo Steel after Gas Nitriding", Transaction of Materials and Heat Treatment, 32, 12 (2011): pp. 143–146.

[47] Z. Liu, "Research on the Corrosion and Wear Performance of the Nitriding and Sherardizing Complex Treatment in Oil Output Liquid", China Academy of Machinery Science and Technology (2011): pp. 36-48.

[48] Y. Chen, C. Lin, C. Chao, and T. Liu, "Excellent Enhancement of Corrosion Properties of Fe-9Al-30Mn–1.8C Alloy in 3.5% NaCl and 10% HCl Aqueous Solutions Using Gas Nitriding Treatment". Journal of Alloys and Compounds, 633 (2015): pp. 137–144.

[49] S. Yeh, L. Chiu, and H. Chang. "Effects on Gas Nitriding on the Mechanical and Corrosion Properties of SACM 645 Steel", Engineering, 3 (2011): pp.942-948.

[50] R. L. O. Baaso, R. J. Candal, C. A. Figueroa, D. Wisnivesky, and F. Alverz, "Influence of Microstructure on the Corrosion Behavior of Nitro carburized AISI H13 Tool Steel Obtained by Pulsed DC Plasma". Surface and Coating Technology, 203, 10 (2009): pp. 1293–1297.

[51] S. Niu, S. Yang, Y. Li, "Improvement in Corrosion Resistance of Anchor Steel by Low Temperature Plasma Nitriding". Journal of Wuhan University of Technology-Material, Science Edition. 29, 3 (2011): pp. 590–593.

[52] L.N. Tang and M.F. Yan. "Influence of Plasma Nitriding on the Microstructure, Wear, and Corrosion Properties of Quenched 30CrMnSiA Steel". Journal of Materials Engineering and Performance, 22, 7 (2013): pp.2121 – 2129

[53] E. Almeida, J. Milan, C. Costa, "Acquired Properties Comparison of Solid Nitriding, Gas Nitriding and Plasma Nitriding in Tool Steels", Materials Research, 18, 1 (2015): pp. 7–35.

[54] T. Weber, L. Wit, F. W. Saris, A. Koniger, B. Rauschenbach, G. K. Wolf, S. Krauss. "Hardness and Corrosion Resistance of Single-phase Nitride and Carbide on Iron", Material Science and Engineering, A199 (1995): pp. 205 -210.

[55] J. Prasek, L. Trankova, I. Gablech, P. Businova, J. Drbohlavova, J. Chomoucka, V. Adam, R. Kizek, J. Hubalec, "Optimization of Planar Three-Electrode Systems for Redox System Detection", International Journal of Electrochemical Science, 7 (2012): pp. 1785-1801.

[56] K. K. Kasmen and S. Jones, "Platinum as Reference Electrode in Electrochemical Measurements", Platinum Metals Review, 52, 2 (2008); pp. 100-106.

[57] A. Lasia, "Electrochemical Impedance Spectroscopy and Its Application", Modern Aspects of Electrochemistry, 32 (1999), pp. 143-248.

[58] Gamry Instruments, "Introduction to Electrochemical Impedance Spectroscopy", retrieved from: https://www.gamry.com/assets/Uploads/Basics-of-Electrochemical-Impedance-Spectroscopy.pdf

[59] Gamry Instruments, "Basics of Electrochemical Impedance Spectroscopy (updated on 2015)", retrieved from: https://www.gamry.com/application-notes/EIS/basics-of-electrochemical-impedance-spectroscopy/.

[60] W. Pinc, D. Heller, W. Fahrenholtz, M. O'Keefe, "Electrochemical and Structural Changes in Cerium Based Conversion Coatings during Exposure to Salt Spray", Electrochemical Society Transactions, 25, 29 (2010): pp. 3-17.

[61] I. Dehri, "Impedance Measurements of Polyester-Coated Galvanized Mild Steel in 10x Acid Rainwater after an Accelerated Wet-Dry Test", Turkey Journal of Chemistry, 24 (2000): pp.239-245.

[62] Gasem, Z. M., "Chapter 3: Electrochemical Kinetics of Corrosion (Polarization)", ME 472: Corrosion Engineering I, KFUPM, 2013.

[63] Princeton Applied Research, "Application Note Corr-1. Subject: Basic of corrosion Measurements", 2012.

[64] Zang, L., Lecture 3 Brief Overview of Traditional Microscopes, Department of Materials Science and Engineering, University of Utah.

[65] H. Inada, D. Su, R.F. Egerton, M. Konno, L. Wu, J. Ciston, J. Wall and Y. Zhu, "Atomic Imaging Using Secondary Electrons in a Scanning Transmission Electron Microscope: Experimental Observations and Possible Mechanisms", Ultramicoscopy (2010); pp. 1-20.

[66] U. Scheithauer, "Application of the Analytical Methods REM/EDX, AES and SNMS to a Chloride Induced Aluminum Corrosion", Fresenius' Journal of Analytical Chemistry, 341 (1991): pp. 445-448.

[67] C. G. Pope, "X-ray Diffraction and the Bragg Equation", Journal of Chemical Education, 74, 1 (1997): pp.129-131.

[68] Continental Alloys and Service, L80, Materials, retrieved from http://www.contalloy.com/products/grade/l80.

[69] Barnstead Thermolyne Corporation, "Types F79300 & F79400 Tube Furnaces – Operation Manual and Parts List (2004)", retrieved from: http://www.masterflex.com/assets/Manual_pdfs/00124VO%20manual.pdf.

[70] V. Fajardo, B. Brown, D. Young, S. Nesic, "Study of the Solubility of Iron Carbonate in the Prescience of Acetic Acid Using an EQCM", NACE International Corrosion 2013 Conference and Expo, Paper No. 2452 (2013); pp. 1-20.

[71] Special Metals Corporation, "High-Performance Alloys for Resistance to Aqueous Corrosion", SMC-026 (2000): pp.1-7.

[72] Craig, B., "Materials for Deep Oil and Gas Well Construction, Advanced Materials and Process", ASM international, AMP16605P033 (2008): pp.33 -35.

[73] Special Metals Corporation, "Incoloy alloy 800", SMC-046 (2004): pp.1–12.

[74] R. C. Newman, H. S., Isaacs and B. Alman , "Effects of Sulfur Compounds on the Pitting Behavior of Type 304 Stainless Steel in Near-Neutral Chloride Solutions", Corrosion, 28, 5 (1982): pp. 261–265.

[75] W.M. Bos, "Chapter 4 - Outdoor Exposure of Coating Systems Monitored with EIS", Prediction of Coating Durability Early Detection Using Electrochemical Methods (2008), ISBN 978-90-9022815-0: pp. 67–73.

[76] A. Tiwari, J. Rawlins, L. H. Hihara, "6.2.2.2 Characterization of Paint Coating and Low Carbon Steel Substrates" Intelligent Coating for Corrosion Control (2015), ISBN 978-0-12-411467-8: pp. 203-204.

[77] J. Banas, B. Mazurkiewiez, U. Lelek-Borkowska, H. Krawiec, W. Solarski, K. Kowalski, "The Effect of CO_2 and H_2S on the Passivation of Chromium and Stainless Steels in Aqueous Solutions at Elevated Temperature and under High Pressure", Passivation of Metals and

Semiconductors, and Properties of thin Oxide Layer: A Selection of Papers from the 9th International Symposium, Paris, France (2005): pp.417–423.

[78] K.M. Chang, C.C. Kuo, Y.W. Chang, C.G. Chao, T.F. Liu, "Effects of Gas Nitriding Pressure on the Formation of Nanocrystalline AlN in Plasma Nitrided Fe-9Al-28Mn-1.8C Alloy", Surface and Coating Technology, 254 (2014): pp. 313-318.

[79] S. A. Gerasimov, V. A. Golikov, M. A. Gress, G. G. Mukhin, and V. I. Snop, "High-Pressure Gas Nitriding of Steels", Metal Science and Heat Treatment, 46, 5-6 (2004): pp. 227 - 232.

[80] H. J. Abercrombie, "Evolution of Groundwater Hydrochemistry, North Athabasca Oil Sand Region", GeoConvention 2015: Geoscience New Horizons (2015): pp. 1-2.

[81] R. Case, S. Mahajanam, J. Dunn, M. Joosten, M. Achour, H. Marchebois, S. Mahajanama, J. Dunn, and M. Bonis. "Evaluation of Corrosivity of Produced Fluids during SAGD Operations". Corrosion (2014), Paper no. 4273: pp. 1-6.

[82] L. Garverick, "Corrosion in Petroleum Production Operations", Corrosion in the Petrochemical Industry (1994), ASM International, ISBN-10 0871705052: pp. 259-260.

[83] J. Michalski, P. Wach, J. Tacikowski, M. Betuik, K. Burdynski, S. Kowalski, and A. Nakonieczny, "Contemporary Industrial Application of Nitriding and Its Modification", Materials and Manufacturing Processes, 24 (2009): pp.855–858.

[84] C. Palmgren, I. Walker, M. Carlson, M. Uwiera, M. Torlak, "Reservoir Design of a Shallow LP-SAGD Project for in-Situ Extraction of Athabasca Bitumen", World Heavy Oil Congress (2011), WHOC11-520: pp. 1-8.

[85] R. Malka, S. Nesic, and D. A. Guilino, "Erosion Corrosion and Synergistic Effects in Disturbed Liquid-Particle Flow", Corrosion NACE XPO 2006), Paper No. 06594: pp. 1-22.
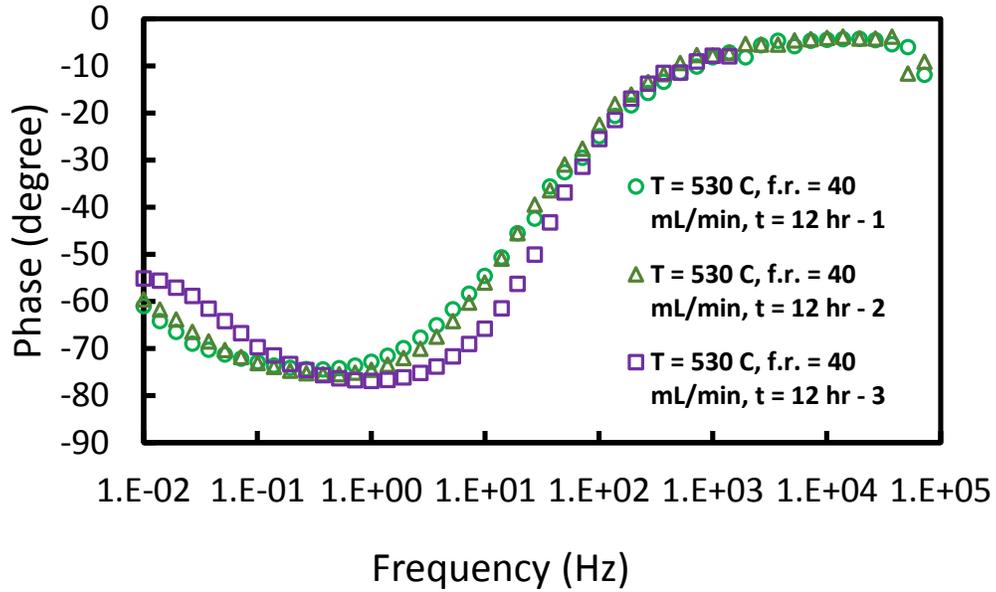
Figure A-1. The Phase Bode Plot L-80 Treated with the Same Nitriding Parameters in Simulated Environment (sample).
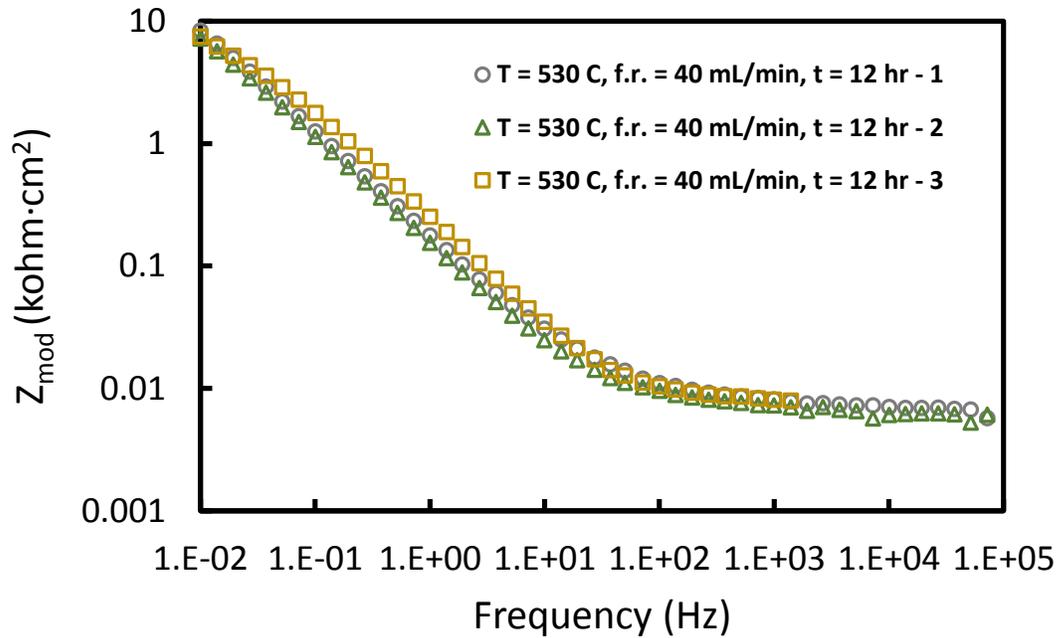

Figure A-2. The Impendence Bode Plot of L-80 Treated with Same Nitriding Parameters in Simulated Environment (sample).
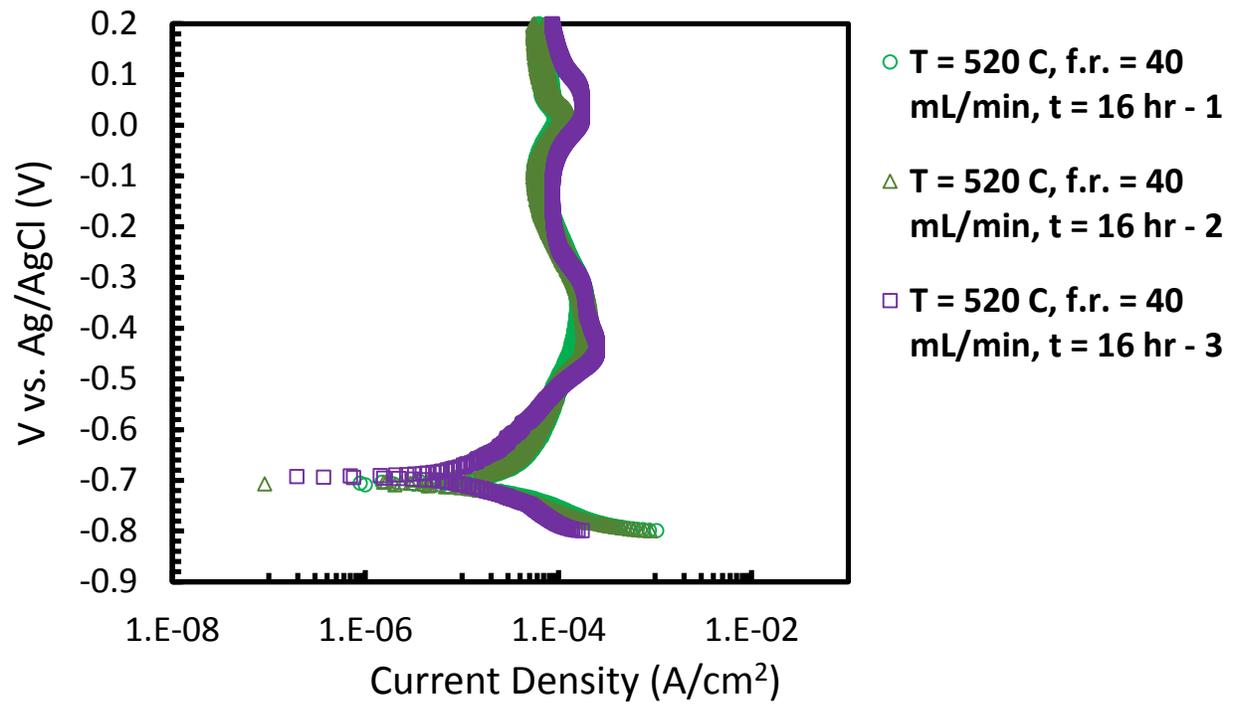
Figure A-3. The L-80 Nitriding Treated with Same Parameters in the Same Simulated Environment (sample).

Electrochemistry Tests Data

530, 40, 12, 20, S6, CO2 - 2								
area	0.9 cm							
Zreal	Zimag	abs Zimag	Zreal	Zimag	Zmod	Zmod	Phase	Frequency
ohm	ohm	ohm	ohm*cm^2	ohm*cm^2	ohm	kohm.cm^2	degree	Hz
6.928785	-1.02216	1.022158	0.006236	0.00092	7.003776	0.006303	-8.39194	100078.1
6.673168	-1.0782	1.078203	0.006006	0.00097	6.759711	0.006084	-9.17813	72046.88
5.728737	-1.1837	1.183695	0.005156	0.001065	5.849749	0.005265	-11.6744	51796.87
6.804047	-0.45395	0.453952	0.006124	0.000409	6.819174	0.006137	-3.817	37359.37
6.929843	-0.51232	0.512321	0.006237	0.000461	6.948755	0.006254	-4.22817	26859.38
6.921384	-0.50763	0.507635	0.006229	0.000457	6.939975	0.006246	-4.19473	19359.38
6.822134	-0.45209	0.452093	0.00614	0.000407	6.837098	0.006153	-3.79137	13921.87
6.728172	-0.48395	0.483948	0.006055	0.000436	6.745554	0.006071	-4.11412	10078.13
6.275129	-0.47504	0.475039	0.005648	0.000428	6.293084	0.005664	-4.32914	7265.625
7.217964	-0.58371	0.583708	0.006496	0.000525	7.241527	0.006517	-4.62338	5203.125
7.390254	-0.7151	0.715096	0.006651	0.000644	7.42477	0.006682	-5.52685	3722.427
7.7707	-0.74495	0.744953	0.006994	0.00067	7.806327	0.007026	-5.47604	2659.255
7.230588	-0.67569	0.675687	0.006508	0.000608	7.262091	0.006536	-5.3387	1938.101
7.730915	-0.97981	0.97981	0.006958	0.000882	7.792758	0.007013	-7.22311	1397.236
7.996369	-1.09303	1.093028	0.007197	0.000984	8.070727	0.007264	-7.78356	998.264
8.018698	-1.08883	1.088833	0.007217	0.00098	8.092284	0.007283	-7.73272	724.4318
8.329007	-1.37899	1.378988	0.007496	0.001241	8.442391	0.007598	-9.40087	516.4195
8.507513	-1.77574	1.77574	0.007657	0.001598	8.690859	0.007822	-11.7899	370.0658
8.705528	-2.08518	2.085184	0.007835	0.001877	8.951772	0.008057	-13.47	268.9549
8.998635	-2.59978	2.599783	0.008099	0.00234	9.366659	0.00843	-16.1145	192.1107
9.336598	-3.05864	3.058638	0.008403	0.002753	9.82483	0.008842	-18.1386	137.8676
9.78171	-4.05559	4.055589	0.008804	0.00365	10.58913	0.00953	-22.5194	100.4464
10.01468	-5.23595	5.235946	0.009013	0.004712	11.30084	0.010171	-27.6018	71.74745
10.57831	-6.34126	6.341258	0.00952	0.005707	12.33338	0.0111	-30.9409	49.86702
10.86533	-8.02729	8.027286	0.009779	0.007225	13.50899	0.012158	-36.4569	37.20238
12.14579	-10.0063	10.00628	0.010931	0.009006	15.73677	0.014163	-39.4833	27.25291
13.19787	-13.461	13.46095	0.011878	0.012115	18.85155	0.016966	-45.5654	19.21107
14.02707	-17.289	17.28896	0.012624	0.01556	22.26358	0.020037	-50.9465	13.95089
15.31248	-22.7462	22.7462	0.013781	0.020472	27.42009	0.024678	-56.052	9.93114
16.9723	-29.7309	29.73088	0.015275	0.026758	34.23425	0.030811	-60.2795	7.233796
18.94289	-39.2043	39.2043	0.017049	0.035284	43.5409	0.039187	-64.2109	5.208333
21.5248	-52.0147	52.01469	0.019372	0.046813	56.2925	0.050663	-67.5192	3.75601
24.98598	-68.9444	68.94441	0.022487	0.06205	73.33234	0.065999	-70.0791	2.703287
30.27687	-93.4711	93.47105	0.027249	0.084124	98.2524	0.088427	-72.052	1.914828
36.77496	-123.656	123.6563	0.033097	0.111291	129.0088	0.116108	-73.4377	1.392602
45.85852	-165.442	165.4422	0.041273	0.148898	171.6803	0.154512	-74.5073	0.999041
58.37354	-219.875	219.8745	0.052536	0.197887	227.4912	0.204742	-75.1318	0.721154
75.76643	-292.079	292.0794	0.06819	0.262871	301.7465	0.271572	-75.4578	0.520833
100.5582	-388.555	388.5552	0.090502	0.3497	401.3565	0.361221	-75.4902	0.375
135.9879	-517.212	517.2122	0.122389	0.465491	534.7907	0.481312	-75.2689	0.269397
187.2055	-686.257	686.2574	0.168485	0.617632	711.3333	0.6402	-74.7414	0.193698
261.565	-909.291	909.2905	0.235409	0.818361	946.1635	0.851547	-73.9517	0.139095
365.0083	-1200.45	1200.446	0.328507	1.080401	1254.712	1.129241	-73.0876	0.10016
520.6399	-1584.17	1584.167	0.468576	1.42575	1667.529	1.500776	-71.8068	0.072005
740.5846	-2070.95	2070.948	0.666526	1.863853	2199.384	1.979446	-70.3226	0.051796
1060.707	-2692.92	2692.916	0.954636	2.423624	2894.286	2.604857	-68.5011	0.037291
1507.428	-3470.16	3470.158	1.356685	3.123142	3783.43	3.405087	-66.52	0.026832
2156.554	-4401.56	4401.563	1.940899	3.961407	4901.478	4.41133	-63.8974	0.019314
2970.146	-5535.44	5535.439	2.673131	4.981895	6281.946	5.653751	-61.7834	0.013897
4039.16	-6886.98	6886.979	3.635244	6.198281	7984.065	7.185659	-59.6087	0.010001

Figure A-4. Sample data for the EIS test.

520, 40, 16, 20, S6 CO2 - 1				
area	0.95	cm		
Vf	Im	Vf	abs Im	abs Im
V vs. Ref.	A	V	A	A/cm2
-7.99E-01	-9.87E-04	-7.99E-01	0.000987	0.001039
-7.98E-01	-8.24E-04	-7.98E-01	0.000824	0.000868
-7.97E-01	-7.08E-04	-7.97E-01	0.000708	0.000746
-7.96E-01	-6.21E-04	-7.96E-01	0.000621	0.000654
-7.95E-01	-5.53E-04	-7.95E-01	0.000553	0.000582
-7.94E-01	-4.99E-04	-7.94E-01	0.000499	0.000525
-7.93E-01	-4.56E-04	-7.93E-01	0.000456	0.00048
-7.92E-01	-4.19E-04	-7.92E-01	0.000419	0.000441
-7.92E-01	-3.89E-04	-7.92E-01	0.000389	0.000409
-7.91E-01	-3.62E-04	-7.91E-01	0.000362	0.000382
-7.90E-01	-3.40E-04	-7.90E-01	0.00034	0.000358
-7.89E-01	-3.20E-04	-7.89E-01	0.00032	0.000337
-7.88E-01	-3.03E-04	-7.88E-01	0.000303	0.000319
-7.87E-01	-2.88E-04	-7.87E-01	0.000288	0.000303
-7.86E-01	-2.74E-04	-7.86E-01	0.000274	0.000288
-7.85E-01	-2.61E-04	-7.85E-01	0.000261	0.000275
-7.84E-01	-2.49E-04	-7.84E-01	0.000249	0.000262
-7.83E-01	-2.39E-04	-7.83E-01	0.000239	0.000251
-7.81E-01	-1.93E-04	-7.81E-01	0.000193	0.000204
-7.81E-01	-2.20E-04	-7.81E-01	0.00022	0.000232
-7.79E-01	-1.80E-04	-7.79E-01	0.00018	0.000189
-7.79E-01	-2.04E-04	-7.79E-01	0.000204	0.000215
-7.77E-01	-1.68E-04	-7.77E-01	0.000168	0.000177
-7.77E-01	-1.91E-04	-7.77E-01	0.000191	0.000201
-7.75E-01	-1.58E-04	-7.75E-01	0.000158	0.000167
-7.75E-01	-1.78E-04	-7.75E-01	0.000178	0.000188
-7.73E-01	-1.49E-04	-7.73E-01	0.000149	0.000157
-7.73E-01	-1.68E-04	-7.73E-01	0.000168	0.000177
-7.71E-01	-1.41E-04	-7.71E-01	0.000141	0.000149
-7.71E-01	-1.58E-04	-7.71E-01	0.000158	0.000166
-7.69E-01	-1.34E-04	-7.69E-01	0.000134	0.000141
-7.69E-01	-1.49E-04	-7.69E-01	0.000149	0.000157
-7.67E-01	-1.27E-04	-7.67E-01	0.000127	0.000134
-7.67E-01	-1.41E-04	-7.67E-01	0.000141	0.000148
-7.65E-01	-1.21E-04	-7.65E-01	0.000121	0.000128
-7.65E-01	-1.33E-04	-7.65E-01	0.000133	0.00014

Figure A-5. Sample data for the PD test (partially displayed).

GN Before Test	
2Theta (°)	Intensity (%)
30	0
30.05	0
30.1	0
30.15	1.76678445
30.2	6.36042403
30.25	9.89399293
30.3	1.06007067
30.35	1.41342756
30.4	4.24028269
30.45	2.82685512
30.5	2.12014134
30.55	3.5335689
30.6	0.35335689
30.65	1.41342756
30.7	0.70671378
30.75	0.70671378
30.8	1.76678445
30.85	0.35335689
30.9	0
30.95	0
31	0.70671378
31.05	0
31.1	2.47349823
31.15	4.24028269
31.2	4.59363958
31.25	0
31.3	0.70671378
31.35	0
31.4	3.8869258
31.45	1.76678445
31.5	0
31.55	1.06007067
31.6	1.76678445

Figure A-6. Sample data for XRD test (partially displayed).